CONCORDIA UNIVERSITY

Technical Note No. TN-EMC-86-04
July 10, 1986

Evaluations of Computer Models
of Steel Tower Power Lines

C.W. Trueman
S.J. Kubina
Concordia University/EMC Laboratory
7141 Sherbrooke St. W.
Montreal, Quebec, Canada
H4B 1R6

FACULTY OF ENGINEERING AND COMPUTER SCIENCE

DEPARTMENT OF ELECTRICAL ENGINEERING
1455 de Maisonneuve Blvd., West
MONTREAL, H3G 1M8, Canada

Technical Note No. TN-EMC-86-04
July 10, 1986

Evaluations of Computer Models of Steel Tower Power Lines

C.W. Trueman
S.J. Kubina
Concordia University/EMC Laboratory
7141 Sherbrooke St. W.
Montreal, Quebec, Canada
H4B 1R6

SCIENTIFIC AUTHORITY
G.M. ROYER

Prepared for:

Communications Research Centre
Ottawa, Ontario, Canada
K2H 8S2

Contract Serial No. 0ST85-00221

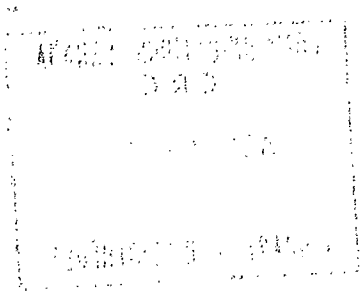

TABLE OF CONTENTS

Page

ACKNOWLEDGEMENT

The work reported herein was carried out for the Communications Research Centre under Department of Supply and Services Contract No. OST85-00221. In the monitoring of this contract, the participation of Dr. J.S. Belrose and Mr. Max Royer of the Communications Research Centre was very much appreciated. The support of the Canadian Electrical Association is gratefully acknowledged.

The authors are indebted to Mr. J. Litchfield and Mr. A. Caruso of the Canadian Broadcasting Corporation for their cooperation, and gratefully acknowledge the CBC's support.

The authors wish to thank Mr. M.A. Tilston for supplying the BASIC language version of the AMPL program.

The authors gratefully acknowledge the work of Mr. Chris Baltassis in preparing the computer programs and the data on the tower footing impedance presented in Chapter 2. The authors wish to thank Mr. Victor Phan for his participation in the digitization of measured radiation patterns and in the preparation of the results for Chapter 3. The authors gratefully acknowledge the work of Mr. Dale Norman in translating AMPL into FORTRAN, in its extensive testing, and in preparing the data for Chapter 4.

CHAPTER 1

INTRODUCTION

This document is the Final Report in DOC/CRC Contract No. OST85-00221, covering the period September, 1985 to May, 1986, and continues the sequence of Final Reports in Refs. (1) to (5). These reports are concerned with MF broadcasting arrays operating in the presence of high-voltage power lines. The power lines studied typically have steel-lattice towers 30 to 50 or more metres tall, and are electrically connected together at their tops by a "skywire", which provides a path to ground for a lightning strike. The broadcast antenna is typically a commercial "standard" broadcast array, operating at a frequency between 535 and 1605 kHz, usually operating with 50 kilowatts of power, and usually required to limit its radiation over specified "restricted arcs", to avoid interference with other stations. The signal from the broadcast array illuminates the power line and induces RF current flow on the towers and skywires. The RF currents on the power line towers "reradiate" the station's signal, and the reradiated signal combines with the array's radiated signal to produce stronger than intended radiation in some directions, and less radiation than intended in others. Two problems arise. One is "scalloping" of the main lobe of the broadcast array's azimuth pattern, resulting in reduced signal strength in parts of the main service area, and hence unsatisfactory coverage. The other problem is "null-filling", in which the power line reradiates into the "restricted arcs" of the station where the broadcast array's pattern has been carefully designed to have sufficiently deep nulls. Reradiation readily causes a greatly increased field strength in the nulls, and hence a violation of the station's licence. "Detuning" refers to the alteration of the power line to suppress the RF current flow, and hence elimination of reradiation, and is intended to restore the array's pattern to its design.

The Final Reports in previous contract periods, Refs. (1) to (5), are concerned with developing and using a computer model of the power line, such that the computer model could be "run" to predict the RF current flow on the power line and hence the reradiated field. The azimuth pattern of the broadcast array operating in the presence of the power line is thus found, and the "damage" due to reradiation can be assessed. The RF current flow on the power line towers pinpoint those towers primarily responsible for reradiation. In this project, much use has been made of the Numerical Electromagnetics Code(NEC,6) for the analysis of the computer model of the power line, using a large computer such as Concordia University's Cyber 174. The 1985 Final Report, Ref. (5), contains a detailed review of the work done in earlier reports, Refs. (1) to (4), and the following briefly summarizes this review of the overall project.

Early work was concerned with the development of the

computer model of the power line(1,2). This was done in conjunction with a 1 to 600 scale model of the power line, taking measurements over highly conducting ground, for a 13-tower power line illuminated by an omnidirectional antenna tower. All the span lengths of the 13 tower line were the same, hence all had the same resonant frequencies. The power line thus carried very strong RF currents near resonance, and gave rise to a strong reradiated field. The mechanism of "loop resonance" was identified as determining the resonant frequencies of the power line.. The "single wire tower" computer model was developed to have about the same two-wavelength loop resonant frequency as the scale-model measured data, and a similar bandwidth for two-wavelength loop resonance. Near resonance, the towers of the resonant span, and their interconnecting skywire, carry a standing-wave pattern of RF current flow, with sharp nulls separated by half a wavelength. The one-wavelength loop resonance frequency band was investigated, both by scale-model measurement and by computation using the "single-wire" tower model. In addition to single-span resonance modes, additional peaks in the response were associated with resonance modes encompassing two and three spans. The development of the computer model was presented in the "open literature" in Ref. (7).

With a useful computer model established, the project became concerned with "detuning" the power line(2,3,5). Detuning can be accomplished by arranging to introduce a high impedance into the power line span at a low-impedance point in the RF current standing-wave associated with the resonance mode. Thus an insulator can be inserted in series with the skywire at an RF current maximum. Or, a quarter-wave stub terminated in a open circuit, which presents a low input impedance, can be connected to the skywire at a RF current minimum, which is a high-impedance point. A stub can be used on the power line tower to provide a suitable impedance change. These methods were investigated by computation and measurement, and the results were reported in the "open literature" in Ref. (8).

The power lines near station CHFA, Edmonton have provided a case study of the analysis of "real" power lines. Distortion of the CHFA array's directional pattern by the nearby "north" and "southeast" power lines was first studied in 1980 prior to the construction of the power lines(9,10). A "real" power line differs from the 13 tower evenly-spaced power line for which the computer model was developed, because on a real power line the towers are far from evenly-spaced. The "span length" or tower-to-tower distance was shown in Ref. (5) to be comparable to a random variable with a Gaussian distribution, where the standard deviation is typically as large as 10 percent of the mean value. Thus the resonant frequencies of the spans of the power line are widely different, and on a real power line only some spans will be resonant. The problem of assessing the amount of reradiation to be expected from a power line prior to its installation, when the exact locations and span lengths have not

yet been determined, is statistical in nature and was dealt with in Ref. (11), which is summarized in Ref. (5).

In 1983, after the construction of the power lines near CHFA, measurements showed substantial reradiation. The need for a practical, simple, inexpensive detuning scheme became acute. Insulating a tower from the skywire is inexpensive and readily installed on selected towers. By insulating a tower from the overhead skywire, a resonant loop path can be "open-circuited", and this approach was taken. The pitfalls of this technique include the creation of resonant "double-spans", which can be strong reradiators themselves. A systematic approach for selecting towers for isolation from the skywire, called the "suppression of resonances", was developed and presented in Refs. (12) and (13), and subsequently included in the 1985 Final Report, Ref. (5). Insulators were installed on the specified towers on the actual power lines near CHFA, and the tower base currents were measured. In the present report, these measured currents are compared with the computer model's predictions before and after the installation of insulators, both as a verification of the computer calculations and as a proof that detuning by isolating selected towers actually works.

Computer models are only as good as their ability to predict the behaviour of real structures. To verify a computer model of a power line, measurements of RF current flow must be made on a real, full-scale power line. Ontario Hydro undertook the measurement of the RF current flow on a five tower section of power line near Thornhill, Ontario, and their measurements were used in Ref. (14) as a basis for the evaluation of a computer model of a power line. It was found that the computer model was in good agreement near 800 kHz, but was poorer near 1600 kHz. Little investigation of computer modelling above 1000 kHz was done prior to this comparison, and thus the accuracy of the computer models as frequencies as high as 1500 kHz becomes suspect.

In this report, a further comparison of computed results with full-scale measurements is presented, at 680 kHz, based on the measurements taken of the RF current flowing at the base of each power line tower near CHFA, both before and after the isolation of towers from the skywire for "detuning". Chapter 5 shows that the computer model is in good agreement with these measurements and thus provides a good basis both for designing detuning, and for predicting the degree of reduction of RF current flow to be expected.

The bulk of the computations done with power line models in Refs. (1) to (5) have used highly-conducting "perfect" ground, because the method-of-images can be used in the NEC program to substantially reduce the cost of the computation. Nevertheless, the effect on reradiation of the conductivity of ground has been of interest. In Ref. (3), the effect of lossy ground was explored using the Sommerfeld-Norton ground model offered in the

NEC program(15,16). It was shown for a 5 tower power line that the resonant frequencies of the power line are not changed, but that lossy ground "damps" reradiation effects considerably. Silva, Balmain and Ford in Ref. (17) describe the use of Monteath's "footing impedance"(18) to include the effect of lossy ground as a lumped impedance at the base of each tower of a computer model to be analysed over perfectly-conducting ground. This report investigates the behaviour of the "footing impedance" in Chapter 2, and shows that it offers an economical and reasonable approximation of the results obtained with the much more costly Sommerfeld-Norton ground model in the NEC code. Chapter 5 shows that inclusion of ground losses using the "footing impedance" improves the agreement of the computations with full-scale measured values for the CHFA power lines.

Previous investigations in Refs. (2), (3) and (4) of the frequency dependence of reradiation effects have extended in frequency from about 200 to about 1100 kHz. Although the existence at higher frequencies of a "three-wavelength loop resonance" mode and a "four-wavelength loop resonance" mode was recognised, these resonances were not explored extensively with computer models. Some measurements of three- and four-wavelength resonance have been made on the 13-tower, evenly-spaced power line model(19,20), and in this report these measurements have been used to evaluate the performance of various computer models up to 1950 kHz in frequency. In Ref. (4) it was suggested that at higher frequencies, top-loading of the tower by the crossarms has a significant effect on the resonant response of the power line, and it is demonstrated in Chapter 3 that a computer model of the type V1S tower which includes a crossarm is best in matching the measured data a high frequencies.

Balmain and Tilston in Ref. (21) presented a computer program called "AM Power Line" or AMPL which was written in BASIC, and could analyse a broadcast antenna and power line problem such as the CHFA array and the "north" power line on a small computer such as an Apple IIe or Commodore-64. The AMPL program is based on transmission-line theory and uses various approximations to simplify the analysis. AMPL is potentially a very valuable tool for analysing power line reradiation for the broadcasting community. In Ref. (5), a FORTRAN version of AMPL was briefly presented. Because FORTRAN is a "compiled" language, the FORTRAN AMPL program runs much faster than its BASIC sibling, and is readily transported between computers with the FORTRAN-77 language, such as the CYBER-174, the LSI-11/23 and an IBM PC computer. In Ref. (5), the performance of AMPL was not extensively evaluated. In Chapter 4 or this report, the AMPL method is briefly reviewed, and then results predicted by the AMPL program are compared with the measured data for the 600-scale factor, 13-tower, evenly-spaced power line model, and with results obtained with the NEC program using the "single wire tower" representation. It is shown that for the 13-tower power line, AMPL does about as well as the "single-wire tower" NEC model in reproducing the measurements over the frequency range

350 to 1950 kHz. In Chapter 5, AMPL is applied to the CHFA plus north power line problem at 680 kHz, and the AMPL results are shown to be close to those obtained with the NEC program. Thus AMPL provides a quick, inexpensive analysis of power lines with modest computer resources.

In summary, this report extends the computer analysis methods for power lines summarized in Ref. (5) in the following ways. The frequency range of the investigations is extended from about 1000 kHz to about 1950 kHz, and so the user has a clearer idea of the accuracy of the computer models, and of the difficulties to be expected, at these higher frequencies. The modelling of ground losses with "footing impedance" is documented and tested systematically against the Sommerfeld-Norton model in the NEC program. It is demonstrated that the user can incorporate "footing impedance" to include the effect of ground loss, and the user is given a clearer idea of the degree of approximation involved. The computer model is tested against full-scale measured tower base currents for a real site, both before and after "detuning" of the power lines by tower isolation. It is shown that the tower currents both before and after "detuning" are in reasonable agreement with measurements. The computer models can thus be used to assess reradiation and design "detuning" with greater confidence. Finally, the AMPL program is extensively tested against the NEC program, and its performance is well documented.

CHAPTER 2

GROUND CONDUCTIVITY AND FOOTING IMPEDANCE

2.1 Introduction

In Refs. (1) to (5), and much other work on reradiation of AM broadcast signals from power lines, the ground has been assumed to be highly conductive or "perfect", because this assumption allows the NEC computer program to use the "method-of-images" to account for the effect of ground, and the "images" solution is fast and economical. The conductivity σ of "real" ground is typically 5 to 20 millisiemens/metre, with a relative permittivity ϵ_r of 15. The loss tangent of the material is given by

$$\tan \phi = \frac{\sigma}{\omega \epsilon_r \epsilon_o} \qquad \ldots (2.1)$$

where ω is the operating frequency in radians per second, and ϵ_o is the permittivity of free space. If the loss tangent is much greater than unity, then the material is generally considered to be a "good conductor"(22). At 430 kHz, with a conductivity of 5 millisiemens/metre, the ratio is about 14, at 860 kHz, the ratio is about 7, and at 1290 kHz the ratio is 4.6, making the "good conductor" assumption less valid as the frequency increases. Results obtained with the "perfect ground" assumption tend to exaggerate reradiation effects, and make the spans of the power line much "higher Q" resonators than they are when ground losses are accounted for. With "perfect ground" the RF currents on the power line towers are larger and the towers which reradiate are readily identified, but the effect on the radiation pattern is also larger than over "real" ground. The conductivity of the ground has the effect of reducing the broadcast antenna's field strength at the towers of the power line, and also of introducing losses into the skywire-and-image transmission line. These ground losses "damp" the resonance effect and reduce the resonant response. The result is less RF current flow on the power line towers, and hence less reradiation. The NEC program is capable of accurately computing the RF current flow on the power line, and the azimuth pattern, using the Sommerfeld-Norton ground model(15,16,23.24), but at greatly increased cost. Nevertheless, the NEC Sommerfeld ground model is the most accurate currently available. Ref. (3) used the Sommerfeld model to explore the resonant behaviour of a five-tower power line with ground conductivities of 5, 10 and 20 millisiemens/metre and relative permittivity 15, in comparison to

"perfect ground". It was found that ground conductivity has a small effect on the frequencies of resonance of the power line, and that ground losses "damp" the resonance and so the response is considerably less than over perfect ground. Silva, Balmain and Ford(17) have proposed the modelling of the conductivity of the ground as a lumped "footing impedance" to be included in series with the base of each power line tower, in the model of the power line operated over highly-conducting ground. This Chapter discusses the "footing impedance" as a means of including the damping effects of lossy ground in the NEC model, while retaining the efficient "method-of-images" solution. It will be demonstrated in Chapter 5 of this report that when the footing impedance is included in the computation, the RF current flow on the towers of a power line is in quite good agreement with full-scale measured values.

2.2 The Footing Impedance

Silva, Balmain and Ford in Ref. (17) use Monteath's "footing impedance"(18) to include ground loss effects in a power line model which is analysed using NEC and the method-of-images solution. Tilston and Balmain(25) present a method for choosing the radius of the "footing". This section reviews the "footing impedance" concept from Refs. (17), (18) and (25), and presents a formula for its computation.

The "footing impedance" method replaces the "real ground" of a given conductivity and permittivity with a perfectly-conducting ground, and lumps the loss effects of ground into a "footing impedance" to be included at the base of each power line tower. This allows the economical method-of-images solution in NEC to be used, with the base of each tower "loaded" with a "footing impedance" representing ground loss effects. The appropriate value for the footing impedance is calculated based on Monteath's formula(18) obtained using the Compensation Theorem. Using Monteath's approach, each power line tower is considered to have a highly-conducting cylindrical "footing" extending downward to great(infinite) depth into a conducting half-space, representing the ground, as shown in Fig. 2.1. Monteath obtains a formula for the difference between the input impedance Z' of a monopole on a footing in real ground, and the input impedance Z of the same monopole over perfectly conducting ground, as illustrated in Fig. 2.2. By including the "footing impedance"

$$Z_{foot} = Z' - Z \qquad \ldots (2.2)$$

at the base of the monopole-above-perfect-ground, its input impedance becomes equal to that of the monopole above real

ground, as illustrated in part (c) of the Fig. 2.2. The "footing impedance" is readily computed using the formula(18)

$$Z_{foot} = \frac{\eta}{4\pi \sin^2 k_o h}\Big[e^{-j2k_oh}\, Ei\left[-j2k_o(r_o-h)\right] + e^{j2k_oh}\, Ei\left[-j2k_o(r_o+h)\right] - 4\cos k_oh\, e^{-jk_oh}\, Ei\left[-jk_o(r_o-h+a_f)\right] - 4\cos k_oh\, e^{jk_oh}\, Ei\left[-jk_o(r_o+h+a_f)\right] + 4\cos k_oh\, Ei\left[-jk_o(r_o+a_f)\right] + 2\cos^2 k_oh\, Ei\left[-j2k_oa_f\right]\Big] \quad \ldots (2.3)$$

where j stands for the square-root-of-minus-one, k_o is the free-space wave number, and η is the intrinsic impedance of the lossy half space which is the ground. Distance r_o is given by

$$r_o = \sqrt{a_f^2 + h^2}$$

where a_f is the "footing radius", and h is the height of the monopole. The intrinsic impedance of the ground is related to its conductivity and relative permittivity by

$$\eta = \sqrt{\frac{j\omega\mu_o}{\sigma + j\omega\epsilon_r\epsilon_o}}$$

where μ_o is the permeability of free space, σ is the conductivity of the ground, ϵ_r is the relative permittivity of the ground and ϵ_o is the permittivity of free space. The function Ei(-jx) is the exponential integral defined by

$$Ei(-jx) = + \int_{\infty}^{x} \frac{e^{-jt}}{t}\, dt$$

The exponential integral can be rewritten in terms of the cosine integral Ci(x) and the sine integral Si(x) defined by

$$Ci(x) = -\int_x^\infty \frac{\cos t}{t}\, dt$$

$$Si(x) = \int_0^x \frac{\sin t}{t}\, dt$$

in the form

$$Ei(-jx) = Ci(x) + j\left[\frac{\pi}{2} - Si(x)\right]$$

and Ci and Si in turn are readily evaluated using series or polynomial approximations(26,27). Appendix 1 lists a FORTRAN program(26) which is readily used to find values of the "footing impedance" at any frequency. In power line computations it is useful to compute the "footing impedance" as if the tower were h = one-quarter wavelength tall, because at resonance the current distribution near the base of the power line tower is quite similar to that on a quarter-wave monopole. Then the footing impedance formula simplifies to

$$Z_{foot} = -\frac{\eta}{4\pi}\left[Ei\left[-j2k_o\left(r_o - \frac{\lambda}{4}\right)\right] + Ei\left[-j2k_o\left(r_o + \frac{\lambda}{4}\right)\right]\right] \quad \ldots (2.4)$$

Note that in this equation, the conductivity and permittivity of the lossy ground enter into the value of η, the intrinsic impedance of the ground. There remains the problem of choosing a reasonable value for the radius of Monteath's cylindrical footing of Fig. 2.1.

The radius of the cylindrical footing ("footing radius") is derived in Ref. (25) from the geometry of the base of a power line tower, illustrated in Fig. 2.3. The four cylindrical

footings are taken to be a "cage" and an equivalent radius for a single conductor replacing the "cage" is taken from Schelkunoff(28) to be

$$a_f = a_{cage} \left(\frac{na}{a_{cage}} \right)^{1/n} \quad \ldots (2.5)$$

Power line towers have n = 4 corners, and the "cage" radius a_{cage} is the distance from the center of the tower to one of its four corners, and is $a_{cage} = \sqrt{w^2/2}$, where w is the side length of the square base in Fig. 2.3. The radius a is that of the concrete footing which supports each of the four legs of the tower. Later in this Chapter, results obtained with the footing impedance will be compared with those obtained with the Sommerfeld-Norton ground model, using a five-tower "test line" with type V1S towers. V1S towers have n = 4 corners, with a tower base of w = 7.62 m square, and each of the four concrete footings has a radius estimated to be about a = 0.7 m, and so the above formula gives a footing radius of about 4.57 m. For the type Z7S towers used on the power lines near CHFA, Edmonton, the tower base is 7.5 metres square, and estimating the radius of each concrete footing to be 0.7 m, the footing radius is a_f = 4.52 m. The following section demonstrates the behaviour of the "footing impedance" as a function of its radius, of the ground conductivity, and of the frequency.

2.3 Behaviour of the Footing Impedance

In this section, the footing impedance formula, Eqn. 2.4, is evaluated to demonstrate the dependence of the footing impedance on the ground conductivity, footing radius and frequency.

If the footing impedance $Z_{foot} = Z' - Z$ of Eqn. 2.2 is separated into real and imaginary parts according to

$$Z' - Z = R' - R + j(X' - X) \quad \ldots (2.6)$$

then the "footing resistance" R'-R and the footing reactance X'-X can be plotted separately to show their dependence on footing radius, as in Figs. 2.4 and 2.5. The values were obtained by

evaluating Eqn. 2.4, in which the intrinsic impedance of the ground η is the parameter which is dependent on the conductivity of the ground, σ . Fig. 2.4 shows the variation of the footing impedance with footing radius at 420 kHz, and Fig. 2.5 at 840 kHz. Recall from Fig. 2.1 that the footing is a cylinder of high conductivity embedded in the imperfectly conducting ground, and that as the radius of the footing post becomes large, the base of the tower becomes centred in a large area of high conductivity. Hence the footing impedance would be expected to decline to zero with increasing footing radius. This is clearly shown in the figures, where both R'-R and X'-X asymptotically approach zero with increasing footing radius. It is seen that the value of the footing impedance is strongly dependent on radius for footing radii less than about 1 metre, but for the values of 4 to 5 meters found for the type V1S and the type Z7S towers, the footing impedance varies quite slowly with the footing radius. The figures show that the value of both the footing resistance R'-R and the footing reactance X'-X decline with increasing ground conductivity, for conductivities of 5, 10 and 20 millisiemens/m, all for the relative permittivity equal to 15. The value with conductivity 20 mS/m is about half that with conductivity 5 mS/m.

Comparing Figs. 2.4 and 2.5 shows that the footing resistance R'-R is almost the same at 420 and at 840 kHz, but the reactance X'-X tends to decrease to zero more quickly at the higher frequency. Typically, the footing impedance has a value of about 10 ohms resistive and 10 ohms reactive. At 420 kHz the radiation resistance of a 51 m power line tower carrying a resonant standing-wave current distribution is about 15 ohms, and so the footing resistance is comparable to the radiation resistance and will have a large "damping" effect on the magnitude of the resonant response. At 840 kHz, the radiation resistance of the power line tower about 45 ohms and is larger than at 420 kHz because the tower is taller in terms of the wavelength. The resonance mode is already "damped" considerably by radiation resistance, and a further 10 ohms of resistance due to footing impedance will not have a major effect on resonant response. Thus footing impedance is expected to have a major "damping" effect on resonance in the one-wavelength loop resonance frequency range, and a less dramatic effect in the two-wavelength range.

Fig. 2.6 shows the variation of the footing impedance with frequency, for the type V1S tower of footing radius 4.57 m. (Note that the legend in Fig. 2.6 uses "RHO" as a symbol for the footing radius a_f .) It is seen that neither R'-R nor X'-X are strong functions of frequency. In the following section, the behaviour of a power line with frequency is studied, and an individual footing impedance value has been used at each frequency. Fig. 2.6 shows that if working over a narrow frequency range, a mean value might be used for R'-R and X'-X, allowing the "frequency stepping" feature of the NEC code to be used to make the calculation less cumbersome.

Fig. 2.7 shows how the footing impedance varies with the ground conductivity at two frequencies, for a footing radius of 4.57 m. It is seen that for values of ground conductivity less than 5 millisiemens/metre, the footing resistance increases rapidly, and the footing reactance has a local maximum, then decreases rapidly to zero. Evidently the footing impedance is poorly behaved for small ground conductivity. Monteath's method is a perturbation technique and would be expected to be accurate only for "high" ground conductivity.

Thus the footing impedance has values of the same order of magnitude as the radiation resistance of the power line tower, is not a strong function of frequency, and is not strongly dependent on the radius of the footing for values of radius which are typically encountered. The following section compares results obtained using the "footing impedance" to those obtained using NEC's Sommerfeld-Norton ground model.

2.4 Comparison with Sommerfeld-Norton Results

In order to assess the effect that the actual conductivity of the ground has on the resonant behaviour of a power line, Ref. (3) explored the behaviour of the power line configuration of Fig. 2.8 using a version of the Numerical Electromagnetics Code which accounts for the interaction of the power line with ground of a given conductivity and permittivity(15,16,23,24). The solution of Maxwell's Equations for thin wires above a lossy half-space, that is, a ground of given conductivity and permittivity, gives rise to Sommerfeld Integrals for the fields due to the interaction of the wires with the ground. Norton(23) obtained asymptotic expressions for the evaluation of the Sommerfeld Integrals when the distance from the wire to the observation point is large. Banos(24) derived approximations for very close distances. Miller et al.(15,16) have used numerical integration and interpolation to construct an efficient method for approximating the interaction terms for any distance from the radiating wire to the observation point. It should be noted that the Sommerfeld Integral expressions give the exact interaction of each wire of the antenna with the ground. The only approximations introduced into the Numerical Electromagnetics Code are those associated with evaluating the integrals, and the treatment of the junction between a wire and the ground. These approximations are not expected to introduce significant error for the ground parameters discussed above, which result in a "good" ground in all cases. Thus the computation using the Sommerfeld-Norton ground model is the best answer presently available.

Ref. (3) plots the max-to-min ratio of the azimuth pattern of the "omnidirectional" broadcast antenna of Fig. 2.8 operating near the five tower "test power line", as a function of frequency

and ground conductivity. An initial study was carried out to determine empirically whether the footing radius given by Eqn. 2.5 represents a "optimal" value. Thus in Fig. 2.9 the max-to-min ratio of the azimuth pattern for the configuration of Fig. 2.8 is plotted as a function of the footing radius, and the result is compared with the value obtained from the Sommerfeld-Norton solution, at 840 kHz for a conductivity of 5 millisiemens/metre. It is seen that the max-to-min ratio increases as the footing radius is increased, and hence as the "local" ground conductivity at the base of each power line tower is made larger. The "footing impedance" approximation predicts a max-to-min ratio equal to that obtained from the Sommerfled-Norton solution when the footing radius is about 4.7 m, which is close to the value of 4.57 m obtained from Eqn. 2.5. The study was repeated for other ground conductivities at other frequencies, with the general conclusion that Eqn. 2.5 results in a reasonable value for the footing radius.

The usefulness of the "footing impedance" approximation of the effect of lossy ground can be judged relative to the Sommerfeld-Norton ground calculations of Ref. (3). Figs. 2.10 and 2.11 plot the max-to-min ratio of the azimuth pattern of the configuration of Fig. 2.8 throughout the one-wavelength and two-wavelength resonance range of frequencies. Fig. 2.10 compares the results obtained at 420 kHz for highly-conducting "perfect" ground, and for ground conductivities of 5, 10 and 20 millisiemens/metre. In all cases the resonant response including ground losses is much less than it is over "perfect" ground, because, as discussed above, the magnitude of the "footing impedance" is comparable to the radiation resistance of the power line tower at 420 kHz. It is seen that the magnitude of the resonant response rises with increasing ground conductivity, and that the values obtained with the "footing impedance" approximation generally follow those obtained with the Sommerfeld-Norton ground model. There are some differences, particularly at frequencies near the resonance peak at 420 kHz. Thus in parts (b) and (c) of Fig. 2.10, it is seen that the Sommerfeld-Norton model predicts a larger response by as much as 6 dB at resonance. Away from the resonant frequency the footing impedance approximation is excellent.

Fig. 2.11 shows the max-to-min ratio at frequencies near two-wavelength loop resonance, for the three ground conductivities of 5, 10 and 20 millisiemens/metre. In this frequency range, the radiation resistance of the tower is twice the magnitude of the footing impedance, and so the footing impedance does not have as marked an effect as it did at lower frequencies. The value of the resonant response rises somewhat with increasing ground conductivity. The footing impedance approximation is excellent for all three ground conductivities and closely traces out the curve obtained with the Sommerfeld-Norton method.

It is of interest to note that the resonant frequency of the power line is not strongly dependent on the ground conductivity in Figs. 2.10 and 2.11. Thus a downward shift in resonant frequency of perhaps 10 kHz can be noted in Fig. 2.10(b), but this is only a small percentage of the operating frequency of 420 kHz. Similarly a small downward shift in resonant frequency can be seen in Fig. 2.11.

Overall, the footing impedance provides a good approximation to the behaviour of the Sommerfeld-Norton ground model, and is especially good in the two-wavelength loop resonance frequency region. Thus the inclusion of "footing impedance" can reasonably account for the damping of resonance by ground conductivity and for the small shift in resonant frequency due to ground conductivity, at a much smaller cost to the user than is incurred by using the Sommerfeld-Norton ground model.

2.5 Conclusion

This Chapter has shown that the "footing impedance" provides a reasonable approximation to the effect of lossy ground on the resonances of a power line. The "footing impedance" is readily computed using Eqn. 2.5 to estimate the "footing radius", and then using Eqn. 2.4 to evaluate the "footing impedance" itself, with the aid of the FORTRAN program of Appendix 1. Inclusion of the footing impedance at the base of each power line tower allows ground losses to be incorporated into the NEC solution using a perfectly-conducting ground, and the method-of-images, and thus provides a means of accounting for ground losses with little increase in the cost of the computer "run" to analyse the model. This chapter has shown that the "footing impedance" approximation is, in most cases, close to the Sommerfeld-Norton solution, and thus the footing impedance can be used with confidence to model ground loss effects.

CHAPTER THREE

EXTENDED FREQUENCY RANGE

3.1 Introduction

This Chapter studies the behaviour of three power line tower models, using the NEC program, at frequencies up to 1950 kHz. Previous studies(1,2,3,5) have extended to 1100 kHz using as a parameter the max-to-min ratio of a site of the azimuth pattern of an omnidirectional antenna operating near a 13 tower power line with evenly-spaced towers, as shown in Fig. 3.1. The geometrical dimensions are the same as in Fig. 2.8. The behaviour of the "single-wire tower" model was studied with reference to the measurements by Lavrench and Dunn(19,20) on a 600 scale factor model, over highly-conducting ground. This Chapter reviews these results and extends the frequency range of the study. Also, the skywire loop impedance has been studied in Ref. (4) at frequencies up to 1400 kHz, in comparison to measured data by Belrose(29). In that work, it was found that a "tapered" tower model reproduces the measured impedance data much better than the "straight" tower of 3.51 m radius, which has been called the "single wire tower" model. In the "tapered" tower, the radius of the vertical wire representing the power line tower is tapered toward the tower top, to match the silhouette of the actual tower. It was found that the crossarm of the tower has a significant effect on the response of the power line above 1000 kHz. The present Chapter explores the behaviour of the "single wire" tower model, and "tapered" tower model at frequencies up to 1950 kHz.

3.2 Measured Patterns

The present study uses measurements made by Lavrench(30) in 1980 of the radiation pattern of the 13-tower, 600-scale factor power line of Fig. 3.1 between 1100 and 1300 kHz, and between 1550 and 1850 kHz. The objective is to establish the degree of confidence that can be placed in the computer models above 1000 kHz. The 13 tower power line shown in Fig. 3.1 is based on the CBC site at Hornby, Ontario, and has been used extensively in previous studies(1,2,3,4). The model configuration and dimensions are those shown in Fig. 2.8. The power line is straight, has all spans of length 274.32 m, and all towers of height 51 m. The line is illuminated by a omnidirectional

broadcast antenna, being a single tower directly opposite the centre tower of the power line, and 448 m away. The antenna height used here was 195 m below 1050 kHz, 64.77 m between 1050 and 1550 kHz, and 49.53 m above 1550 kHz. These heights were those used to obtain Lavrench's measured data. The measurement setup used 600-scale factor models of Ontario Hydro type V1S towers, but only one skywire was strung at the end of the top crossarm, and not the parallel pair of skywires as is the case on the actual power line. Unfortunately, this introduces an ambiguity in the interpretation of the agreement of computer models. At the time the measurements were made, it was thought that there would be little difference in the azimuth pattern of a power line with one thin skywire at one end of the top crossarm of the tower, compared to the azimuth pattern if both skywires were strung on the towers, one at each end of the top crossarm. Indeed, this was verified with a few patterns near the two-wavelength resonance frequency of 860 kHz. Most of the measurements were then carried out with one thin skywire at one end of the top crossarm. In retrospect, the absence of the pair of skywires may make a difference in the bandwidth of the one- and two-wavelength loop resonance response, and may have a major effect on the resonant frequencies above 1000 kHz, where crossarms make a significant difference. It will be demonstrated later in this chapter that the best agreement with measured results in the high frequency range was obtained with a tapered tower model, explicitly representing the top crossarm, with the skywire connected at the end of the crossarm. Lavrench(30) expresses a doubt about the quality of the data above 1500 kHz.

The max-to-min ratio of the azimuth pattern of the "omni" antenna of Fig. 3.1 operating near the 13 tower power line has customarily been plotted as a function of frequency to investigate the frequency dependence of reradiation from the power line, and Fig. 3.2 shows the behaviour of the measurement model. There are four resonance ranges. From about 400 to about 530 kHz the power line shows "one-wavelength loop resonance", and three distinct resonance peaks are seen. Refs. (3) and (5) discuss the origin of the peaks as follows. The 430 kHz peak is due to resonance of a "single-span" path, in which one wavelength of the RF current distribution "fits" the electrical path length. The 470 kHz peak is due to resonance of a "double-span" path encompassing two adjacent spans, in which two wavelength of RF current standing-wave "fit" a path encompassing two towers, the skywires of two adjacent spans, and their images in ground. The 510 kHz peak arises due to a "triple-span" resonance model covering three adjacent spans. Thus resonant behaviour is quite complex, involving several closely-spaced resonance modes in the "one-wavelength loop resonance" frequency range.

Fig. 3.2 shows "two-wavelength loop resonance" around 860 kHz, with rather incomplete measured data. As discussed in Ref. (5) in conjunction with Table 2.1, "four-wavelength double-span resonance" is expected at about 990 kHz, and so it would be expected that significant response would be seen in the

measurement model to frequencies above 1000 kHz. Indeed where the measured data starts once again, at 1083.33 kHz, a significant max-to-min ratio of 5.83 dB is seen.

The "three-wavelength loop resonance" frequency can be estimated as 1290 kHz, using Eqn. 2.7 in Ref. (5). The measurements show a large response from 1150 to 1300 kHz, with a maximum response at 1258.33 kHz. Thus the simple estimate is not far wrong. It is unfortunate that the measurement was not extended to cover the range from 1300 to 1550 kHz, because multi-span resonances are expected in that range. Thus at 1495 kHz, a "six-wavelength double span" resonance mode is expected. Also, at 1403 kHz an "eight-wavelength triple-span" resonance model is expected.

The "four-wavelength loop resonance" frequency is expected by the "simple" estimate to be 1720 kHz. The measurements show a large response around 1550 kHz, tapering off to a minimum at 1700 kHz, then increasing once again to a peak at 1816.67 kHz. Evidently the "simple" resonant frequency estimate is not useful in this frequency range.

The following sections evaluate three computer models of the type V1S power line tower in comparison to this measured data.

3.3 Single-Wire Tower Model

The "single-wire tower" computer model of the power line tower, shown in Fig. 3.3, was developed in Ref. (1) such that the two-wavelength loop resonance frequency of the computer model agreed with Lavrench's measured data for the configuration of Fig. 3.1. The choice of the wire radii for the "single-wire tower" model was reviewed in detail in Ref. (5). The tower radius in the "single wire tower" model is uniform and equal to 3.51 m. A "fat" single skywire models the pair of skywires on the actual type V1S towers, and has a radius of 0.71 m. Thus the computer model uses a single, fat skywire of radius 0.71 m as an equivalence to the a pair of "thin" skywires present on the real type V1S tower. But the measurement model used only one "thin" skywire at one end of the top crossarm, as discussed above.

The discussion of the "single-wire tower" model and other models will be organized as follows. First, the frequency dependence of the model will be presented, in the format of the max-to-min ratio of the azimuth pattern of the configuration of Fig. 3.1 from 350 to 1950 kHz. Secondly, individual azimuth patterns will be examined at selected frequencies, to illustrate the similarities and differences between the measured behaviour and the "predictions" of the computer model.

3.3.1 Frequency Dependence

The frequency dependence of a computer model of a power line tower has customarily been studied in this project(1,3,4,5) by plotting the max-to-min ratio of the azimuth pattern of the 13-tower power line configuration of Fig. 3.1 as a function of the frequency. Fig. 3.4(a) shows the frequency dependence of the "single-wire tower" model, in comparison to that of the measured patterns. The data from 350 to 1000 kHz is taken from Ref. (3), and the NEC program was run with the "single-wire tower" model from 1000 to 1950 kHz to complete the figure.

The behaviour of the power line is complex in the one wavelength resonance region and is re-plotted in Fig. 3.4(b). The computer model has a broader response than the measurement model and responds strongly starting at about 400 kHz, about 20 kHz lower than the measurement model. Both the computer model and the measurement model show three peaks in this resonance region, and these have been associated with one-span, two-span and three-span resonance modes as discussed above. The term "alignment" will be used to compare the resonant frequencies of the computer model with the measurements. The measurement model clearly shows resonance at about 430 kHz, while the computer model has its strongest response at 413 kHz, giving a "misalignment" of about 20 kHz. It has been remarked in Ref. (2) that the NEC solution for the RF current on the power line in the one-wavelength resonance frequency range is quite unstable, in the sense that the computed currents change considerably if the lengths of the "segments" used in the NEC model are changed. This partially accounts for the ragged behaviour of the NEC solution between 380 and 450 kHz. The instability is due to the fact that the model is analysed over "perfect" highly-conducting ground, and the only energy loss is the rather small radiation resistance of each power line tower. The NEC solution can be stabilized by adding more "damping" or energy loss to the resonant system, for instance by including the "footing impedance" at the base of each power line tower, to model ground losses.

Returning to Fig. 3.4(a), the response of the measurement model is broader than that of the computer model in the "two-wavelength loop resonance" frequency range, although the frequency of the peak is roughly in agreement. In fact the wire radii in the model were chosen to obtain this agreement(1). It is unfortunate that the measurements were not continued above 910 kHz, because the presence of the peak around 950 kHz in the computation cannot be verified from the measurement.

There is considerable disagreement in the frequency of "three-wavelength loop resonance" between the measured data, and the computed behaviour of the "single-wire tower" model. The measurement model shows a large response from about 1200 to about 1300 kHz, and the computer model from 1250 to 1350 kHz, a "misalignment" of about 50 kHz. It will be shown below that this

misalignment can be corrected by including a crossarm at the top of the tower model, and "stringing" the skywire at the end of the crossarm. Also, the bandwidth of the "single-wire tower" model's response is somewhat broader than that of the measurement model.

The computer model does not appear to reproduce the peak in the measured response from 1550 kHz to 1650 kHz, but does agree with the upward trend in the measured data above 1650 kHz. Overall the "single-wire tower" computer model is reasonably satisfactory in the one- and two-wavelength resonance ranges, resonates at too high a frequency in the three-wavelength range and appears to be a poor model above 1500 kHz.

3.3.2 Pattern Comparisons

The max-to-min ratio frequency spectrum of Fig. 3.4 shows certain resonant frequency "misalignments" between the "single-wire tower" computer model and the measurement model. The nature of the differences between the measured and the computed patterns is illustrated in this section. In general, the patterns will be shown to be similar, with differences in detail giving rise to the max-to-min ratio disagreements.

The power line of Fig. 3.1 is taken to be oriented in an east-west sense, with the broadcast tower being north of the centre tower of the power line. In plotting azimuth radiation patterns, such as in Fig. 3.5(a), compass directions have been used to identify azimuth directions. Thus "N" for "north" refers to zero degrees azimuth, for which the field point lies at a distant point on a line from the centre tower of the power line, through the broadcast antenna. "E" for "east" refers to 90 degrees azimuth, etc.

A "standard" set of frequencies was selected for the comparison of the measured patterns with the patterns "predicted" by various computer models. The computer models often resonant at too low a frequency for one- and two-wavelength loop resonance, and so for comparison, a frequency was selected somewhat below resonance, and very close to resonance in the measurement model. These are 400 and 433.33 kHz for "one-wavelength loop resonance", 826.67 and 860 kHz for "two-wavelength loop resonance". The frequency of three-wavelength loop resonance in computer model depends on the handling of the skywire, and 1200, 1258.33 and 1300 kHz were selected for comparison as being below, right on, and above the three-wavelength loop resonant frequency of the measurement model. Finally, frequencies of 1700 and 1816.67 kHz were selected as giving the smallest max-to-min ratio, and a peak in the max-to-min ratio of the high-frequency measured patterns.

Fig. 3.5(a) and (b) compare the computed pattern and the measured pattern at 400 and 433.33 kHz. At 400 kHz the computer model predicts a much deeper null in the pattern than is seen in the measurement model. At 430 kHz, the patterns are quite similar, but the computer model shows a much broader lobe at zero degrees azimuth than is present in the measurement. These patterns indicate that reradiation predictions involving one-wavelength loop resonance must be interpreted with caution.

Fig. 3.6(a) and (b) compare the "single-wire tower" computed pattern with the measurement at 826.67 and 860 kHz. In both cases the patterns are very similar, and show differences only in the small details. The "iron cross" pattern of Fig. 3.6(b) has been presented in several previous reports(1,2,5) and has often been used to illustrate the nature of pattern changes due to reradiation. Recall that in Ref. (1), the "single-wire tower" model was developed to closely match the measured pattern at 860 kHz, and thus the agreement in Fig. 3.6(b) is about as good as can be achieved with the present state-of-the-art in computer modelling.

Fig. 3.7(a), (b) and (c) evaluate the "single-wire tower" computer model in the three-wavelength resonance frequency range. Recall from Fig. 3.4(a) that this computer model clearly resonates at too high a frequency. This is reflected in the 1200 kHz pattern of Fig. 3.7(a), where the measurement shows large excursions at zero degrees, 65 degrees and 295 degrees azimuth, which are not present in the computation. Also, the measurement has minima at 125 and 245 degrees, which are not seen in the computed pattern. At 1258.33 kHz, the measurement model is strongly resonant, and Fig. 3.7(b) shows that the computed and measured patterns are similar, showing peaks and nulls at much the same angular position. The measurement model has considerably deeper nulls, however, hence a larger max-to-min ratio. As most features of the measured pattern are also present in the computed pattern, the "agreement" is quite reasonable. At 1300 kHz, Fig. 3.7(c) shows that the measured and computed patterns are quite similar, displaying remarkably good agreement.

Fig. 3.8(a) and (b) compare the measurement and the computation at 1700 and 1816.67 kHz, respectively. At 1700 kHz, the computer model reproduces many of the features of the measured pattern, with some differences in angular position, such as the lobe near 90 degrees, and some differences in the size of certain features, such as the lobe at 110 degrees. The computer model predicts the size of the reradiation effect quite well at this frequency, but not the fine details of the radiation pattern. Much the same can be said about the pattern comparison at 1816.67 kHz. The size of the reradiation effect is predicted quite well once again. Most of the features of the measured pattern are present in the computation, notably the lobe structure near 90 degrees and 270 degrees. There is some disagreement in angular position of the lobes and minima. There

is detail differences between the two patterns near azimuth 165 and 195 degrees.

In overall summary, the "single-wire tower" model has resonant frequency "misalignment" in the one- and three-wavelength loop resonance frequency ranges, resulting in computed patterns which are similar to the measured patterns but which display differences in the magnitude of the reradiated field, particularly at 400 and 1300 kHz. The model remains a useful indicator of the size of reradiation effects at frequencies as high as 1700 and 1816 kHz.

3.4 Tapered Tower Model

Ref. (4) studied the behaviour of various models of the type V1S power line tower with reference to measurements of the "skywire loop impedance", made using 200-scale factor models of the towers. It was found that the "single-wire tower" fared poorly in reproducing the measured impedance vs. frequency curves, and that the "tapered tower model" of Fig. 3.9 did much better. Without the crossarm at the tower top, the "tapered tower" alone reproduced the measured loop impedance data quite well up to 1000 kHz. If the crossarm was included in the model then the frequency range extended to 1300 kHz or even higher. Note that in this model the "fat" skywire of radius 0.71 m is still intended to be "electrically equivalent" to the pair of skywires used on the actual full-scale type V1S towers. Recall also that the measurement model uses only one "thin" skywire at one end of the top crossarm, and so the comparison of the measured max-to-min ratio frequency dependence with the computed data may amount to comparing "apples" to "oranges" to a certain extent. It might be expected that the "tapered tower" would be better at predicting radiation pattern behaviour, as well as skywire loop impedance. This section investigates whether or not this is so.

3.4.1 Frequency Dependence

The wire radii and crossarm length of the "tapered tower" model of Fig. 3.9 were chosen according to Ref. (4), sections 2.3.2 and 2.4, and optimize the agreement of the predicted "skywire loop impedance" with the measured data. Fig. 3.10(a) and (b) presents the frequency response of the "tapered tower with crossarm" model. Fig. 3.10(b) expands the frequency scale in the one-wavelength loop resonance frequency range and can be compared with Fig. 3.4(b) for the "single wire tower" model. The

tapered tower model's response is not as broad as that of the single wire tower model, and consequently the disagreement with the measurement below 420 kHz is not as severe. There is still a resonant frequency misalignment, but it is only of the order of 5 kHz for the "tapered tower" model. In the two-wavelength loop resonance region, this model has its maximum response at a frequency about 30 kHz lower than the 860 kHz resonance frequency of the measurement model. This is poorer than the "single wire tower" model's behaviour.

The "three-wavelength loop resonance" frequency of the "tapered tower" model is still too high compared with that of the measurement model, the misalignment being about 30 kHz. However, the bandwidth of the three-wavelength resonance response is narrower for the tapered tower than for the single-wire tower, and so is closer to that of the measurement model. The two models exhibit similar behaviour above 1500 kHz and neither is "close" to the measurement. In particular neither model appears to predict the strong peak seen in the measurement at 1570 kHz.

3.4.2 Pattern Comparisons

Fig. 3.11 compares the measured patterns with those of the "tapered tower" model at 400 and 433.33 kHz. In part (a) at 400 kHz, the computed pattern has a minimum at zero degrees azimuth which is much deeper than that of the measured pattern, although not as deep as that of the computed pattern in Fig. 3.5(a). The computed patterns in Fig. 3.5(b) and Fig. 3.11(b) are quite similar. Thus in individual patterns in the one-wavelength resonance frequency range, the "tapered tower" model's patterns are not greatly different from those of the "single-wire tower".

Fig. 3.12 compares the "tapered tower" model's predictions with the measured patterns at 826.67 and 860 kHz. The measured and computed patterns are quite similar at 826.67 kHz in part (a) of the figure. The nulls in the computed pattern are much deeper than those in the measured pattern, giving rise to the larger max-to-min ratio at 826.67 kHz seen in the frequency sweep of Fig. 3.11. The patterns at 860 kHz in Fig. 3.12(b) are also quite similar. The measured pattern has a notably larger lobe at 55 degrees, and a deeper null at 135 degrees than does the computed pattern. The agreement between measurement and computation in Fig. 3.6(b) is better than in Fig. 3.12(b), although in both cases the agreement is good and the computer model is quite a useful representation of the power line.

The "single wire tower" and the "tapered tower" models have much the same defect in the three-wavelength loop resonance frequency range, in that both resonate at too high a frequency,

as can be seen by comparing Figs. 3.4(a) and 3.10(a). Fig. 313(a) compares the "tapered tower" model's azimuth pattern at 1200 kHz with the measurement, and it is seen that the measured pattern has a larger lobe at 65 degrees and a deeper null at 115 degrees. Also, the measured pattern has a lobe at zero degrees and a null at 180 degrees which are not present in the computed pattern. At 1258.33 kHz, in Fig. 3.13(b), the measured pattern and the computed pattern are remarkably similar. There is a difference in detail near zero degrees azimuth. The agreement here is better than that in Fig. 3.7(b) for the "single-wire tower" model. At 1300 kHz, in Fig. 3.13(c), the agreement is also quite good. Thus the computer model clearly remains useful throughout the three-wavelength loop resonance frequency range.

Fig. 3.14(a) compares the measured and computed pattern with the "tapered tower" model at 1700 kHz. Many of the features of the measured pattern are present in the computed pattern, but with some angular shift. The "tapered tower" model does not do much better than did the "single-wire tower" model in Fig. 3.8(a). At 1816.67 kHz, in Fig. 3.14(b), there is once again a good correspondence between lobes in the measured pattern and those in the computed pattern, particularly from 50 to 130 degrees azimuth, but there is some angular shift in the position of these features. The max-to-min ratio in Fig. 3.14(b) corresponds better to that of the measurement than does the max-to-min ratio in Fig. 3.8(b).

The pattern comparisons show that the agreement between the computation and the measurement is no worse in the 1200 to 1300 kHz range than in the 400 to 500 kHz range, and indeed remains useful as high as 1816 kHz. Both the "single-wire tower" model and the "tapered tower" model remain useful throughout the frequency range.

3.5 Skywire at Crossarm End

The measurement model was strung with only one skywire, at the end of the top crossarm, as discussed in Sect. 3.1 above. The computer model would be expected to get the best agreement when the geometrical configuration of the computer model is closest to that of the measurement model. If the skywire were strung at the end of the crossarm, as in Fig. 3.15, and made of "thin" radius, then the computer model more closely duplicates the measurement model than does the computer models of Figs. 3.3 and 3.9. This model will be called the "tapered tower with offset skywire" model, or simply the "offset skywire" model. The length of the top crossarm is 35 feet or 10.7 m, corresponding to the length of the actual crossarm, and the skywire radius was made 0.05 m.

3.5.1 Frequency Dependence

The frequency response of the "offset skywire" model is shown in Fig. 3.16(a) and (b). There is a general downward shift in all resonant frequencies due to the additional path length added to the resonant loop path. Thus the two-wavelength loop resonance frequency now falls at 820 kHz, or 40 kHz lower than the measurement model. The one-wavelength loop resonance frequency is also shifted down to 410 kHz, as shown in Fig. 3.16(b), compared to 430 kHz for the measurement model. The bandwidth of the main resonant peak now agrees quite well with the measurement. Fig. 3.16(a) shows that the frequency of the three-wavelength response is now in reasonable agreement with the measured data. The model now shows peaks at 1560 and 1640 kHz, which is behaviour more nearly resembling the measured data than was seen in either Figs. 3.4(a) or 3.10(a). Thus the "tapered tower with offset skywire" configuration appears to make a significant difference in the response of the model.

3.5.2 Pattern Comparisons

Fig. 3.17(a) shows that the "offset skywire" model predicts a pattern at 400 kHz which is about the same as that of the "single-wire tower" model, in Fig. 3.5(a), and both have a much deeper minimum at zero degrees azimuth than does the measurement. The patterns at 433.33 kHz, in Figs. 3.5(b) and 3.17(b), are also similar, although the "offset skywire" model does significantly worse near 180 degrees azimuth. None of the models presented in this Chapter are very close to the measurements in max-to-min ratio throughout the one-wavelength loop resonance frequency range.

Figs. 3.18(a) and (b) evaluate the model's performance in the two-wavelength loop resonance frequency range. At 826.67 kHz, the "single-wire tower" model in Fig. 3.6(a) agrees best with the measured pattern, while both the "tapered tower" model in Fig. 3.12(a) and the "offset skywire" model in Fig. 3.18(a) resonant at too low a frequency, resulting in nulls in the pattern which are too deep. The agreement at 860 kHz with the "offset skywire" model in Fig. 3.18(b) is somewhat worse than with other models. Nevertheless, the "offset skywire" model is a useful predictor of reradiation effects throughout the two-wavelength resonance frequency range.

Fig. 3.19 shows that the "offset skywire" model does significantly better than the other models in the three-wavelength resonance frequency range. Thus in part(a) of the figure, there is good agreement in pattern features, both in position and magnitude. The narrow lobe at zero degrees azimuth

is present, but the null at 180 degrees is not seen in the computer model. At 1258.33 kHz, in Fig. 3.19(b), the patterns agree well, except for small detail differences near zero degrees, and a small lobe which is present in the measurement at 45 and 315 degrees, but is not seen in the computation. At 1300 kHz, good agreement is also found. The agreement here is every bit as good as that in the "iron cross" of Fig. 3.6(b), which was used in Ref. (1) to establish the validity of the "single-wire tower" model at two-wavelength loop resonance.

Fig. 3.20 tests the "offset skywire" model at the high end of the frequency range. There is no clear cut difference between the computed patterns at 1700 kHz, in Figs. 3.8(a), 3.14(a), and 3.20(a). At resonance at 1816.67 kHz, the "offset skywire" model shows much better angular alignment of the lobes near azimuth 90 degrees than do the models of Figs. 3.8(b) and 3.14(b). The agreement between the measurement and the computation in Fig. 3.20(b) shows that the "offset skywire" computer model remains useful in this frequency range.

The "offset skywire" model thus resembles most closely the actual tower and skywire configuration used for the measurement and is clearly superior in the three- and four-wavelength loop resonance frequency range.

3.6 Conclusion

This chapter has compared the performance of three tower models analysed by the NEC program with measured data. The measurements were made with one skywire strung at the end of the top crossarm of 200-scale factor towers. The actual towers have a parallel pair of skywires. This introduces some uncertainty about the correspondence of the resonant frequencies and bandwidth of the measurement model with the actual type V1S tower. The "single-wire tower" computer model has its skywire configuration based on the presence of the parallel pair of skywires, and thus may not precisely correspond to the single, offset skywire configuration of the measurement model. The "single wire tower" model does well for the low frequency resonances but is resonant at too high a frequency for three-wavelength loop resonance. The "tapered tower" more closely resembles the actual tower geometry but uses the same skywire equivalence as the "single-wire tower", and suffers from the same problem in the three-wavelength loop resonance" frequency range. The "tapered-tower with offset skywire" model most closely resembles the actual tower geometry of the measurement model, and does in resonant frequency and bandwidth in the three-wavelength resonance range, and also does quite well for pattern comparisons up to 1816 kHz. All three models do rather poorly in the one-wavelength resonance frequency range,

especially for the depth of minima in pattern comparisons.

The present study does not unequivocally point to one model as clearly superior over the whole frequency range. In fact, the "tapered tower" does best for one-wavelength loop resonance, the "single wire tower" does best for two-wavelength loop resonance, and the "offset skywire" model is best above 1000 kHz. Evidently, the detail of the model is important in establishing agreement with measurements in a specific frequency range. It is also evident that the crossarms and the offset of the skywire become increasingly important above 1000 kHz. It would be desirable to repeat the measurements using the pair of skywires at all frequencies, and covering the entire frequency range systematically, so that some of the ambiguities of the present study could be removed.

CHAPTER 4

EVALUATION OF THE AMPL PROGRAM

4.1 Introduction

In this chapter Tilston and Balmain's AM Power Line (AMPL,21) is evaluated as a tool for assessing the reradiation from a power line using a small computer such as an IBM-PC. The version of AMPL tested here(31) is a FORTRAN-77 translation of the BASIC program in Ref. (21), and obtains virtually the same results for the configurations tested. This "compiled language" version of AMPL runs for a complex site in less than 10 minutes on an IBM-PC computer, which is much faster than the "interpreted" BASIC-language version. Thus AMPL is potentially a highly practical, inexpensive tool for broadcast consultants to use in assessing reradiation from power lines. In this Chapter, AMPL is evaluated as a tool by comparing its "predictions" with the measurements used in the last chapter to assess the performance of various NEC models, and also by comparing AMPL results with those obtained using the "single wire tower" model and the NEC program. It will be demonstrated that AMPL is a useful tool over a wide frequency range.

The AMPL program determines the RF current flowing on the towers and skywires of the power line by modelling the RF behaviour of the skywires and the towers using transmission-line theory. The skywire and its image in the ground is regarded as a two-wire transmission line, as illustrated in Fig. 4.1. The characteristic impedance Z_{cs} and the propagation constant γ_s are computed to take approximate account of the lossiness of the ground(21,32). The skywire current distribution is given by the standard transmission line formula(22)

$$I_{s,k}(z_k) = I_k^+ e^{-\gamma_s z_{sk}} + I_k^- e^{+\gamma_s z_{sk}} \qquad \ldots(4.1)$$

where z_{sk} is the distance along the skywire on span # k, measured from tower # k, and I_k^+ and I_k^- are the positive-going and the negative-going current travelling-wave amplitudes, respectively. The voltage on the skywire is similarly given by

$$V_{s,k}(z_k) = \frac{I_k^+}{Z_{cs}} e^{-\gamma_s z_{sk}} - \frac{I_k^-}{Z_{cs}} e^{+\gamma_s z_{sk}} \qquad \ldots(4.2)$$

These give rise to the standard transmission line impedance

transformations given, for example, in Ref. (22).

The tower is modelled as a uniform cylinder with no crossarms, as shown in Fig. 3.3, and the AMPL model is thus comparable to the "single wire tower" model discussed in the last Chapter. The tower is regarded as a transmission line above ground, similar in nature to the bicone transmission line discussed in Ref. (33). The bicone geometry has a constant, uniform characteristic impedance and propagation constant, but the cylindrical geometry has characteristic impedance and propagation constant which vary with position above the ground. To keep the method simple, an "average" value for the characteristic impedance Z_{ct} of the tower transmission line, and the propagation constant γ_t have been used, and these values are assumed to be uniform. The propagation constant includes losses due to radiation from the tower. The tower is illuminated uniformly along its length by the electric field of the broadcast array E_a, and the current satisfies the differential equation

$$\frac{d^2 I}{dz^2} - \gamma_t^2 I = \frac{-E_a}{Z_{ct}} \qquad ...(4.3)$$

The current is shown in Ref. (21) to be of the form

$$I_{tk}(z) = A_k + B_k \sinh(\gamma_t z_{tk}) + C_k \cosh(\gamma_t z_{tk}) \qquad ...(4.4)$$

where z_{tk} is the distance along the tower starting at the ground plane, and the constants A_K, B_K, and C_K must be found for each tower, such that the solution, Eqn. 4.4, satisfies appropriate boundary conditions. Thus it is readily shown that

$$A_K = \frac{E_a}{\gamma_t Z_{ct}} \qquad ...(4.5)$$

AMPL accounts for the lossiness of the ground by including the "footing impedance" at the base of each tower, by the method discussed in this report in Chapter 2.

The travelling wave amplitudes on each span and the coefficients A, B and C for each tower are found by enforcing Kirchoff's Laws at the tower-skywire junctions. AMPL uses a method based on superposition which implicitly eliminates the skywire travelling-wave amplitudes and yields a tri-diagonal matrix which is readily solved for the tower current amplitudes. AMPL effectively enforces the following conditions. At the top

of tower # k, KCL is enforced such that

$$I_{s,k-1}(\rho_k) = I_{s,k}(0) + I_{t,k}(h_{t,k}) \quad \ldots(4.6)$$

where the currents are illustrated in Fig. 4.1. Symbol ρ_k is the length of span number k, and $h_{t,k}$ is the height of tower # k. Also, at tower # k, continuity of the skywire voltage is enforced, such that

$$V_{s,k-1}(\rho_k) = V_{s,k}(0) = V_{t,k}(h_{t,k}) \quad \ldots(4.7)$$

Finally, at the base of each power line tower, the current and voltage must satisfy

$$V_{t,k}(0) = -Z_f I_{t,k}(0) \quad \ldots(4.8)$$

Equation 4.5 relates the A_k coefficient on each tower to the applied excitation field E_α. Together, these equations provide enough information to find the values of the travelling-wave current amplitudes on each span and of the coefficients A,B and C on each tower.

The principal assumptions made in AMPL are the following. The results obtainable are inherently limited by the model used for the tower. Thus at best AMPL would reproduce the behaviour of the "single wire tower" model as analysed by the NEC program. Any deviation is likely due to simplifying assumptions made in determining the tower currents in AMPL. The analysis of the tower has been simplified by assuming that it behaves as a uniform transmission line, thus effectively modelling the tower as a bicone transmission line. The characteristic impedance and propagation constant have a major effect on the resonant frequencies predicted by AMPL for the transmission line. Tower-to-tower interactions via the skywire transmission line have been explicitly included, but tower-to-tower interactions due to the electric field radiated from each tower have not been included. Also, each tower is immersed in the electric field which is present across the skywire-and-image transmission line, and the presence of this component of field along the tower wire has been ignored. Also, the far field expressions for the broadcast antenna's field have been used to evaluate the excitation of each power line tower, thus assuming that the transmission line is sufficiently far from the broadcast antenna that "far field" is a reasonable approximation.

In spite of these simplifying assumptions, it will be shown in the following that AMPL generates useful results over a wide

frequency range.

4.2 AMPL vs. Measured Results

This section compares the behaviour of the thirteen tower power line of Fig. 3.1 as predicted by AMPL with the measured behaviour of the power line, using the set of measured data described in Sect. 3.2. The comparison is made at the same set of frequencies used in Chapter 3. For this comparison, AMPL was run with highly-conducting ground, because the measurements were made over a metal ground plane. In the next section of this Chapter, AMPL results will be compared with those obtained with the NEC program.

Fig. 4.2 shows the max-to-min ratio of the azimuth pattern of the omni-antenna plus 13 tower power line configuration, and compares AMPL's results to the measurement. In the one-wavelength resonance frequency range, shown enlarged in Fig. 4.2(b), it is seen that AMPL predicts a series of peaks starting at about 400 kHz and extending to about 440 kHz. The measurement model shows a single resonance peak at about 433 kHz. Thus the "one-wavelength loop resonance" effect predicted by AMPL starts at too low a frequency, and has a much larger bandwidth than that seen in the measurement. AMPL does quite well in predicting the existence of the multi-span resonance at about 475 kHz, although the bandwidth of the effect predicted by AMPL is less that seen in the measurement. The peak at 515 kHz in the measurement appears at about 507 kHz in the AMPL calculation. The magnitude of the response predicted by AMPL is generally quite close to that of the measurement, except from about 380 to 415 kHz.

Fig. 4.2(a) shows the two-wavelength and higher resonances. AMPL shows a large resonance peak at about 823 kHz, compared to the measured maximum response at about 848 kHz. The magnitude of the AMPL response is too large. Thus the two-wavelength resonance response is "misaligned" by about 30 kHz. The three-wavelength resonance response is quite well aligned with the measured response, with AMPL showing a strong peak centred at about 1230 kHz, and the measurement's peak centred at about 1240 kHz. The AMPL response from 1500 kHz onward is not similar to that of the measurement model.

Figs. 4.3 to 4.11 show comparisons of the azimuth pattern predicted by AMPL with that measured on the 600 scale factor model. Fig. 4.3 shows that at 400 kHz, the AMPL pattern has a deep null not seen in the measurement, and this gives rise to the large max-to-min ratio seen in Fig. 4.2(b). Fig. 4.4 shows that at 433 kHz, the AMPL and measured patterns are similar, with the

AMPL pattern showing a broader beam at zero degrees, which is split into two peaks, where the measured pattern shows a narrow beam with only one peak. At 827 kHz in Fig. 4.5 the AMPL and measured patterns are quite similar, but AMPL shows a much higher max-to-min ratio because the AMPL pattern has deeper nulls. At 860 kHz in Fig. 4.6 the AMPL and measured patterns are also similar, with AMPL showing less-deep nulls at this frequency. At 1200, 1258 and 1300 kHz, in Figs. 4.7, 4.8 and 4.9, the AMPL and the measured patterns are very similar. There are some detail differences at 1258 kHz, near zero degrees azimuth, and at 1300 kHz in the ripple structure of the lobes from 5 to 45 degrees and from 130 to 170 degrees. At 1700 kHz, in Fig. 4.10, the AMPL and the measured patterns are similar in some features, such as the structure near 90 degrees azimuth, but differ in some features, such as the large ripples between 0 and 30 degrees. At 1816.67 kHz, in Fig. 4.11, the AMPL and measured patterns are quite similar.

These comparisons lead to the following conclusions. The AMPL program gives a useful, approximate prediction of reradiation from power lines which can be quite good even up to frequencies as high as 1800 kHz, and perhaps higher. However, the resonances of the spans of the power line are somewhat different in the AMPL model than those seen in the measurement model. Thus around 400 kHz, AMPL predicts a response not seen in the measurement, and the two-wavelength loop resonance is misaligned by 30 kHz. The AMPL response in the three-wavelength loop resonance range agrees very well with the measurement. Although the structure of the max-to-min ratio frequency response differs between AMPL and the measurement above 1550 kHz, AMPL can still predict useful pattern approximations in this frequency range. Much the same comments can be made about the "single wire tower" model analysed with the NEC program, and the following section compares AMPL's response with that model.

4.3 AMPL vs. NEC

As discussed above in Sect. 4.1, the model of the tower that AMPL uses is similar to the "single wire tower" model which was discussed in Sect. 3.3. If the method used in AMPL to compute the tower currents included an exact analysis of the cylindrical tower wire, and if all interactions from tower to tower, and from tower to skywire were included in analysis, then the results obtained would be expected to be very close to those found using the NEC program. Because AMPL uses an approximation in modelling the tower wire as a transmission line with uniform parameters, and because AMPL omits some interactions between towers and between the skywires and the towers, the AMPL solution is not exactly the same as that obtained with NEC. This section serves

to document some of these differences for the specific configuration of the "omni" broadcast tower and the 13 tower power line of Fig. 3.1, by comparing the results obtained with NEC and the "single wire tower" model, presented in Sect. 3.3, with those obtained with AMPL. The ground is highly-conducting.

Fig. 4.12 compares the max-to-min ratio frequency response of AMPL with that of the NEC "single-wire tower model". Fig. 4.12(b) compares the two models in the one-wavelength loop resonance frequency range. The large peak present in the AMPL result at 400 kHz is not reproduced in the NEC calculation, although there is a minor peak on the shoulder of the NEC response near 400 kHz. The NEC model has the sharp peaks seen in the AMPL model at 413 and 425 kHz, but lacks the peak at 440, instead declining more gradually to the minimum at about 460 kHz. The NEC and AMPL models agree quite well in the multi-span resonance mode peaks at 470 and 510 kHz. In Fig. 4.12(a), it is seen that the NEC model and the AMPL model differ increasingly as the frequency goes up. In the two-wavelength loop resonance frequency range, the AMPL model has a much larger response than the NEC model, and the peak in the AMPL model's response, at about 823 kHz, is a lower frequency than that of the NEC model at 850 kHz. There are some sharp peaks in the AMPL response between 1000 and 1100 kHz which are not seen in the NEC response. In the three-wavelength loop resonance frequency range, the NEC model has its maximum response at 1320 kHz, compared to AMPL's maximum centred at about 1230 kHz. There is little resemblance between the AMPL and the NEC max-to-min ratio above 1500 kHz.

Figs. 4.13 through 4.21 compare the azimuth patterns and the power line tower currents between the AMPL solution and the NEC solution. Fig. 4.13(a), at 400 kHz, shows that the azimuth patterns are very similar, although the AMPL pattern has a much larger max-to-min ratio due to a deeper null at zero degrees. Part (b) plots the magnitude of the tower current against the tower number, where the numbers are given in Fig. 3.1. It is seen that the AMPL model predicts 20 percent stronger currents on most towers. Part (c) shows excellent agreement in the phase of the tower currents. Fig. 4.14(a) compares the AMPL and NEC azimuth patterns at 433 kHz, and shows excellent agreement at this "one-wavelength loop resonance" frequency. Parts (b) and (c) show a close correspondence of the tower current magnitudes and phases, with a small difference showing on the centre tower of the power line. Fig. 4.15(a) shows some differences between the AMPL azimuth pattern and the NEC pattern at 860 kHz, particularly in the depth of the nulls and the size and angular position of the lobes near azimuth 50 degrees. Part (b) shows that the tower current distribution is somewhat different, with stronger currents on the centre towers and end towers in the AMPL model. Part (c) shows that there is about 30 degrees difference in phase between the AMPL and the NEC tower currents. Incidentally, it may appear that there are large phase

differences for towers number 5, 7, and 9, but note that the phase is plotted from -180 to 180 degrees, and that the difference between -155 degrees and plus 175 degrees is actually only 30 degrees. Fig. 4.16(a) compares the azimuth patterns at 860 kHz, and shows that they are very similar, but that there are structure differences in the nulls. Part (b) shows a similar distribution in the tower current magnitudes, with stronger currents on the end towers in the AMPL model, and on the centre towers in the NEC model. The phase difference is about 15 degrees between the two models. Fig. 4.17(a) compares the azimuth patterns at 1200 kHz, and shows that a marked difference exists, with much larger lobes in the AMPL model at zero and 63 degrees azimuth, and a much deeper null at 115 degrees. Recall that the AMPL model agrees better with the measurement in this frequency range. Part (b) shows much stronger currents flowing on the power line towers in the AMPL model, and part (c) shows a considerable phase difference, amounting to about 40 degrees. Fig. 4.18(a) shows better agreement at 1258 kHz, although the null in the AMPL pattern at 55 degrees is not seen in the NEC calculation. Part (b) shows similar current magnitudes but the currents are distributed differently among the towers in the two models. Part (b) looks alarming but amounts to a phase difference of about 50 degrees between the two models. Fig. 4.19(a) shows similar azimuth patterns at 1300 kHz, with deeper nulls in the NEC pattern, giving rise to the larger max-to-min ratio for the NEC model at this frequency. Part (b) shows a large difference in the current magnitude on the centre tower and a generally different distribution, but with similar overall magnitudes. Part (c) shows a somewhat different phase distribution.

In the four-wavelength loop resonance frequency range, the AMPL and the NEC models show considerably different max-to-min ratio frequency responses, and this is reflected in the azimuth patterns. At 1700 kHz, the patterns show detail differences, with the large ripples between 10 and 25 degrees in the AMPL pattern being absent in the NEC pattern. The magnitude current distribution is now quite different between the two models, with the AMPL model having much larger current flow on the end towers on the power line, and the NEC model not showing the near zero current flow on towers number 5 and 9, as predicted by the AMPL model. Part (c) shows a systematic 80 degree phase shift between the two models. Fig. 4.21(a) compares the azimuth patterns at 1816.67 kHz, and once again there are many differences in detail between the two patterns. This is due to a quite different RF current distribution on the towers, and shown in part (b) of the figure. Thus the AMPL model predicts a much larger current flow on the centre tower, and much smaller currents on the end towers. There are large phase differences, as well.

Overall conclusions can be based on the max-to-min ratio frequency response graph of Fig. 4.12. The NEC model does somewhat better below 413 kHz than does the AMPL model. The NEC model has somewhat too large a max-to-min ratio below 413 kHz,

and the AMPL model has much too large tower currents. The models are comparable in performance for the rest of the one-wavelength resonance region. The AMPL model presents too-strong a resonant response at too-low a frequency in the two-wavelength resonance range. The AMPL model does much better than the NEC model in the three-wavelength loop resonance range, in comparison to the measurements, but bear in mind the discussion of Sect. 3.2, which casts some doubt on the details of the measurement model and hence makes a firm conclusion in this frequency range difficult. If the "single-wire tower model" were being analysed with perfect accuracy by NEC, and if the AMPL solution were also perfectly precise, then the two would be expected to agree at all frequencies. It would be expected that the NEC solution is the more accurate since it accounts for all interactions present between the towers and skywires of the power line. Finally, the AMPL and NEC models disagree throughout the four-wavelength frequency range and neither is in good agreement with the measurement.

4.4 Conclusion

The user of any computer model of a power line should bear in mind the following. The main usefulness of such computer models is in identifying those spans of the power line which are resonant. It is thus desirable that the computer model not "miss" resonant spans. In the one-wavelength resonance range, the AMPL model will tend to identify more spans as resonant than there are on the real power line, because the AMPL bandwidth extends about 30 kHz lower in frequency in Fig. 4.2(b) than does the measured response. Still, the AMPL bandwidth encompasses all of the measured response. The NEC "single-wire tower" model will also encompasses the full frequency range of one-wavelength resonance. Thus the error is conservative. Fig. 4.2(a) indicates that in the two-wavelength resonance range, the AMPL model will tend to have more spans resonant than does the actual power line, and that those spans most strongly resonant in AMPL may not be most strongly resonant on the measurement model. The error is still conservative.

In the three wavelength loop resonance frequency range, neither the AMPL model nor the NEC model can be used with perfect confidence. Although it appears in Fig. 4.2(a) that the AMPL model agrees well with the measurements in this frequency range, there is doubt about the details of the actual measurement model. Thus the scale model may have been different in this frequency range if it had been strung with two instead of one skywire. The computer model in this frequency range may identify some spans as being not resonant which will actually show a significant resonant response. The computer model must then be used with caution.

In the four-wavelength range the predictions of these models must be regarded with considerable skepticism. The comparison of individual radiation patterns with the measured patterns at 1700 and 1826.67 kHz show that AMPL can still generate useful results at these high frequencies. However, the user should be aware that the computer model may not "predict" enough current on the towers at some frequencies.

The following chapter deals with the use of computer models on a real site, that of the CHFA antenna at 680 kHz, and the nearby "north" power line. The results obtained with the NEC and the AMPL computer models will be compared.

CHAPTER 5

Computations vs. Measurements for the CHFA Site

5.1 Introduction

In this Chapter, computer modelling techniques are applied to analysing a real situation, namely that of the CHFA broadcast array, and the "north" power line. In Ref. (5), the CHFA site was discussed and analysed extensively. The results presented here extend that work to include the modelling of the conductivity and permittivity of the ground using the "footing impedance", as discussed above in Chapter 2. Also, a comparison is made between the calculated tower base currents and full scale measured values, providing an important corroboration of the calculations with full-scale data. This comparison is done with all power line towers connected to the skywire, and with some tower isolated to "detune" the power line. Finally, the AMPL program is used to analyse the "north" power line, and the results are compared with those of the NEC program. This evaluation tests AMPL in the context of a realistic, complex site.

Chapter 2 in Ref. (5) presents a detailed summary of the resonant behaviour of power lines, and in subsequent Chapters, gives a comprehensive analysis of the "north" and "southeast" power lines near the CHFA antenna. Station CHFA has a three tower broadcast array operating at 680 kHz with the azimuth pattern shown in Fig. 5.1(a). The maximum field strength is 960 mV/m at about 10 degrees azimuth, and the R.M.S. field strength is 590 mV/m. Fig. 5.1(b) plots the "far field" strength of the antenna scaled to a distance of 1 mile from the array. The station must maintain a "protection requirement" from 168 to 236 degrees azimuth, and the antenna's field strength is about 12 mV/m over this "protected arc". The pattern is about 10 mV/m below the protection limit, and any reradiation from the power line in excess of 10 mV/m may cause the protection limit to be exceeded. The power lines near CHFA are shown in Fig. 5.2. It is seen that the "north" line passes within 3500 m of the CHFA array, and is illuminated with a field strength of 440 mV/m at that point. The computer model used to analyse the power lines with NEC is described in Sect. 3.7 of Ref. (5), with Fig. 3.7 giving the geometry of the power line tower.

Chapter 3 of Ref. (5) contrasts the behaviour of real power line sites, in which the length of each span is different from the length of any other span, with uniformly-spaced power line models, such as that discussed above, in which all spans have the same resonant frequencies. Thus Fig. 4.4 of Ref. (5) shows the

span lengths on the "as-built" north line, and these are readily used to estimate the resonant frequencies of the spans, using Eqn. 2.7 of Ref. (5). The resulting set of resonant frequencies is shown in Fig. 5.3 of the present report, and was shown in the "resonance chart" of Fig. 5.2 of Ref. (5). The RF current flowing on the towers of the "north" line, with high ground conductivity, were computed in Chapter 4 of Ref. (5), and presented in Fig. 4.7. Fig. 5.4 of the present report repeats this data in schematic form. A comparison of Figs. 5.3 and 5.4 shows that spans of the power line with resonant frequencies within about 50 or 60 kHz of CHFA's operating frequency of 680 kHz can be excited strongly and can carry very strong RF current flow. Also, spans adjacent to resonant spans can couple and carry strong RF currents. The principal conclusion is that on a real site with many different span lengths, it is essential to identify those specific spans which are of resonant length at the operating frequency. Thus the computer method used to analyse the site must be capable of accurately assessing the resonant behaviour of individual spans.

Reference (5) in Chapter 5 contains a detailed description of a procedure for "detuning" the power lines near CHFA, by the method of "suppression of resonances". In this technique, individual towers are selected for isolation from the skywire, such that any span which is resonant is "open circuited". The creation of resonant double- or triple-spans must be avoided. It is shown that by isolating towers 150, 153, 158, 161, 165, 167, 168, 174, 176, 178, 182 and 184, the "north" line can be effectively detuned, and the resulting azimuth pattern and RF current flow is shown in Fig. 5.6 of Ref. (5), which is reproduced schematically in Fig. 5.5. In comparison to the "all-towers-connected" current in Fig. 5.4, the "selected towers isolated" current of Fig. 5.5 shows that a large reduction in RF current flow has been achieved. These results are recomputed in the following, using the tower footing impedance to account for the effects of ground conductivity. The resulting power line tower base currents are compared with full-scale measured values.

5.2 North Line with All Towers Connected

This section presents the azimuth pattern of the CHFA antenna operating near the "north" power line, and compares the RF current flow at the power line tower bases with full-scale measured values. The calculation takes into account the ground conductivity by including the "footing impedance" described in Chapter 2.

The conductivity of the ground has the effect of reducing the broadcast antenna's field strength at the towers of the

power line, and also of introducing losses into the skywire-and-image transmission line, and so results in less RF current flow on the power line towers, and hence less reradiation when ground conductivity is included in the computer model. The value of the footing impedance is calculated using Eqn. 2.4, which calls for a footing radius a to be derived from the tower geometry using Eqn. 2.5. For the present purpose, each of the n = 4 corners of the power line tower is supported by a reinforced-concrete footing of radius a = 0.7 meter(estimated). The "cage" radius a_{cage} is the distance from the center of the tower to one of its four corners, and is $a_{cage} = \sqrt{w^2/2}$, where w = 7.5 meters is the side length of the square base, giving a_{cage} = 5.3033 m. Thus the footing radius is a_f = 4.52 m. With this value, Eqn. 2.4 obtains the footing impedances given in Table 5.1 for ground conductivities of 5, 10 and 20 millisiemens/metre. In the following, results will be shown for these three ground conductivities, incorporated into the model by including the footing impedance at the base of each power line tower.

TABLE 5.1

Footing impedance values at 680 kHz, with footing radius 4.52 m, for three ground conductivities. The relative permittivity of the ground is taken to be 15.

Ground Conductivity millisiemens/metre	Footing Impedance Ohms	
	Real	Imaginary
5	13.41	5.98
10	9.38	4.50
20	6.59	3.28

The NEC model of the power line used in Ref. (5) was altered by loading the base of each of the power line towers with the "footing impedance". Fig. 5.6(a) compares the azimuth pattern computed with "perfect" or highly-conducting ground to the azimuth patterns found with ground conductivities of 5, 10 and 20 millisiemens/metre. It is seen that as the conductivity is reduced, the null-filling reradiated field is also reduced in strength. Thus at azimuth 215 degrees, the field strength with perfect ground is 116.5 mV/m at one mile, and is reduced to 91.3 for ground conductivity 20 mS/m, 83.1 for 10 mS/m, and 74.1 for 5 mS/m. Fig. 5.6(b) compares the power line tower base currents for perfect ground with those computed including the footing

impedance. It is seen that the tower base currents also decrease with decreasing ground conductivity. Thus for perfect ground conductivity, the maximum current on tower number 168 is 86.2 mA relative to 1 amp on the centre tower of CHFA. But the current decreases to 56.0 mA for ground conductivity 20 mS/m, 47.4 mA for conductivity 10 mS/m, and to 38.6 mS/m for ground conductivity 5 mS/m. Thus both the current flow on the power line towers, and the reradiated field strength, decrease with decreasing ground conductivity.

Fig. 5.7 compares full-scale measured data with the computations. Fig. 5.7(a) shows the measured field strength(34) for the actual CHFA array operating in the presence of both the "north" and the "southeast" power lines of Fig. 5.2. Computations in Ref.(5) show that the reradiation effect is primarily due to the "north" line. Comparing the measured values with those computed with the "north" line alone shows that for ground conductivity 20mS/m there is reasonable agreement. The RF currents flowing on the power line towers can be measured either using a "toroid" probe, described in Ref. (14), or by using a pair of loop antennas, as in Ref. (35). Fig. 5.7(b) is a comparison of the measured tower base currents from Ref. (35) with the computed values for the three ground conductivities of 5, 10 and 20 ms/m. The currents in Fig. 5.7(b) have been scaled relative to a current of 1 amp on the centre tower of the CHFA array. It is seen that towers 165, 166, 167, and 168 carry substantial current flow, and the computed RF current values agree well for a ground conductivity of 5 ms/m. Note that the closest towers to the broadcast antenna, towers 170 to 172 in Fig. 5.2, do not carry the largest RF current flow. The measurements were made with both the "north" and the "southeast" lines in place, whereas the calculation in Fig. 5.7(b) includes only the "north" line. The "southeast" line is expected to have the strongest effect on the current flow on the "north" line where the two lines are parallel, from tower 174 on the "north" line to higher numbered towers. This may account for some of the disagreement in Fig. 5.7(b) between the measurement and the computation on towers 174, 176, 177 and 178.

The measurements in both Figs. 5.7(a) and 5.7(b) were taken in June, 1984, and no explanation is readily apparent for the difference in the conductivity value needed for the computed pattern to agree with the measurement, and for the computed tower base currents to agree. The differences between the computed and measured currents on towers 174 through 179 may be due to the presence of the "southeast" power line, which runs closely parallel near these towers, as seen in Fig. 5.2. This is discussed more fully in Ref. (5). Figs. 5.7(a) and 5.7(b) together show that the computer model predicts both the azimuth pattern and the RF current flow on the power line towers with reasonable precision, although the computation should evidently be repeated for a range of representative ground conductivities.

5.3 North Line with Towers Isolated from the Skywire

Ref. (5) discusses the method of "suppression of the resonances" for choosing towers for isolation from the power line in order to detune the power line. For the "north line", Ref. (5) recommends isolating towers number 184, 182, 178, 176, 174, 168, 167, 165, 161, 158, 153 and 151, and Figs. 5.4 and 5.5 can be compared to see the reduction in tower and skywire current flow which is obtained by isolating this set of towers from the overhead skywire, when the computation is done using "perfect" ground conductivity. The calculation was repeated using the "footing impedance" to account for the effect of ground conductivity, to obtain the azimuth pattern shown in Fig. 5.8(a). A very substantial reduction in the reradiated field has been achieved by isolating the selected set of towers from the skywire, and there is only one small excursion over the protection limit. It is interesting to note that the "detuned" pattern is independent of the ground conductivity, because the RF impedance seen at the base of each power line tower which is part of a non-resonant structure is quite large in comparison to the values of a few ohms for the "footing impedance" representing the effect of ground losses. Hence a change of a few ohms in the footing impedance makes little difference in the azimuth pattern for a non-resonant structure. It is only when the span is resonant that the "footing impedance" makes a significant difference in the response of the span.

Prior to the isolation of towers from the skywire on the real power lines, the RF current flowing at the base of each power line tower was measured, with the result presented above in Fig. 5.7(b). The specified set of towers were then isolated, and the currents on the isolated towers and their neighbours were again measured(36), with the result shown in Fig. 5.8(b). A substantial reduction in the measured tower base currents has been achieved by isolation of the set of towers specified by the method of "suppression of resonances". The figure shows that the computer model predicts the reduction in tower base currents quite accurately, because the level of the measured tower base currents is quite similar to that of the computed currents. Note that the value of the RF current is substantially independent of the ground conductivity for the detuned, non-resonant power line.

This section has shown that the predictions of the NEC computer model of the RF current flow at the tower bases of the power line when selected towers on the power line are isolated from the skywire are substantially in agreement with full scale measurements on the "north" line near CHFA. Thus computer modelling can be used with some confidence to select towers for isolation and subsequently predict the reduction in tower base current to be expected on the actual power line.

5.4 AMPL for the CHFA Site

In this section, the AMPL program is used to find the azimuth pattern and tower currents for the CHFA array operating near the north power line. AMPL was discussed in Chapter 4, and was tested for a 13 tower power line with a uniform span length. This section provides an evaluation of AMPL for a "realistic" site, in which the span length is non-uniform, and so some of the spans are resonant but most are not. Since AMPL can be "run" on a small computer, it is an attractive tool for such reradiation problems. it should be noted that the input data for AMPL is much the same as that required to for a power line model to be analysed with the NEC program. That is, the coordinates of the base of each power line tower relative to the "reference" tower of the broadcast array must be known to high precision. Deriving this data from the engineering drawings for the power line and from maps is a tedious, time-consuming task, and is the substantial cost factor in computer-modelling a power line. This section compares AMPL's results with those obtained with the NEC program for the specific case of the CHFA site with the "north line", at one frequency. Also, results obtained by modelling ground conductivity with footing impedance in the AMPL program are compared with NEC's results using footing impedance.

5.4.1 Matching the Array Pattern

In order to allow the simplest possible comparison of the AMPL and the NEC azimuth patterns and power line tower currents, it is desirable that the azimuth pattern for the CHFA antenna alone be identical for the two programs. In AMPL, the broadcast towers carry ideal sinusoidal current distributions, of the form

$$I(z) = I_o \sin(\beta (h - z)) \qquad ...(5.1)$$

The tower base currents are given by

$$I(0) = I_o \sin(\beta h) \qquad ...(5.2)$$

and are specified in the AMPL input to obtain the desired azimuth pattern from the antenna array. In the NEC program, the tower base voltages must be specified, and the program computes a matrix which is solved for the current distribution on the array towers, and hence the tower base currents. Thus the difficulty in using NEC to model broadcast antennas has been that of finding the required tower base voltages such that the array produces the "design" azimuth pattern. In Ref. (9) this problem

was solved in an approximate way, such that the NEC program produced a pattern very similar to the design pattern. All of the work reported in Ref. (5) and earlier documents uses this approximate representation of the CHFA array in analysis with the NEC program. In the following, a much more precise correspondence between the NEC and the AMPL azimuth patterns for the CHFA array is established, in order to simplify the comparison of the NEC and AMPL results with the "north" power line in place.

In order to provide a straightforward comparison between AMPL results and NEC results, it was desired to adjust the tower base currents used in AMPL such that the antenna-alone pattern from the AMPL program would be identical with that produced by the NEC program. The following provides a straightforward procedure. In the azimuth plane, the field radiated by a vertical antenna tower is proportional to the "current-moment" of the tower, defined as

$$I_m = \int_0^h I(z)\, dz \qquad \ldots(5.3)$$

where h is the height of the tower, and I(z) is the complex current flowing on the tower. In AMPL, the current on a tower is given by Eqn. 5.1 above, where I_o is the "complex amplitude" of the current flowing on the tower. Inserting Eqn. 5.1 into Eqn. 5.3 and integrating obtains the current-moment of the tower for AMPL which is

$$I_m^{AMPL} = \frac{I_o}{\beta}\left(1 - \cos(\beta h)\right) \qquad \ldots(5.4)$$

If the current-moment of each tower in the AMPL model is made the same as the current-moment of each tower in the NEC model, then the azimuth patterns will be identical. To find the current moment of a tower in the NEC program, the data reported in the NEC output file can be used. NEC reports the current at the centre of each "segment" used to model the tower. If Δ is the length of each "segment" on the antenna tower, then the current-moment of the tower is approximately

$$I_m^{NEC} = \Delta \sum_{k=1}^{N} I_k \qquad \ldots(5.5)$$

where N is the number of segments on the tower. Eqn. 5.5 is a

rectangular-rule approximate integration of Eqn. 5.3, using the data NEC provides at evenly-spaced points on the antenna tower. Other, more accurate numerical integrations can be devised, and a Simpson's Rule(37) method was used for the present purpose. To make the current-moment on a sinusoidal tower equal to that on the same tower in the NEC result, choose

$$I_o = \frac{\beta\, I_m^{NEC}}{(1 - \cos(\beta h))} \qquad ...(5.6)$$

With this choice of sinusoidal current amplitudes for AMPL, the CHFA array's pattern computed by AMPL is identical to that computed by the NEC program, and so a straightforward comparison of AMPL's array-plus-power-line pattern with that from NEC is possible.

The method of equating "current-moments" described above can be worked in the reverse direction, to allow the tower base voltages required for input to NEC to be found, such that the NEC computation of the azimuth pattern for the antenna array will be identical to the "design" pattern, which is specified in terms of sinusoidal current distributions on the antenna towers. This method is far superior to the use of the array's mutual impedance matrix for finding the tower base voltages. The reason lies in that the current distribution computed by NEC for each tower of the array differs substantially from a sinusoidal distribution. Hence the tower base currents, related to the base voltages by the mutual impedances, can be substantially different in phase from the "loop current" at the current-maximum part way up the tower(for towers taller than a quarter-wavelength). The method is fully described in Ref. (38), where it has been used to derive tower base voltages for NEC to model a six-tower directional array, such that NEC's azimuth pattern is exactly the same as the "design" azimuth pattern.

5.4.2 AMPL vs. NEC for CHFA

With the sinusoidal current amplitudes for the AMPL program chosen so that the azimuth pattern of the CHFA array computed by AMPL is identical to that computed by NEC, the results for the CHFA array operating near the "north" power line can be compared between the two programs. With a highly-conducting "perfect" ground plane, Fig. 5.9(a) compares the azimuth patterns in the region of CHFA's restricted arc. Perfect ground tends to exaggerate reradiation effects and is quite useful in pinpointing resonant spans on a power line. Comparing the two patterns in

Fig. 5.9(a) shows that they are very similar. In general the AMPL peaks are coincident in angular location with those predicted by the NEC program, but AMPL's peaks are smaller than NEC's, the difference being about 10 to 20 percent. The RF current flow at the base of the power line towers is compared in Fig. 5.9(b). AMPL's current on the strongly-resonant span, towers 167 and 168, is about 10 percent less than that predicted by NEC. The reason for this difference is associated with the precise resonant frequency "predicted" for a span by AMPL and by NEC. This span is near two-wavelength loop resonance. Fig. 4.12(a) shows that the AMPL resonant response and the NEC resonant response for two-wavelength loop resonance are not well in agreement. Evidently, in the NEC model, span 167-168 is closer to resonance and has a larger response. For later reference, note that the current on towers 173 to 176 is almost the same in the two models. Overall, the comparison between AMPL and NEC for perfect ground shows good agreement, and at this frequency AMPL provides an excellent tool for assessing power line reradiation.

Figs. 5.10 and 5.11 compare AMPL and NEC results when the "footing impedance" is incorporated at the base of each power line tower to model the effect of lossy ground. Fig. 5.10(a) shows that the both programs predict a "damping" or reduction of the reradiation from the power line when the ground is lossy, in this case with a conductivity of 20 millisiemens per metre, and a relative permittivity of 15. The height of the reradiation peaks predicted by AMPL is somewhat less than that predicted by NEC, as before. Fig. 5.10(b) compares the tower current magnitudes, and shows that the reduction in the tower currents from those of Fig. 5.9(b) is similar for all towers. It is interesting to note that the footing impedance has caused a disagreement in the current flow on towers 174 and 176 between the two programs, whereas for perfect ground there is agreement. For ground conductivity 5 millisiemens per metre, Fig. 5.11 compares the azimuth pattern and the tower currents. Once again, a reduction in ground conductivity leads to a damping of the reradiation effect, and the current on most towers is reduced by about the same factor from the "perfect" ground case of Fig. 5.9, for both AMPL and NEC. The disagreement for towers 174 and 176 is now more pronounced than in Fig. 5.10(b).

This section has demonstrated that at 680 kHz, for a "realistic" power line configuration with variable span length along the line, the AMPL program running on a small computer generates results which are in very good agreement with the NEC program running on a Cyber 174. Thus AMPL provides a useful, inexpensive tool which can be used to assess power line reradiation problems.

5.5 Conclusions

This Chapter has applied computer modelling to a "realistic" site, in which a directional array at 680 kHz operates near a power line with a realistic route and with a non-uniform span length. Results of a computer model of the power line, using the simple "single-wire" power line tower model analysed with the NEC computer program, have been compared with full-scale measurements. It has been shown that there is a good correlation between the calculated current flow on the towers of the power line, and the actual currents measured on the real power line. Towers "predicted" to carry strong currents are actually found to be those with strong currents. It was noted above that the computed currents differ from the measured for towers where the "southeast" line closely parallels the "north". The "southeast" line was not included in the computer model. If the computation includes the effect of ground loss by incorporating the "footing impedance" discussed in Chapter 2, then the strength of the RF current flow is in reasonable agreement with the measurement. However, in the absence of a direct measurement of the actual ground conductivity, it is recommended that the computer model be "run" for a typical "low" conductivity value for the area, and also for a typical "high" conductivity. The expected current magnitudes will likely lie somewhere in between these extremes. It was also shown in this Chapter that the predicted level of the azimuth field strength is in agreement with the full-scale measured value, although the pattern was not measured at points sufficiently closely spaced in angle for a detailed comparison of the fine lobe structure.

It was shown in Ref. (5) that the power line could be "detuned" by isolating some of the towers from the skywire, provided that these towers are chosen judiciously. The specified set of towers was isolated on the "north" line near the CHFA antenna, and the tower base currents were measured. This Chapter demonstrated that the level of the measured "detuned" currents is in good agreement with the level predicted by the NEC program, and hence the reduction in the power line tower currents predicted by the computer modelling technique is actually achieved on the real power line.

This Chapter compared the results obtained with the AMPL program with the azimuth pattern and power line tower currents obtained with the NEC program, at one frequency for the "realistic" CHFA and "north" line site. It was shown that AMPL and NEC agree quite well and that AMPL is certainly a useful tool for predicting power line reradiation at this frequency. There is some difference in the magnitude of the response predicted by the two programs, and some of this disagreement is attributable to the "misalignment" of the resonant frequencies of the power lines, as discussed in Chapter 4.

CHAPTER 6

CONCLUSIONS

The present report, taken together with the 1985 Final Report(5), provide a detailed guide to computer modelling power lines, to the use of a computer model in the assessment of the reradiation likely from a proposed power line, to the evaluation of reradiation from an existing power line, and to the detuning of a power line by isolating towers from the overhead skywire. The present report has extended the technique in various ways. The frequency range has been extended by investigating the behaviour of various computer models of power line towers up to 1950 kHz. The modelling of the conductivity of ground with the "footing impedance" has been compared with the Sommerfeld-Norton ground model, and used in a comparison with full-scale measurements. The AMPL program has been thoroughly investigated and its results compared with NEC and with scale-model measurements. A corroboration of the predictions with full-scale measured tower base currents has shown reasonable agreement. The following summarizes the computer modelling of power lines, with emphasis on the contributions of the present report.

The first step in dealing with a broadcast antenna and power line problem is the modelling of the broadcast antenna itself. The design of a broadcast antenna is usually based on the assumption of "ideal" sinusoidal current flow on the antenna towers, and the design specifies the amplitude and phase of each tower current. The design's azimuth pattern is had by integration of the sinusoidal current distributions. To model the broadcast array with AMPL, the tower currents are specified directly, and since AMPL itself uses the sinusoidal current distribution assumption directly, the design's azimuth pattern is obtained. To model the broadcast array with NEC, the user must specify the voltage excitation of each antenna tower. In the NEC model, the current flow on each antenna tower differs from the ideal sinusoidal current distribution. The amplitude is not sinusoidally distributed, and the phase is not constant. The best approach is to determine the tower base currents so that the current-moment of each antenna tower in the NEC model of the antenna, given by Eqn. 5.3, is the same as the current-moment of each tower in the sinusoidal model, given by Eqn. 5.4. The unknown vector is the tower base voltage for each of the N towers of the broadcast array. The voltages are found assembling an NxN matrix, for a N tower broadcast array. Row # k of the matrix consists of entries which give the current-moment of each tower of the array when tower # k is excited with 1 volt, and all others are shorted to ground. The right-hand side consists of

the current-moments of the sinusoidal current distributions. The method is explained in Ref. (38). In this way, the azimuth pattern computed by NEC for the broadcast array can be made identical to the azimuth pattern in the design.

The second step is the derivation of a model for the power line tower, and for the skywire configuration. Chapter 2 of Ref. (5) reviews the derivation of the radii for the tower and skywire of the "single-wire" tower model of a power line tower. The tower geometry is used to derive cross-sectional dimensions at various heights above the ground, which are used with the "isoperimetric inequalities"(39) to derive equivalent radii for the tower wire at various heights. The various radii result in a "tapered tower" model such as that of Fig. 3.9, which can be simplified to a "straight" tower model, such as the "single wire tower" of Fig. 3.3, by taking a suitable mean value. The skywire radius is equal to the actual radius if there is only one skywire. If there is a parallel pair, the skywire radius is usually determined by making the characteristic impedance of the skywire-image transmission line equal to that of the transmission line formed by the pair of skywires and the pair of images(1,5,7). The bulk of the scale-model measured data which has been used for model validation has been based on type V1S towers. The "single-wire tower" model's ability to represent other tower types, with suitably chosen radii, has not been tested systematically against scale model measurements as a function of the frequency. It is not known whether the bandwidths of resonance modes are reasonable for other tower types nor whether three- and four-wavelength loop resonance is reasonably reproduced.

This report has investigated the higher-frequency behaviour of the "single-wire tower" model, and of a tapered-tower model with an "equivalent skywire", and of a tapered-tower model with a single, thin skywire at a crossarm end. The behaviour of the three models in the three- and four-wavelength loop resonance frequency range is significantly different, hence the predictions of a computer model of a power line above 1100 kHz will be dependent on the specific tower model used. Doubts about the conditions under which the measurements were made, as discussed in Sect. 3.2, make it quite difficult to choose one of these three computer models as the "best fit". It appears that the "single-wire tower" does best below 1000 kHz, and the "tapered-tower" with a thin skywire at the crossarm end does best for three- and four-wavelength loop resonance. It would be desirable to repeat the measurements, taking careful note of the configuration of skywires on the measurement model. Patterns should be taken every 10 kHz(full-scale) across the whole band from 300 to 2000 kHz, so that a systematic comparison of the computer model with solid measured data could be made. Indeed, such a measurement for several diverse tower types would establish whether the tower geometry, and the presence or absence of crossarms, plays a significant role in the higher-frequency behaviour of power lines. It may be necessary to have a computer

model specifically tailored to a certain tower type to obtain high-quality computer predictions of three- and four-wavelength loop resonance. At present, the computer models can be used with good confidence for one- and two-wavelength loop resonance, but with much less confidence for three- or four-wavelength resonance predictions. It is possible that a computer model will overlook a resonant span at these higher frequencies, because the computer model's resonant behaviour is poorly aligned with that of the real power line.

Previous work has largely ignored the effect of the conductivity of ground on reradiation. Silva, Balmain and Ford(17) use Monteath's "footing impedance"(18) to include ground losses in a simple way in a computer model to be analysed over highly-conductive ground. This report has systematically investigated the behaviour of the "footing impedance" and compared predictions made with the "footing impedance" with the behaviour of the Sommerfeld-Norton ground model. It has been shown that the "footing impedance" model provides a good approximation to the more costly, and cumbersome Sommerfeld-Norton model at most frequencies. It is recommended that the "footing impedance" be included in power line models, and that a power line be analysed for both a typical "low" local ground conductivity, and a typical "high" value, to see the range of tower currents likely to be encountered on the power line.

This report has presented a specific test of the computer modelling methodology at the "low" frequency of 680 kHz, namely the CHFA broadcast antenna and the "north" power line. This case-study provides a test of the usefulness of the "single-wire" tower model for a tower type quite different from the V1S. The derivation of the wire radii for the CHFA site was reviewed in Ref. (5). To construct a computer model of such a power line, the precise tower positions relative to the broadcast antenna must be found from maps used in the construction of the power line. Given such precise tower positions, it has been shown that the RF current flow predicted for the towers of the power line is in quite reasonable agreement with full-scale measured values, provided that the "footing impedance" is included to model ground losses. The towers in the computer model which are predicted to carry high current flow are confirmed by the measurement to be the reradiators. Some difficulties were observed on the portion of the "north" line which runs closely parallel to the "southeast" power line, and so a computer model should be used with caution for closely parallel power lines. The reduction in RF current flow on the power line towers which the computer model predicted after detuning the power line by isolating selected towers from the skywire was compared with the reduction as measured on the actual site, and it was shown that the expected reduction was achieved. Thus the computer model provides both a good indication of the level of the RF current flow to be expected on the towers of a power line, and the reduction in RF current flow which can be achieved by detuning by isolating towers.

Thus it is expected that a computer model of a power line can be relied on for one- and two-wavelength resonance predictions, but that the computer model's results must be regarded as less reliable when the frequency and span lengths are such that three- and four-wavelength loop resonance is encountered. At higher frequencies, the computer model's predictions are quite dependent on the tower model used, and the computer model may predict certain spans resonant which are not resonant, or may miss some resonant spans entirely. It may be necessary to develop a specific computer model for each type of power line tower of interest, if precise predictions at higher frequencies are to be made.

Computer-modelling of power lines has become a well-developed methodology, and will continue to provide for both the analysis of reradiation from proposed and from existing power lines, and to serve as a guide to detuning such power lines to suppress unwanted RF current flow, and undesirable reradiation of the broadcast antenna's signal.

LIST OF REFERENCES

1. C.W. Trueman and S.J. Kubina, "AM Reradiation Project", Final Report, Communications Research Centre Contract No. OSU79-00066, Technical Note No. TN-EMC-80-03, Dept. of Electrical Engineering, Concordia University, March, 1980.

2. C.W. Trueman and S.J. Kubina, "Prediction by Numerical Computation of the Reradiation from and the Detuning of Power Transmission Lines," Final Report, Communications Research Centre Contract No. OSU80-00121, Technical Note No. TN-EMC-81-03, Dept. of Electrical Engineering, Concordia University, May 13, 1981.

3. C.W. Trueman and S.J. Kubina, "Corrective Measures for Minimizing the Interaction of Power Lines with MF Broadcast Antennas," Final Report, Communications Research Centre Contract No. OSU81-00192, Technical Note No. TN-EMC-82-02, Dept. of Electrical Engineering, Concordia University, May 17, 1982.

4. C.W. Trueman and S.J. Kubina, "Recent Advances in the Computer Modelling of Type V1S Power Line Towers at MF Frequencies," Final Report, Communications Research Centre Contract No. OSU82-00157, Technical Note No. TN-EMC-83-04, Dept. of Electrical Engineering, Concordia University, Sept. 29, 1983.

5. C.W. Trueman and S.J. Kubina, "Initial Assessment of Reradiation from a Power Line and Its Detuning by Tower Isolation", Final Report, DOC/CRC Contract No. OST83-00290, Techincal Note No. TN-EMC-85-05, Dept. of Electrical Engineering, Concordia University, May 31, 1985.

6. G.J. Burke, A.J. Poggio, J.C. Logan and J.W. Rockway, "NEC - Numerical Electromagnetics Code for Antennas and Scattering", 1979 IEEE International Symposium on Antennas and Propagation Digest, IEEE Publication No. 79CH1456-3AP, Seattle, Washington, June, 1979.

7. C.W. Trueman and S.J. Kubina, "Numerical Computation of the Reradiation from Power Lines at MF Frequencies," IEEE Trans. on Broadcasting, Vol. BC-27, No. 2, pp. 39-45, June 1981.

8. C.W. Trueman, S.J. Kubina and J.S. Belrose, "Corrective Measures for Minimizing the Interaction of Power Lines with MF Broadcast Antennas," IEEE Trans. on Electromagnetic Compatibility, Vol. EMC-25, No. 3, pp. 329-339, August 1983.

9. C.W. Trueman and S.J. Kubina, "Analysis of Reradiation from the Southeast Route Power Line into the Restricted Arc of the Pattern of CHFA, Edmonton," Report No. CHFA-1, prepared for the Canadian Broadcasting Corporation, Sept. 25, 1980.

10. C.W. Trueman and S.J. Kubina, "Analysis of Reradiation from the Northern Route Power Line into the Restricted Arc of the Pattern of CHFA, Edmonton," Report No. CHFA-2, prepared for the Canadian Broadcasting Corporation, Nov. 25, 1980.

11. C.W. Trueman and S.J. Kubina, "Initial Assessment of Reradiation from Power Lines", IEEE Trans. on Broadcasting, Vol. BC-31, No. 3, pp. 51-65, Sept. 1985.

12. C.W. Trueman and S.J. Kubina, "The Radiation Pattern of CHFA, Edmonton near the As-Built North and Southeast Power Lines and Their Detuning by Isolating Towers," Interim Report, Communications Research Centre Contract No. OST83-00290, Technical Note No. TN-EMC-84-01, Dept. of Electrical Engineering, Concordia University, Jan. 31, 1984.

13. C.W. Trueman and S.J. Kubina, "Analysis and Procedures for Detuning the Power Lines near CHFA, Edmonton, by Isolating Towers," Interim Report, Communications Research Centre Contract No. OST83-00290, Technical Note No. TN-EMC-84-03, Dept. of Electrical Engineering, Concordia University, May 31, 1984.

14. C.W. Trueman, S.J. Kubina, R.C. Madge and D.E. Jones, "Comparison of Computed RF Current Flow on a Power Line with Full Scale Measurement," IEEE Trans. on Broadcasting, Vol. BC-30, No. 3, pp. 97-107, Sept. 1984.

15. J.N. Brittingham, E.K. Miller, and J.T. Okada, "SOMINT : An Improved Model for Studying Conducting Objects near Lossy Half Spaces," Lawrence Livermore Laboratory Report No. UCRL-52423, Feb. 24, 1978.

16. G.J. Burke, E.K. Miller, J.N. Brittingham, D.L. Lager, R.J. Lytle, and J.T. Okada, "Computer Modelling of Antennas Near the Ground," Lawrence Livermore Laboratory Report No. UCID-18626, May 13, 1980.

17. M.M. Silva, K.G. Balmain and E.T. Ford, "Effects of Power Line Re-Radiation on the Pattern of a Dual-Frequency MF Antenna," IEEE Trans. on Broadcasting, Vol. BC-28, No. 3, Sept. 1982.

18. G.D. Monteath, "Applications of the Electromagnetic Reciprocity Principle," Pergammon Press, New York, 1973.

19. W. Lavrench and J.G. Dunn, private communication, National Research Council of Canada, Division of Electrical Engineering, April 25, 1979.

20. W. Lavrench and J.G. Dunn, private communication, National Research Council of Canada, Division of Electrical Engineering, December 16, 1980.

21. M.A. Tilston and K.G. Balmain, "A Microcomputer Program for Predicting AM Broadcast Re-Radiation from Steel Tower Power Lines," IEEE Trans. on Broadcasting, Vol. BC-30, No. 2, pp. 50-56, June, 1984.

22. C.R. Paul and S.A. Nasar, "Introduction to Electromagnetic Field Theory", Mc-Graw-Hill, 1982.

23. K.A. Norton, "The Propagation of Radio Waves over the Surface of the Earth and in the Upper Atmosphere, Part II", Proc. IRE, Vol. 25, No. 9, pp. 1203-1236, Sept. 1937.

24. A. Banos, "Dipole Radiation in the Presence of Conducting Half-Space," Pergamon Press, New York, 1966.

25. M.A. Tilston and K.G. Balmain, "Medium Frequency Reradiation from an Unstrung Steel Tower Power Line," IEEE Trans. on Broadcasting, Vol. BC-29, No. 3, pp. 93-100, September, 1983.

26. C. Baltassis, "The Concept of Footing Impedance and its Utilization in the Power Line Reradiation Problem", Internal Report, Concordia University, Dept. of Electrical Engineering, April, 1985.

27. M. Abramowitz and I.A. Stegun, "Handbook of Mathematical Functions", Dover, New York, 1972.

28. S.A Schelkunoff and H.T. Friis, "Antennas - Theory and Practice", Wiley, 1966.

29. J.S. Belrose, private communication, Sept. 1, 1982.

30. W. Lavrench, private communication, Dec. 16, 1980.

31. D.E. Norman, "AMPL - A Transmission Line Theory Method of Analysing Interaction Between AM Broadcast Stations and Nearby High Voltage Power Lines", Technical Note No. TN-EMC-85-07, Dept. of Electrical Engineering, Concordia University, Sept., 1985.

32. P. Knight, "Propagation Coefficient of the Beverage Aerial", Proc. IEE, Vol. 119, No. 7, pp. 821-826, July, 1972.

33. E.C. Jordan and K.G. Balmain, "Electromagnetic Waves and Radiating Systems", 2nd Edition, Prentice-Hall, New Jersey, 1968.

34. P. Warmbein and S. Reid, "Effect on CHFA, Edmonton of Reradiation from High-Voltage Transmission Lines", Canadian Broadcasting Corporation, Report No. ER-436, Jan. 15, 1985.

35. W.V. Tilston, T. Tralman, and M.A. Tilston, "Reradiation Measurments of CHFA's Signal at the TransAlta Utilities Power Line Towers", Final Report, Contract No. E-31786, Til-Tek Limited, P.O. Box 550, Kemptville, Ontario, April, 1984.

36. W.V. Tilston and T. Tralman, "Reradiation Measurements of CHFA's Signal at the TransAlta Utilities Power Line Towers", Final Report, Contract No. E-32545, Til-Tek Limited, P.O. Box 550, Kemptville, Ontario, July, 1984.

37. R.L. Burden, J.D. Faires and A.C. Reynolds, "Numerical Analysis", 2nd Edition, Prindle, Weber and Schmidt, Boston, 1981.

38. C.W. Trueman and S.J. Kubina, "Reradiation from a Microwave Tower into the Azimuth Pattern of Station CHUM", Report No. OH-86 01, prepared for Ontario Hydro Transmission Systems Division, by Les Conseillers SJK Inc., May 21, 1986.

39. D.L. Jaggard, "An Application of Isoperimetric Inequalities to the Calculation of Equivalent Radii", Proc. of the National Radio Science Meeting, Boulder, Colorado, Nov. 1979.

APPENDIX 1

LISTING OF THE FOOTING IMPEDANCE PROGRAM

```
C
C  FOOT.1A
C
C  THIS PROGRAM IS USED TO FIND THE FOOTING IMPEDANCE Z'-Z
C  OF A VERTICAL THIN WIRE ANTENNA ABOVE (REAL) GROUND.
C  THE MAIN PARAMETERS USED ARE: RHO   : FOOTING RADIUS
C                                SIGMA : EARTH'S CONDUCTIVITY
C                                ER    : EARTH'S PERMITTIVITY
C                                FMHZ  : FREQUENCY IN MHZ
C THIS VERSION FINDS A SINGLE VALUE OF FOOTING IMPEDANCE
C FOR USE AT A SINGLE FREQUENCY IN A SPECIFIC CASE.
C
C
C PROGRAM "ZMZP" WAS WRITTEN BY C.W. TRUEMAN IN AUGUST, 1982 FOR
C THE INITIAL TESTING OF THE FOOTING IMPEDANCE IDEA.
C PROGRAM FOOT.1A WAS DEVELOPED FROM
C ZMZP BY C. BALTASSIS IN FEB. 1985.
C ADAPTED FOR FORTRAN-77 BY C.W. TRUEMAN
C SEPT. 27, 1985
C
      PROGRAM FOOTIM
C
      REAL MU, L, IND
      COMPLEX CHETA,Z,ETA
C RECORD OF THE VALUE FOUND
      OPEN(6,FILE = 'FOOT.OUT',STATUS = 'NEW')
C
C INITIALIZATION
C
C USEFUL CONSTANTS
      PI = 4.*ATAN(1.)
      EPS = 8.854187E-12
      MU = PI*4.E-07
      ER = 15.
C
      WRITE(*,90)
   90 FORMAT(///,'PROGRAM FOOTZ.1A - SEPT. 27, 1985',
     &//,' COMPUTATION OF THE FOOTING IMPEDANCE' )
C
C FREQUENCY PARAMETERS
C
      FMHZ = 0.840
      WRITE(*,91)
   91 FORMAT(//,' SPECIFY THE FREQUENCY IN KHZ :')
      WRITE(*,96)
   96 FORMAT(' (REAL NUMBER - INCLUDE A DECIMAL POINT)')
```

```
      READ(*,92) FKHZ
   92 FORMAT(F7.4)
      FMHZ = FKHZ / 1000.
      FREQ = FMHZ*1.E+06
      RADFRE = 2.*PI*FREQ
      WAVE = 2.99792457E+08/FREQ
      BETA = 2.*PI/WAVE
C
C EARTH'S CONDUCTIVITY IN MHO/METRE
      SIGMA  =  .010
      WRITE(*,93)
   93 FORMAT(/,' SPECIFY THE GROUND CONDUCTIVITY IN ',
     &' MILLISIEMENS/METRE :')
      WRITE(*,96)
      READ(*,92) SIGMA
      SIGMA = SIGMA / 1000.
C
C
C FOOTING RADIUS
      RHO  =  4.57
      WRITE(*,94)
   94 FORMAT(/' SPECIFY THE FOOTING RADIUS IN METRES :')
      WRITE(*,96)
      READ(*,92) RHO
C
C
C PRINT-OUT STATEMENTS
C
      WRITE(*,1)
      WRITE(6,1)
    1 FORMAT(' '///4X,'CALCULATION OF FOOTING IMPEDANCE'/

     1             4X,'================================'
     &//           4X,'INPUT DATA :')
      WRITE(*,2) FMHZ * 1000.
      WRITE(6,2) FMHZ * 1000.
    2 FORMAT(/4X,'FREQUENCY                          : F      = ',
     &       F6.0,' KHZ')
      WRITE(*,3) ER
      WRITE(6,3) ER
    3 FORMAT(/4X,'GROUND (RELATIVE) PERMITTIVITY : ER     =',
     &',F6.0)
      WRITE(*,4) SIGMA * 1000.
      WRITE(6,4) SIGMA * 1000.
    4 FORMAT(/4X,'GROUND CONDUCTIVITY            : SIGMA  = ',
     1       F6.0,' MILLISIEMENS/METRE')
      WRITE(*,5) RHO
      WRITE(6,5) RHO
    5 FORMAT(/4X,'FOOTING CYLINDER RADIUS        : RHO    = ',
     #       F6.2,' METRE'///4X,'OUTPUT DATA :')
C
C INTRINSIC IMPEDANCE OF GROUND
C
      ETA = CHETA( MU, EPS, ER, RADFRE, SIGMA )
```

```
C
C ANTENNA HEIGHT IN M
C
      L = WAVE/4.
      WRITE(*,11) L
      WRITE(6,11) L
   11 FORMAT(/4X,'ANTENNA HEIGHT (LAMBDA/4)      : ',F6.2,
     &'  METERS')
C
C
C FOOTING IMPEDANCE EVALUATION
C
      CALL ZFOOT( L,RHO,BETA,ETA,PI,Z )
C
C
C
      WRITE(*,6) Z
      WRITE(6,6) Z
    6 FORMAT(/4X,'FOOTING IMPEDANCE                :'
     #,' ZP-Z =  (',F7.4,' , ',F7.4,' ) OHMS')
C
C
C
C EVALUATION OF THE RESISTANCE AND INDUCTANCE (CAPACITANCE)
C
      RES  =  REAL( Z )
      AIM  =  AIMAG( Z )
C
C EXAMINE WHETHER THE FOOTING IMPEDANCE IS INDUCTIVE OR C
CAPACITIVE
C
      IF (AIM.LT.0.) GO TO 30
      IND = AIM/RADFRE
      WRITE(*,9) RES,IND
      WRITE(6,9) RES,IND
    9 FORMAT(/4X,'RESISTANCE R = ',E11.5,' OHMS',
     #/       4X,'INDUCTANCE L = ',E11.5,' HENRIES')
      GO TO 20
   30 CAP = -1./(AIM*RADFRE)
      WRITE(*,10) RES,CAP
      WRITE(6,10) RES,CAP
   10 FORMAT(/4X,'RESISTANCE  R = ',E11.5,' OHMS',
     #/       4X,'CAPACITANCE C = ',E11.5,' FARADS')
   20 CONTINUE
   50 CONTINUE
      WRITE(*,95)
   95 FORMAT(//,' PRINT FILE FOOT.OUT FOR A COPY OF THE RESULT')
      STOP
      END
C
C
C
C
C
```

```
      SUBROUTINE ZFOOT( L,RHO,BETA,ETA,PI,Z )
C
C EXPONENTIAL INTEGRAL EVALUATION
C
      REAL  L
      COMPLEX EI,COF1,COF2,EI1,EI2,Z,ETA,TERM1,TERM2
      DOUBLE PRECISION RO
      RO = L**2+RHO**2
      RO  =  DSQRT(RO)
      ARG1  =  2.*BETA*(RO-L)
      ARG2  =  2.*BETA*(RO+L)
      EI1  =  EI( ARG1 )
      EI2  =  EI( ARG2 )
      ARG  =  2.*BETA*L
      COF1 =  CEXP(CMPLX(0.,-ARG))
      COF2 =  CEXP(CMPLX(0., ARG))
      TERM1  =  COF1*EI1
      TERM2  =  COF2*EI2
C
C FOOTING IMPEDANCE EVALUATION
C
      Z  =  ETA/(4.*PI)
      Z  =  Z * ( TERM1 + TERM2 )
      RETURN
      END
C
C
C
C
C
C
      FUNCTION CHETA( MU,EPS,ER,RADFRE,SIGMA )
C
C CHETA CALCULATES THE INTRINSIC IMPEDANCE OF THE GROUND
C
      COMPLEX CHETA
      REAL MU
C C.W.T. AUGUST 1982
      CHETA  =  CSQRT( CMPLX(0.,RADFRE*MU)
     1     / CMPLX( SIGMA,RADFRE*ER*EPS ) )
C      WRITE(6,1) CHETA
    1 FORMAT(/10X,'INTRINSIC IMPEDANCE OF GROUND :',19X,
     &'ETA  =  (',F9.4,' , ',F9.4,' ) OHMS')
      RETURN
      END
C
C
C
C
C
C
C
C
C
```

```
      FUNCTION EI( ARG )
C
C EI CALCULATES THE EXPONENTIAL INTEGRAL WITH IMAGINARY ARGUMENT
C
      COMPLEX EI
      PI  =  4.*ATAN(1.0)
      PI2  =  PI * 0.5
      CII  =  CI( ARG )
      SII  =  SI( ARG )
      EI  =  CMPLX( CII,PI2-SII )
C     WRITE(6,1) ARG
    1 FORMAT(///10X,'ARGUMENT  = ',E12.5)
C     WRITE(6,2) EI
    2 FORMAT(/10X,'EXPONENTIAL INTEGRAL  = ( ',
     1       E12.6,' , ',E12.6,' )')
      RETURN
      END
C
C
C
C
      FUNCTION CI(Z)
C
C CI CALCULATES THE COSINE INTEGRAL USED IN FUNCTION EI
C
      DOUBLE PRECISION SUM,ZSQ,ZNUMER
      INTEGER FACTOR,SIGN
C COMPUTE THE COSINE INTERGAL
C
      IF( Z .LE. 3. ) GO TO 1
C USE A RATIONAL FUNCTION APPROXIMATION (ABRAMOWITZ: 5.2.8,

C        5.2.9, 5.2.38, 5.2.39)
      CI  =  FI(Z)*SIN(Z) - GI(Z)*COS(Z)
      GO TO 1002
    1 CONTINUE
C SUM UP THE INFINITE SERIES (ABRAMOWITZ : 5.2.16)
C TERM FOR N  =  1
      SIGN  =  -1
      ZNUMER  =  Z*Z
      FACTOR  =  2
      ZSQ  =  Z*Z
      SUM  =  -ZSQ / 4.
C TOLERANCE FOR STOPPING
      TOL  =  1.E-06
C MAX # OF ITERATIONS
      ITERMX = 100
C LOOP FOR SUMMING UP
      N = 2
 1000 SIGN = -SIGN
      ZNUMER = ZNUMER * ZSQ
      FACTOR = (2*N)*(2*N-1)*FACTOR
      SUMO = SUM
      SUM = SUM + SIGN*ZNUMER/(2*N*FACTOR)
```

```
C STOPING CONDITION
      IF( ABS(SUMO-SUM) .LT. TOL ) GO TO 1001
      N = N + 1
      IF( N .LT. ITERMX ) GO TO 1000
C ERROR - TOO MANY ITERATIONS
      WRITE(6,2) Z
    2 FORMAT(/////3X,'ERROR IN COMPUTING CI FOR A =( ',
     1       E12.6,' , ',E12.6,' )')
      WRITE(6,3) SUM
    3 FORMAT(/3X,'TOO MANY ITERATIONS : SUM= ',D18.10)
      STOP
 1001 CONTINUE
      CI = SUM + 0.5772156649 + ALOG(Z)
 1002 CONTINUE
C     WRITE(6,4) Z
    4 FORMAT(//10X,'ARGUMENT =   ',E12.6)
C     WRITE(6,5) CI
    5 FORMAT(/10X, '      CI =    ',E12.6)
      RETURN
      END
C
C
C
C
      FUNCTION SI(Z)
C
C SI CALCULATES THE SINE INTEGRAL USED IN FUNCTION EI
C
      DOUBLE PRECISION ZNUMER,SUM,ZSQ
      INTEGER FACTOR ,SIGN
C COMPUTE THE SINE INTEGRAL
C
C
      IF( Z .LE. 3. ) GO TO 1
      PI2 = 2.*ATAN(1.)
C USE RATIONAL FUNCTION APPROXIMATION (ABRAMIWITZ: 5.2.8,
C            5.2.38, 5.2.39)
      SI = PI2 - FI(Z)*COS(Z) - GI(Z)*SIN(Z)
      GO TO 1002
    1 CONTINUE
C SUM UP THE INFINITE SERIES (ABRAMOWITZ : 5.2.14)
C
C TERM FOR N = 0
      SIGN = 1
      ZNUMER = Z
      FACTOR = 1
      SUM = Z
      ZSQ = Z*Z
C TOLERANCE FOR STOPPING
      TOL = 1.E-06
C MAXIMUM NUMBER OF ITERATIONS
      ITERMX = 100
C LOOP FOR ADDING TERMS
      N = 1
```

```
 1000 SIGN = - SIGN
      ZNUMER = ZNUMER * ZSQ
      FACTOR = ( 2*N+1 ) * ( 2*N ) * FACTOR
      SUMO = SUM
      SUM = SUM + SIGN*ZNUMER / ( ( 2*N+1 ) * FACTOR )
C STOPPING CONDITION
      IF( ABS(SUMO-SUM) .LT. TOL ) GO TO 1001
      N = N + 1
      IF( N .LT. ITERMX ) GO TO 1000
C ERROR - TOO MANY ITERATIONS
      WRITE(6,2) Z
    2 FORMAT(////3X,'ERROR IN COMPUTING SI FOR Z = ( ',
     1       E12.6,' , ',E12.6,' )')
      WRITE(5,3) SUM
    3 FORMAT(/3X,'TTOO MANY ITERATIONS : SUM = ',D18.8)
      STOP
 1001 CONTINUE
      SI = SUM
 1002 CONTINUE
C     WRITE(6,4) Z
    4 FORMAT(///10X,'ARGUMENT   =   ',E12.6)
C     WRITE(6,5) SI
    5 FORMAT(/10X,   '       SI   =    ',E12.6)
      RETURN
      END
C
C
C
C
      FUNCTION POLY(A1,A2,A3,A4,XSQ)
      POLY =  A4 + XSQ*( A3+XSQ*( A2+XSQ*( A1+XSQ )))
      RETURN
      END
C
C
C
C
      FUNCTION FI(X)
      A1 =  38.027264
      A2 = 265.187033
      A3 = 335.677320
      A4 =  38.102495
      B1 =  40.021433
      B2 = 322.624911
      B3 = 570.236280
      B4 = 157.105423
      XSQ = X*X
      FI =(1./X)* POLY(A1,A2,A3,A4,XSQ) / POLY(B1,B2,B3,B4,XSQ)
      RETURN
      END
C
C
C
C
```

```
      FUNCTION GI(X)
      A1 =   42.242855
      A2 =  302.757865
      A3 =  352.018498
      A4 =   21.821899
      B1 =   48.196927
      B2 =  482.485984
      B3 = 1114.978885
      B4 =  449.690326
      XSQ = X*X
      GI =(1./XSQ)* POLY(A1,A2,A3,A4,XSQ) / POLY(B1,B2,B3,B4,XSQ)
      RETURN
      END
```

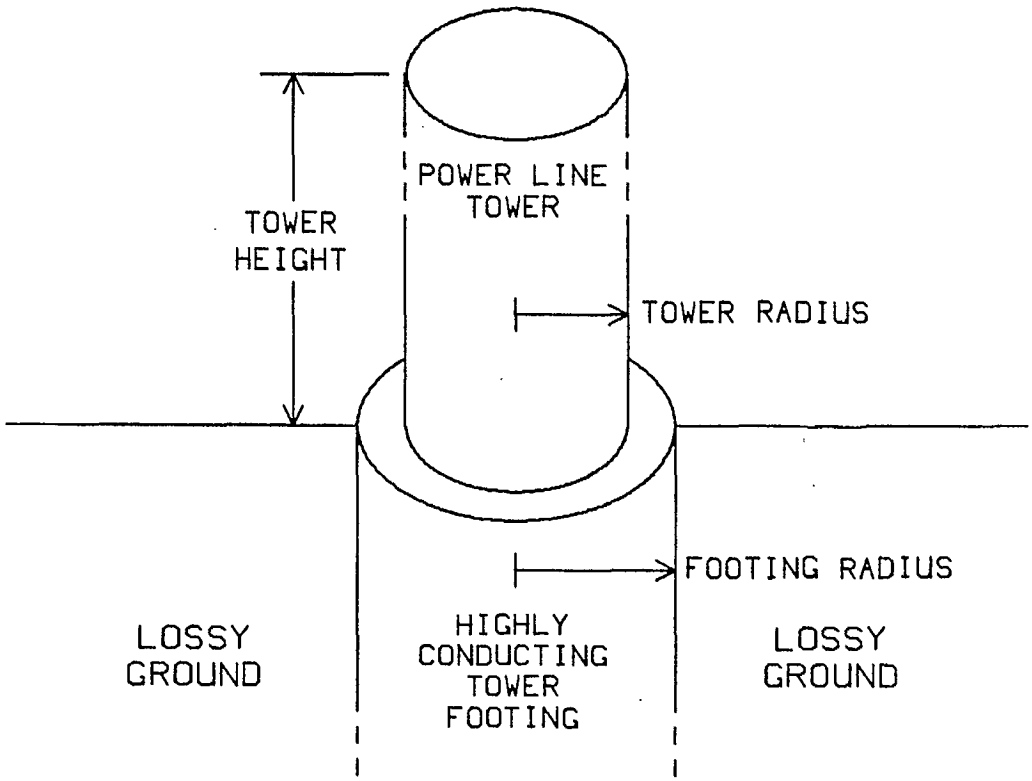

Fig. 2.1 - A tower on a cylindrical, highly-conducting "footing" embedded in a lossy ground.

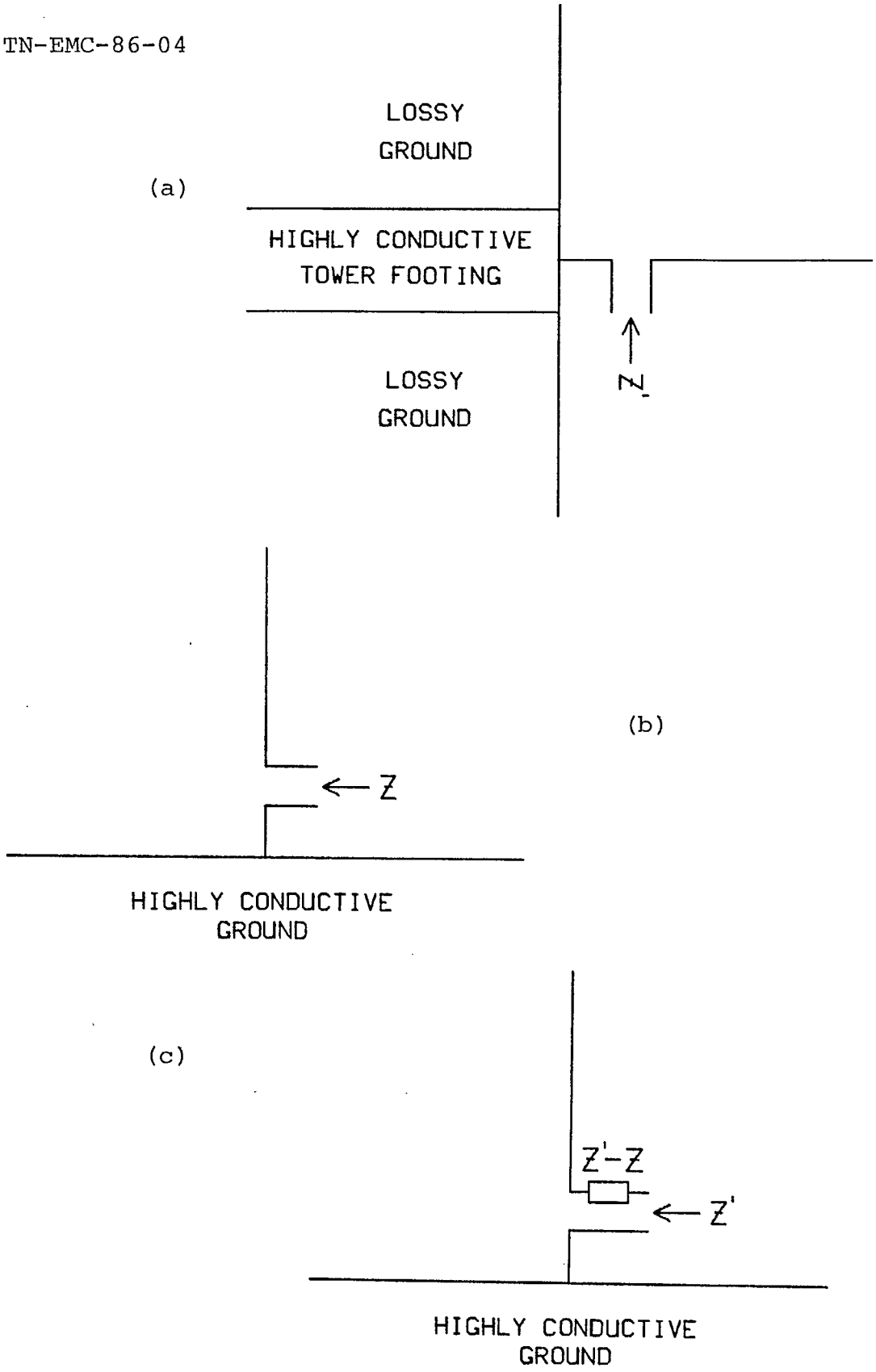

Fig. 2.2 - Definition of the "footing impedance" Z'-Z and its use to make the input impedance of a tower on footing in lossy ground equal to the input impedance of the tower above perfectly-conducting ground.

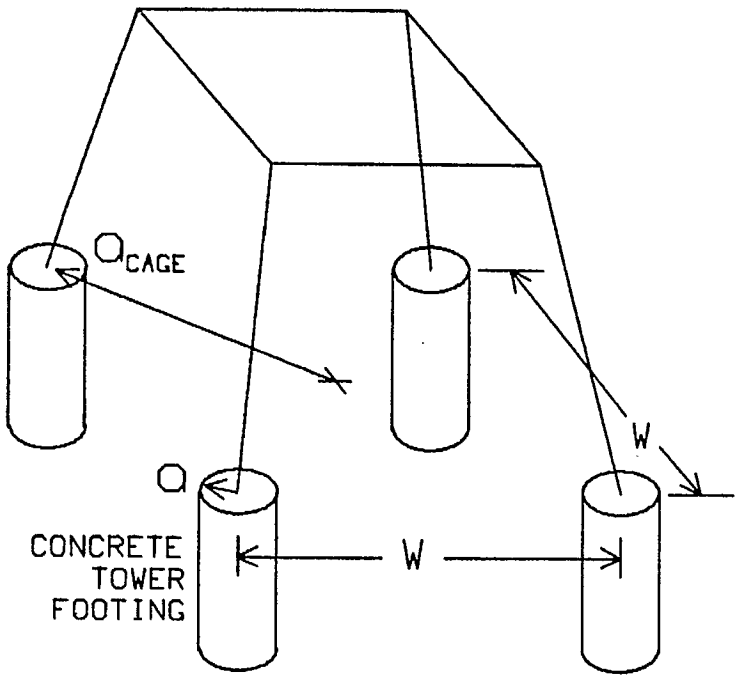

Fig. 2.3 - The geometry of the footing of a real power line tower.

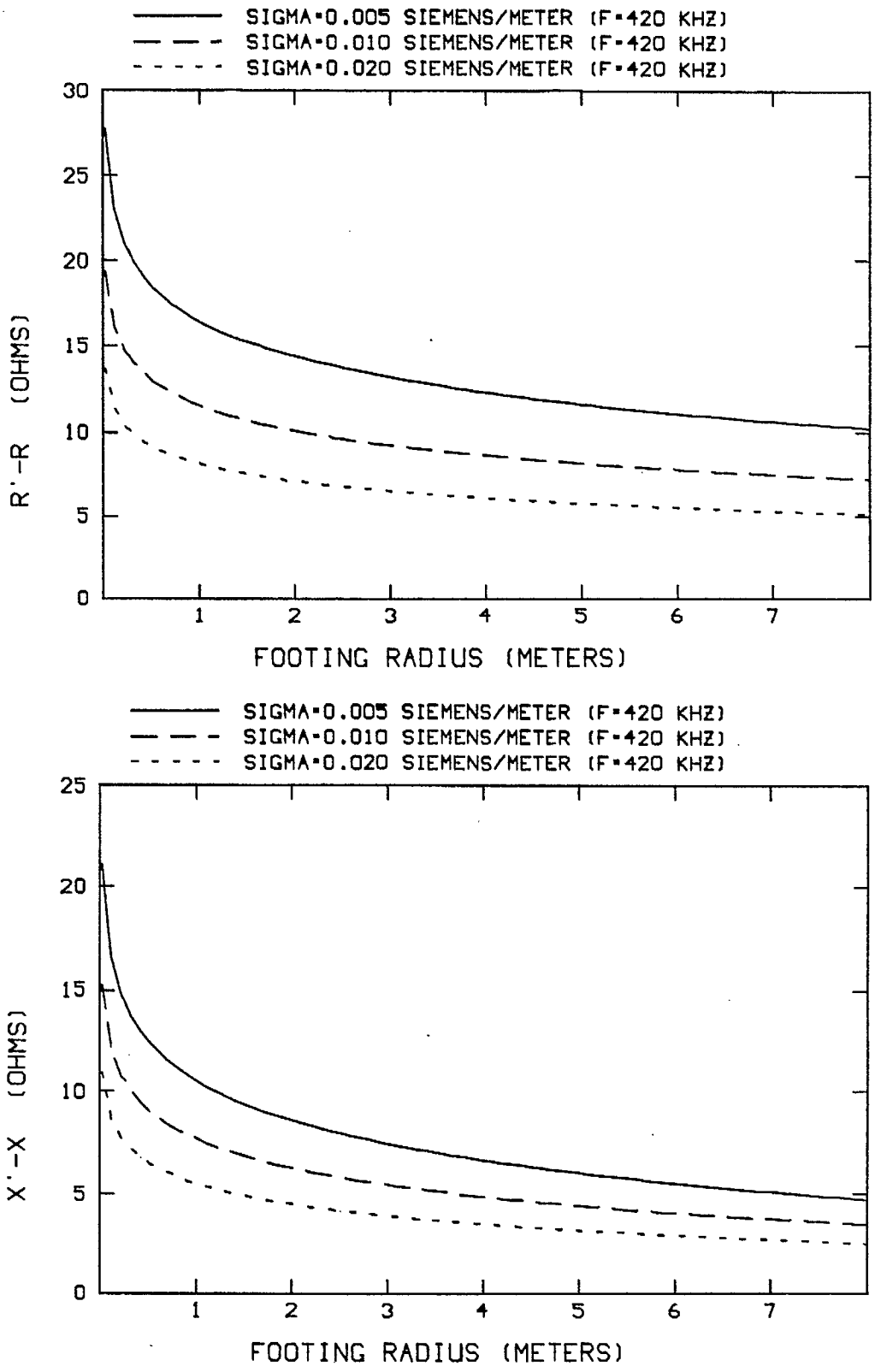

Fig. 2.4 - Variation of the footing resistance and footing reactance with the radius of the footing of Fig. 2.1, at 420 kHz, for three ground conductivities.

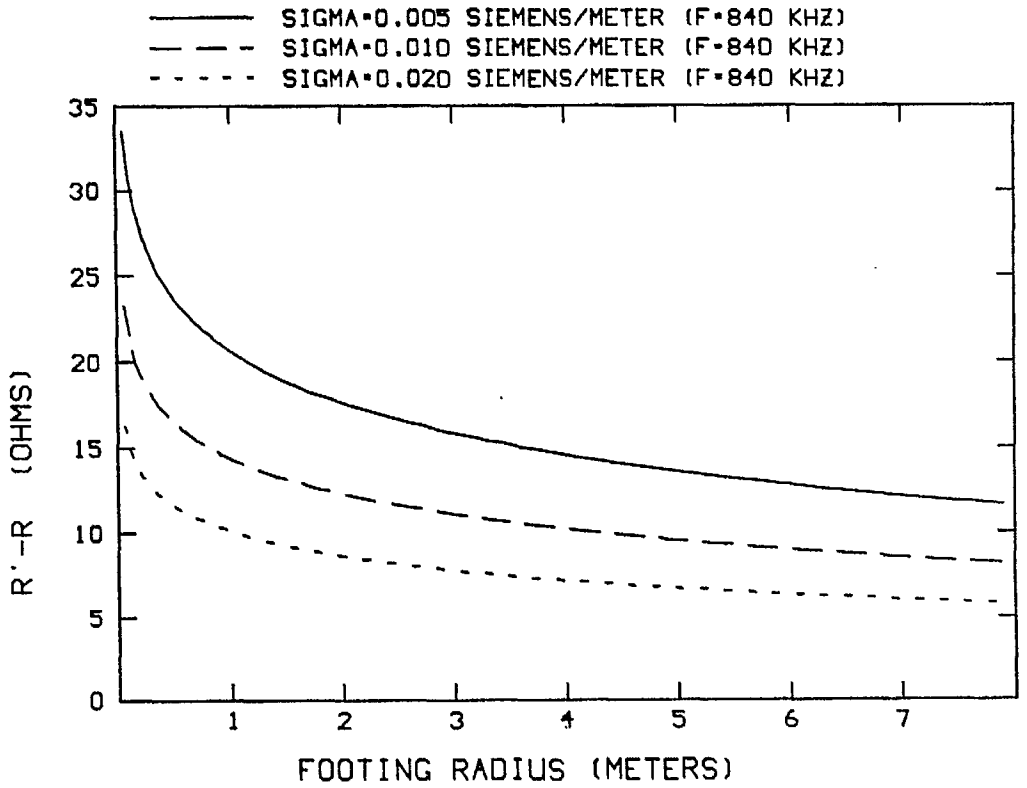

(a)

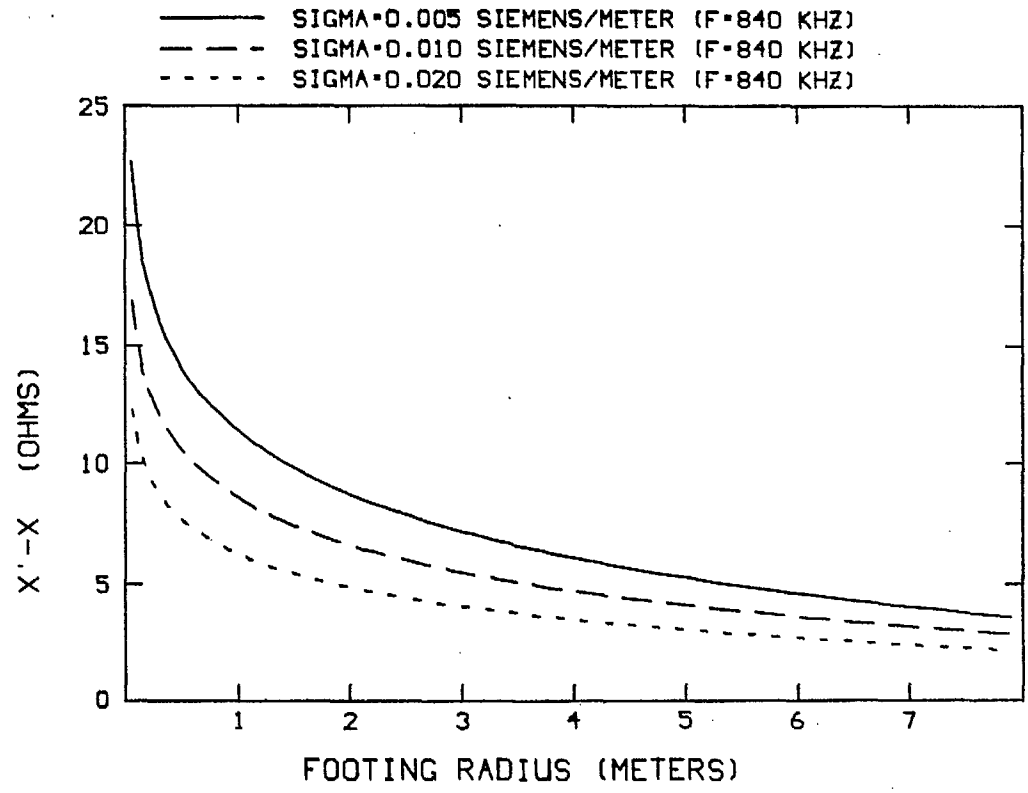

(b)

Fig. 2.5 - Variation of the footing resistance and footing reactance with the radius of the footing of Fig. 2.1, at 840 kHz, for three ground conductivities.

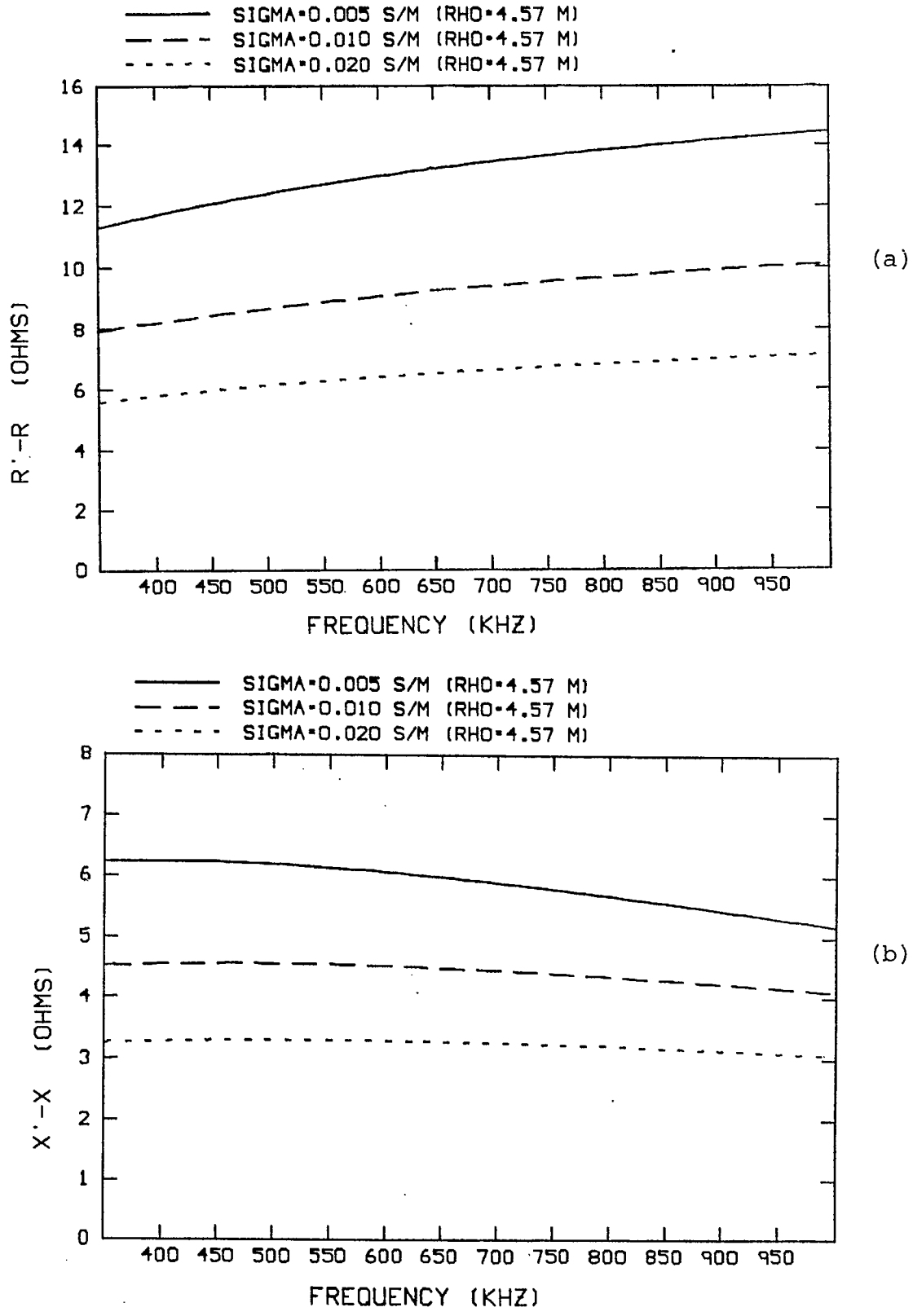

Fig. 2.6 - Variation of the footing resistance and the footing reactance with frequency, for a footing of 4.57 m radius, and three different ground conductivities.

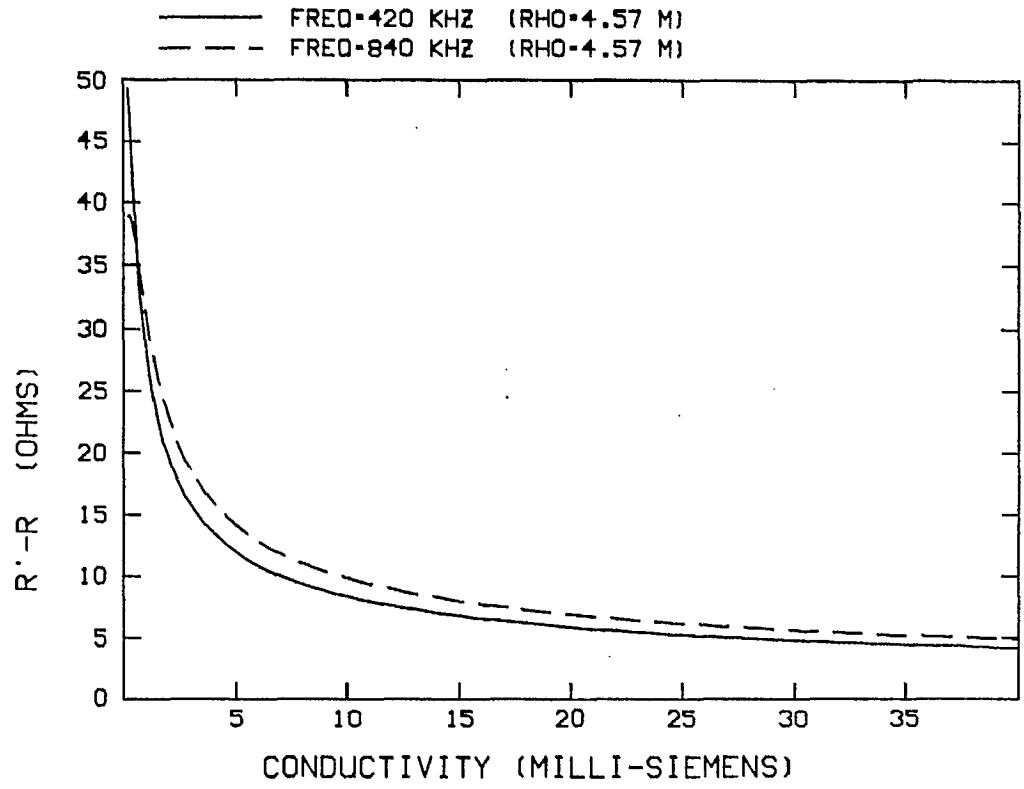

(a)

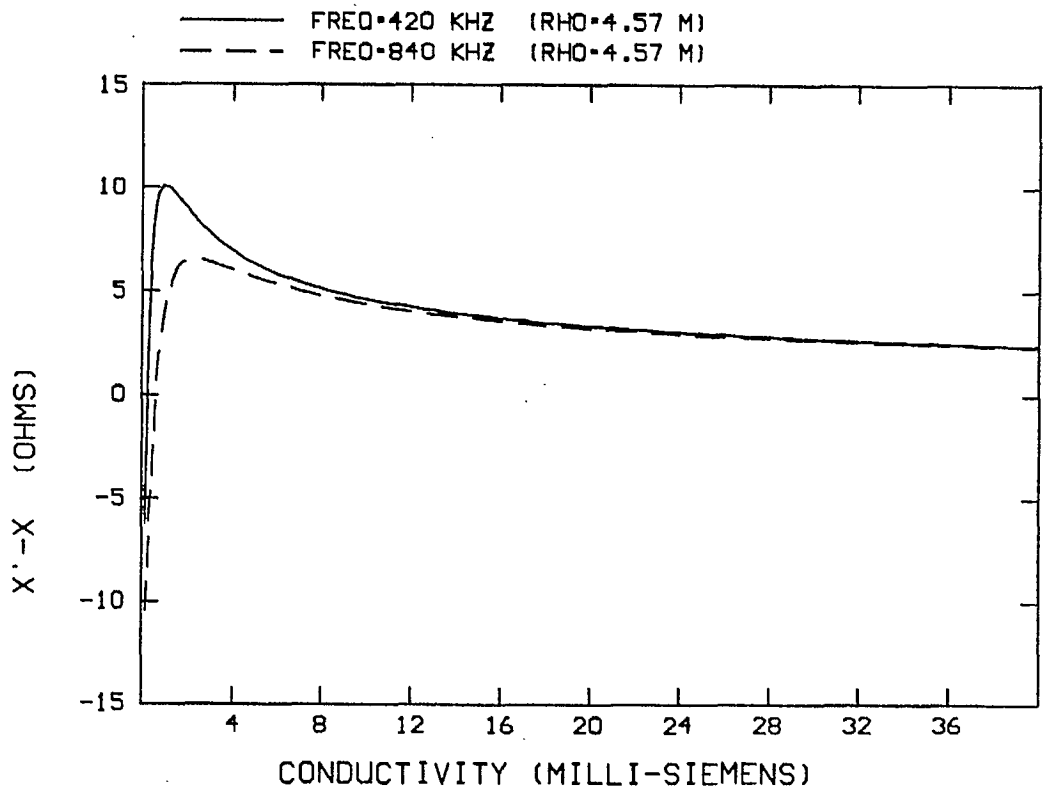

(b)

Fig. 2.7 - Variation of the footing resistance and the footing reactance with the conductivity of the ground, for a footing of radius 4.57 m, at two frequencies.

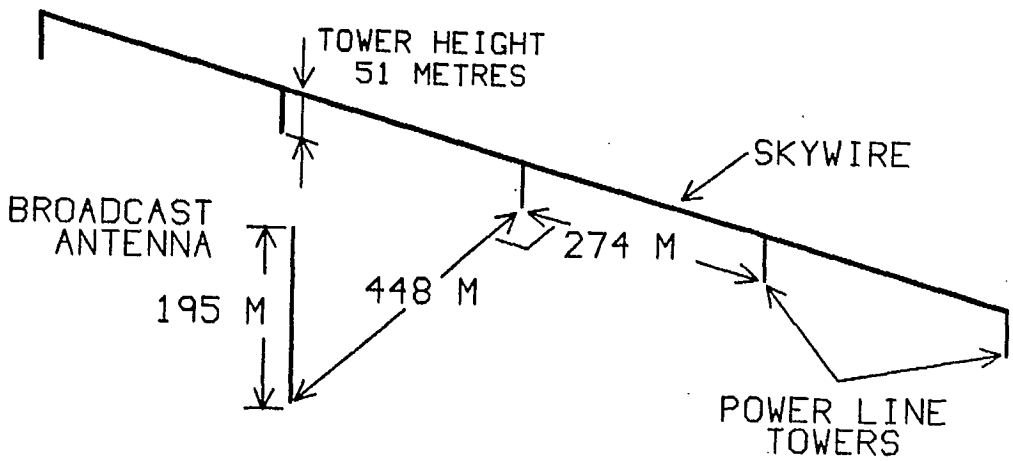

Fig. 2.8 - The five tower "test power line" illuminated by an omnidirectional broadcast antenna, used in Ref. (7) to evaluate the effect of ground conductivity on power line resonant behaviour.

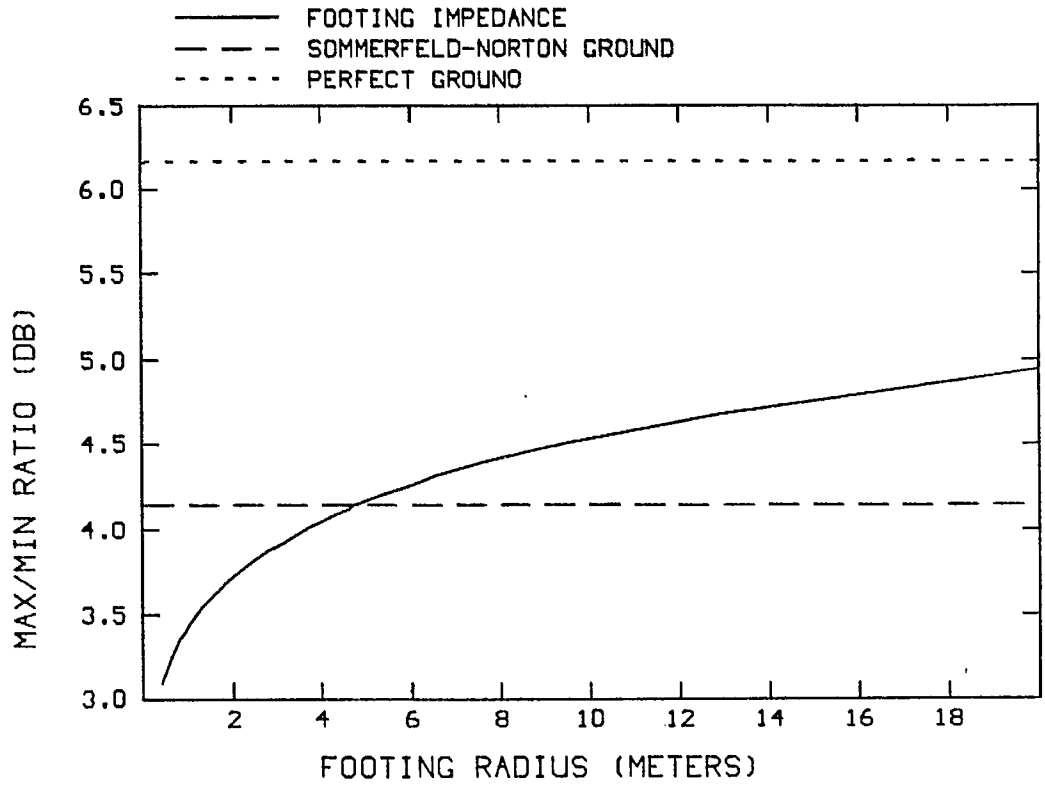

Fig. 2.9 - Variation of the max-to-min ratio of the azimuth pattern of the configuration of Fig. 2.8 with the radius of the tower footing, showing that good agreement with the Sommerfeld-Norton ground model is found when the footing radius is close to that specified by Eqn. 2.5.

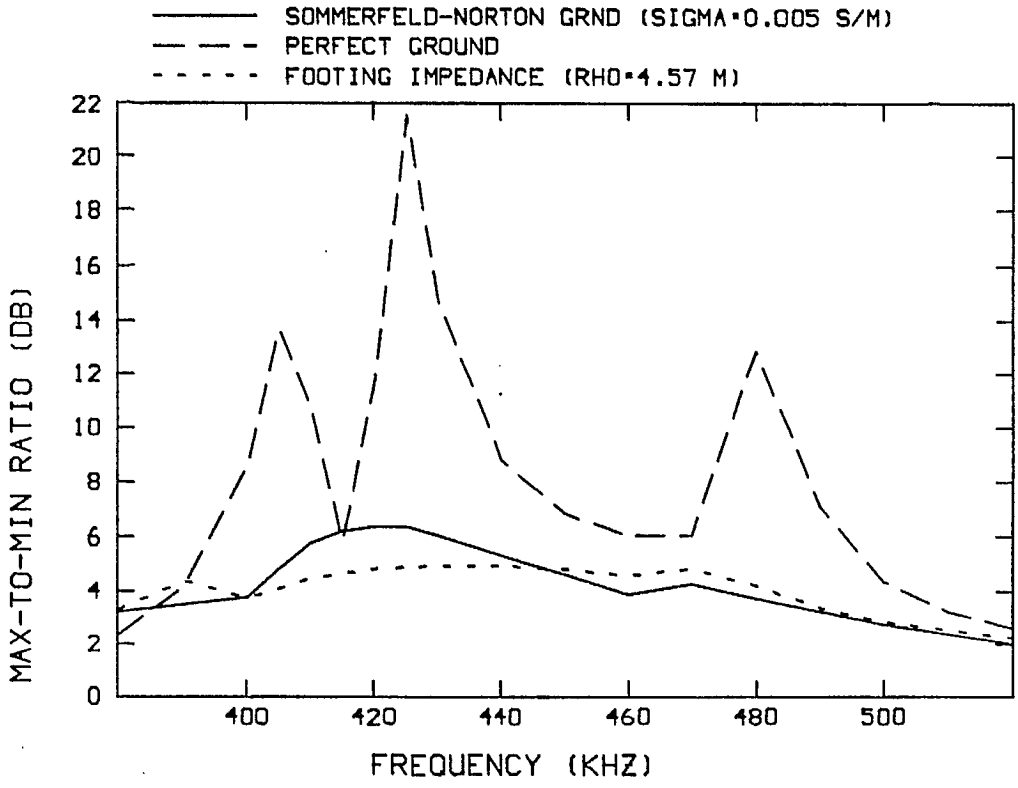

(a)

Fig. 2.10 - Frequency dependence of the max-to-min ratio of the azimuth pattern of the antenna near the power line of Fig. 2.8, throughout the one-wavelength loop resonance frequency range. The results obtained with the footing impedance are close to those found with the Sommerfeld-Norton ground model, except very near the resonant frequency.
(Fig. 2.10 (b) and (c) on next page)

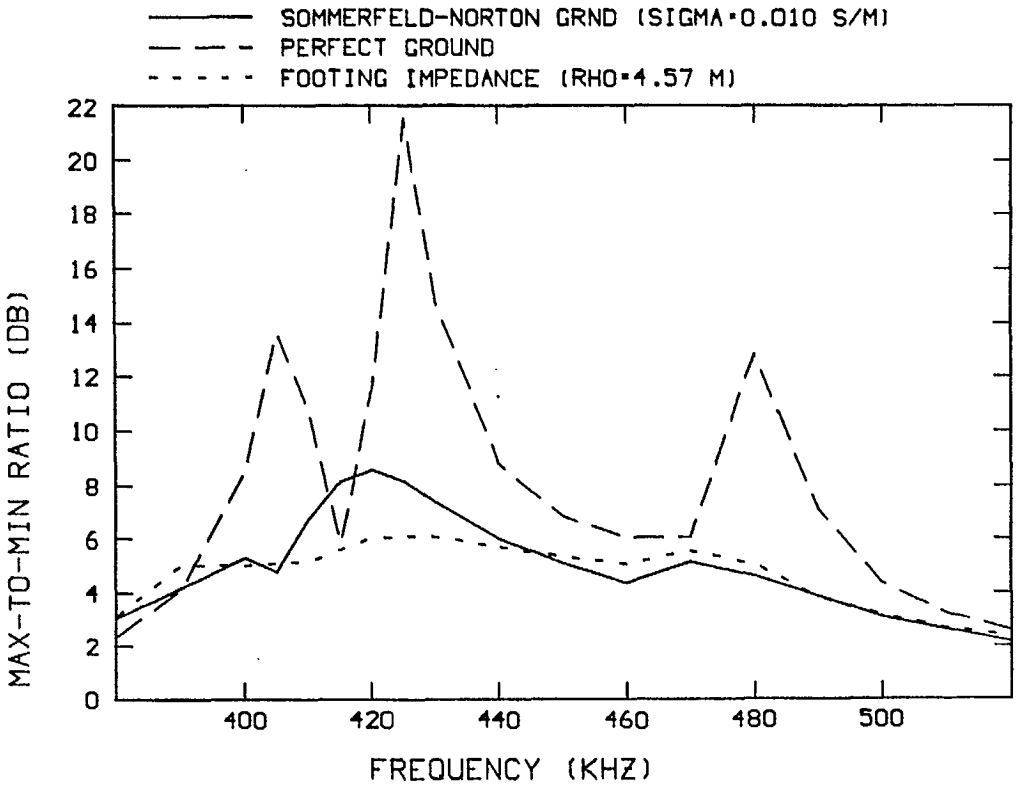
SOMMERFELD-NORTON GRND (SIGMA=0.010 S/M)
PERFECT GROUND
FOOTING IMPEDANCE (RHO=4.57 M)
MAX-TO-MIN RATIO (DB)
FREQUENCY (KHZ)
0
2
4
6
8
10
12
14
16
18
20
22
400
420
440
460
480
500

(b)

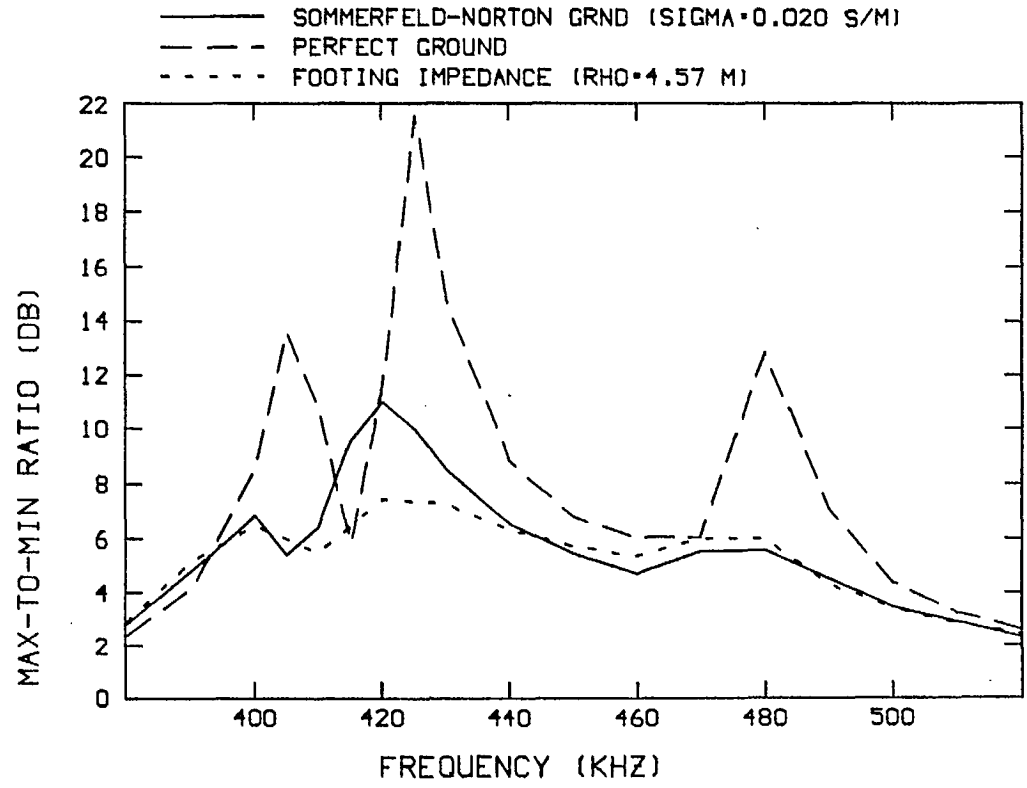
SOMMERFELD-NORTON GRND (SIGMA=0.020 S/M)
PERFECT GROUND
FOOTING IMPEDANCE (RHO=4.57 M)
MAX-TO-MIN RATIO (DB)
FREQUENCY (KHZ)
0
2
4
6
8
10
12
14
16
18
20
22
400
420
440
460
480
500

(c)

Fig. 2.10

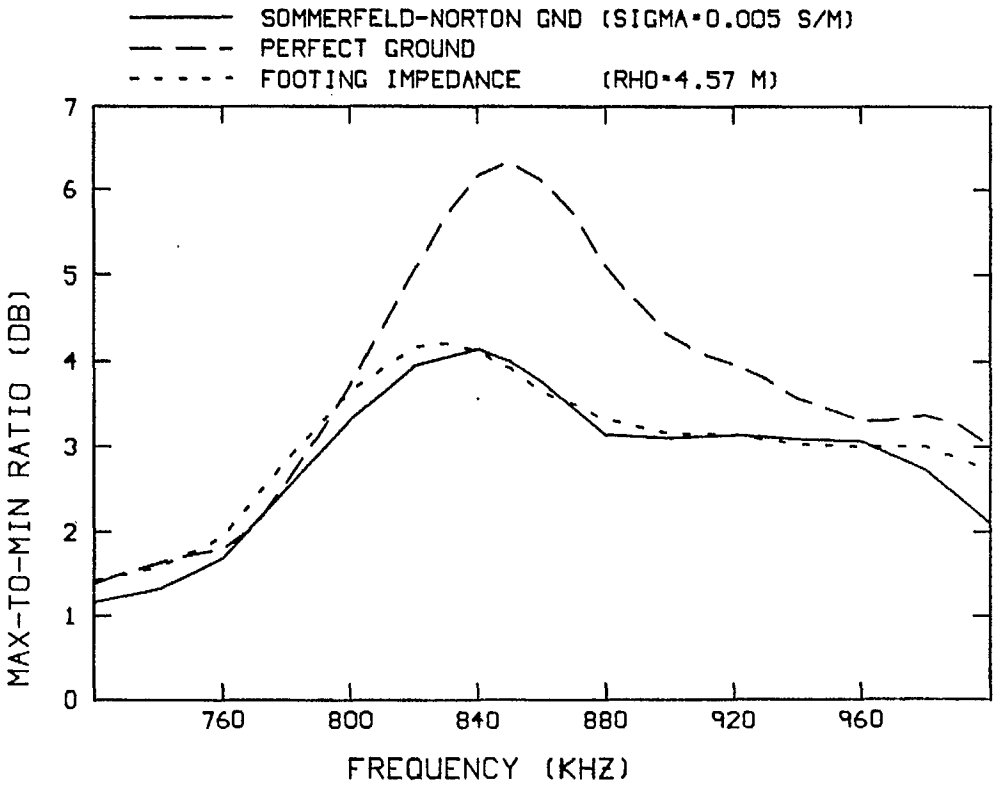

(a)

Fig. 2.11 - Frequency dependence of the max-to-min ratio of the azimuth pattern of the antenna near the power line of Fig. 2.8, throughout the two-wavelength loop resonance frequency range. The results obtained with the footing impedance are uniformly close to those found with the Sommerfeld-Norton ground model.
(Fig. 2.11 (b) and (c) on next page)

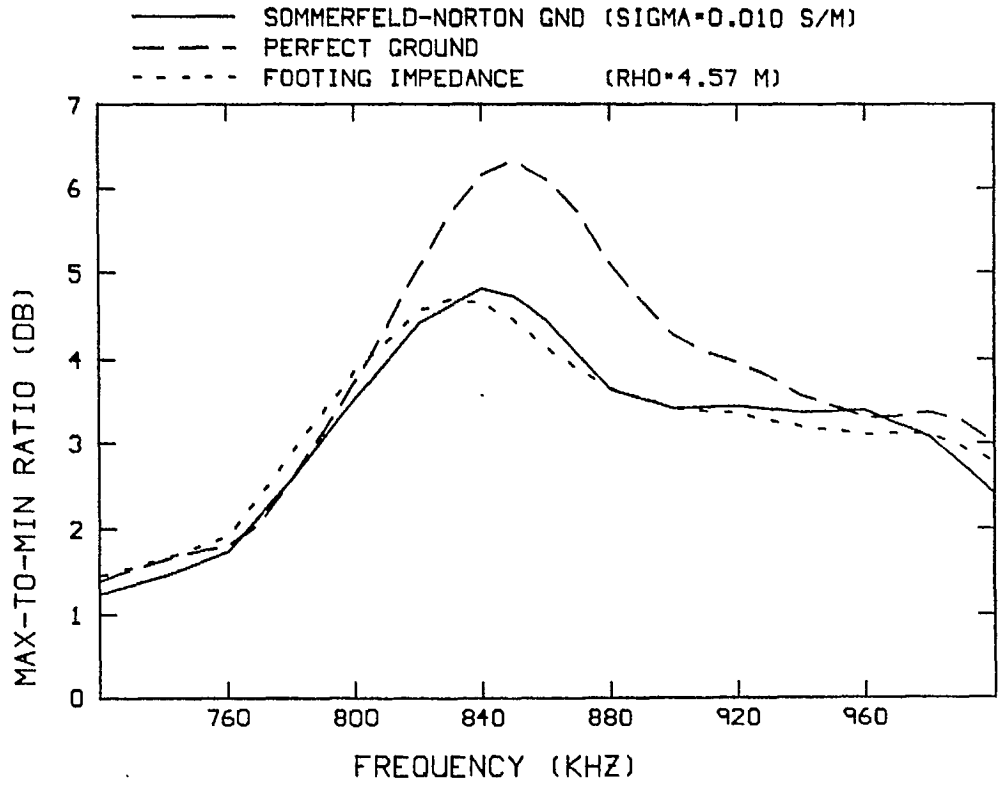
SOMMERFELD-NORTON GND (SIGMA=0.010 S/M)
PERFECT GROUND
FOOTING IMPEDANCE (RHO=4.57 M)
MAX-TO-MIN RATIO (DB)
0
1
2
3
4
5
6
7
760
800
840
880
920
960
FREQUENCY (KHZ)

(b)

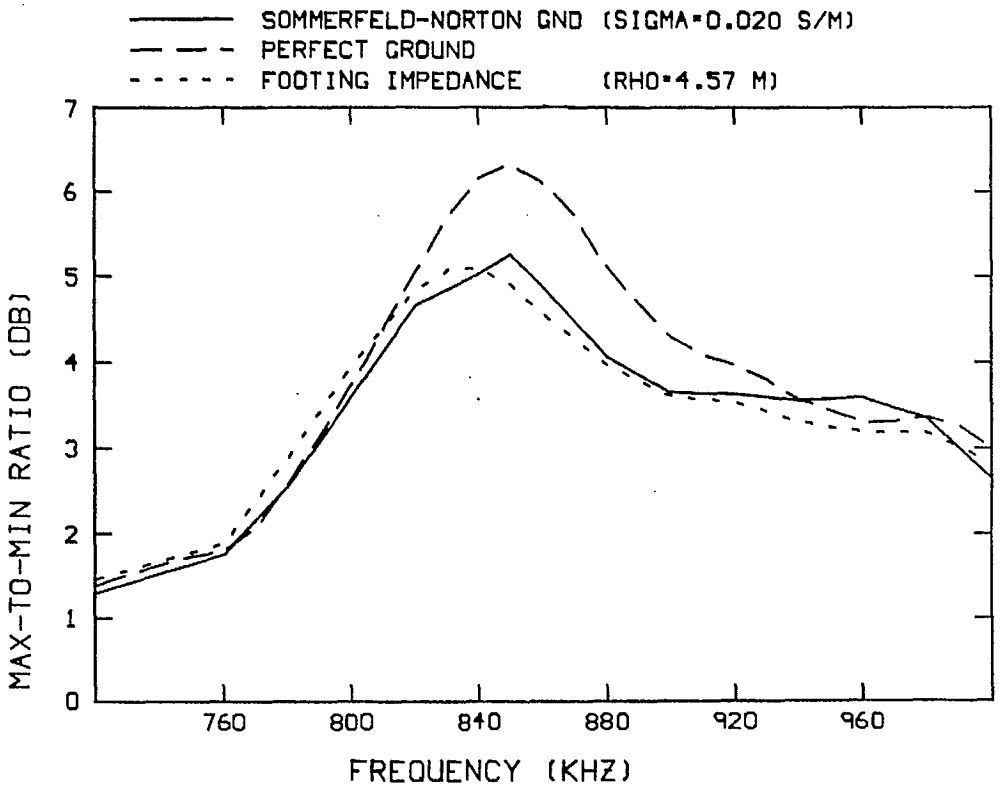
SOMMERFELD-NORTON GND (SIGMA=0.020 S/M)
PERFECT GROUND
FOOTING IMPEDANCE (RHO=4.57 M)
MAX-TO-MIN RATIO (DB)
0
1
2
3
4
5
6
7
760
800
840
880
920
960
FREQUENCY (KHZ)

(c)

Fig. 2.11

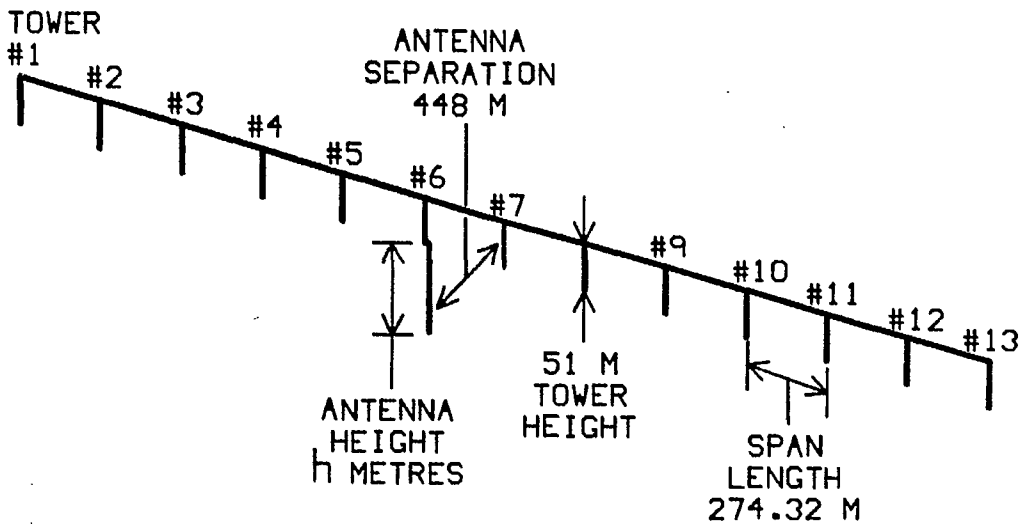

Fig. 3.1 - A 13-tower, straight, evenly-spaced power line illuminated by an omni-directional antenna.

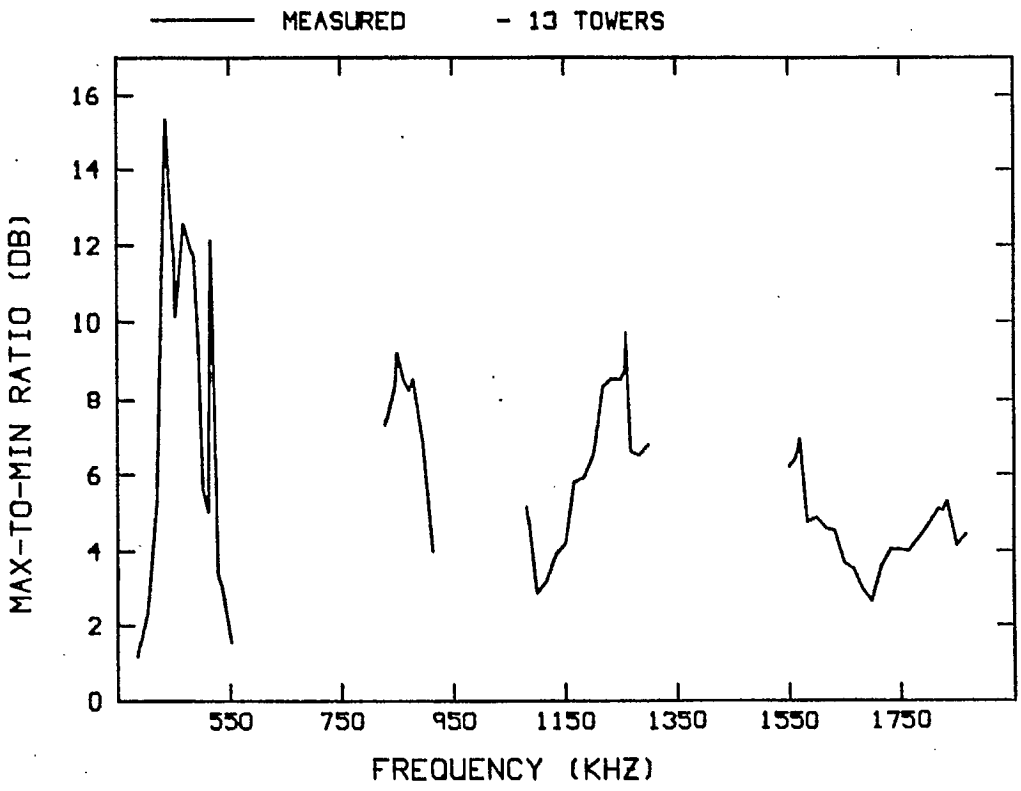

Fig. 3.2 - The measured max-to-min ratio data plotted as a function of the frequency.

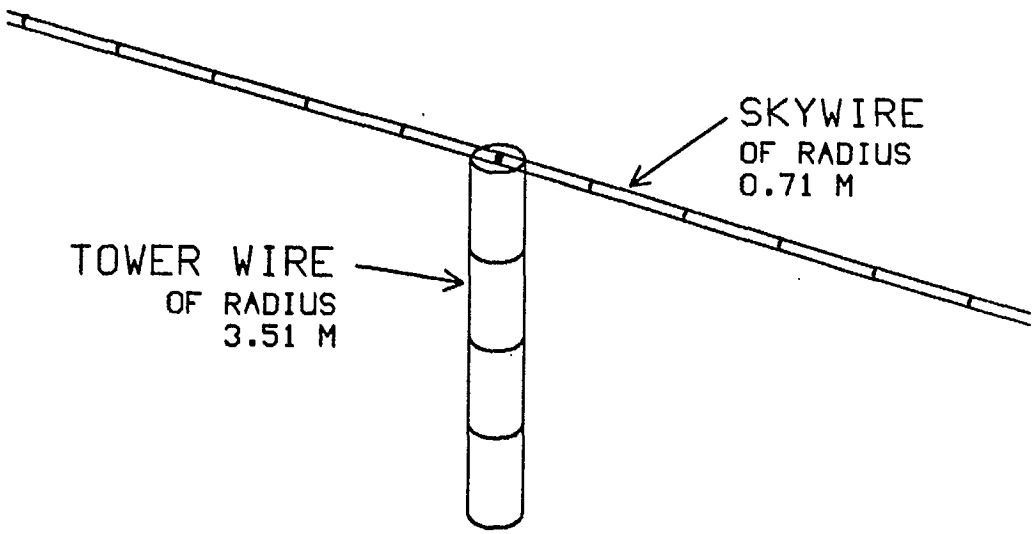

Fig. 3.3 - The "single-wire tower" or "straight tower" computer model.

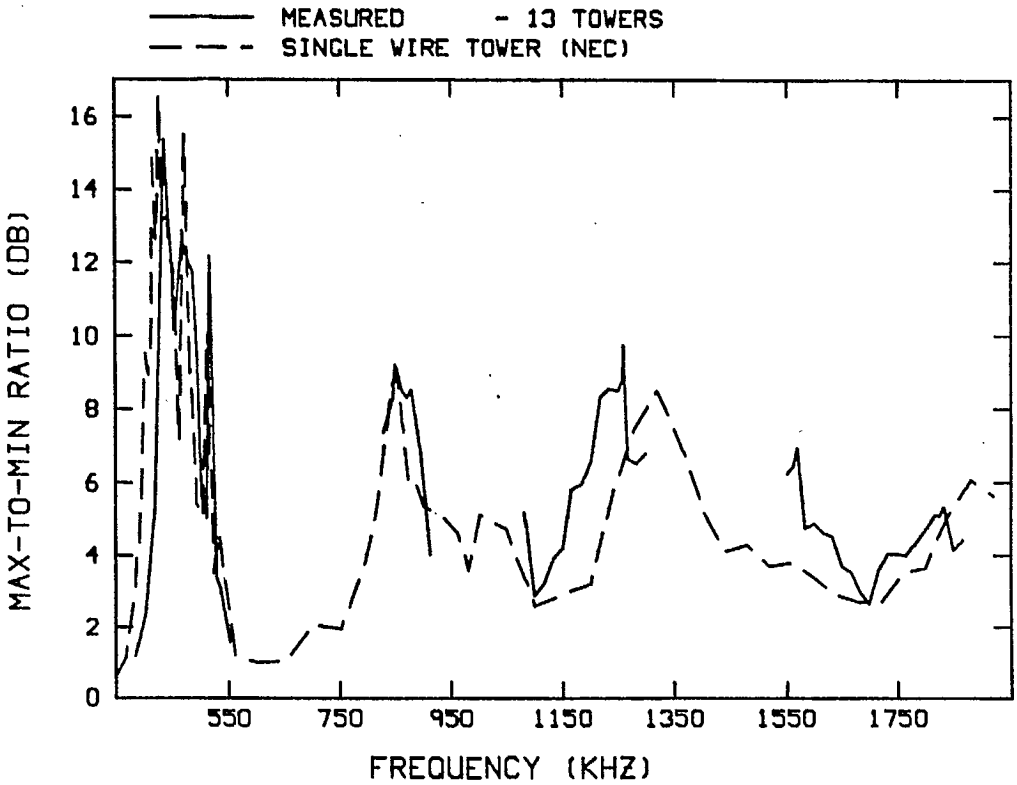

Fig. 3.4(a) - The max-to-min ratio as a function of the frequency for the "single-wire tower" model.

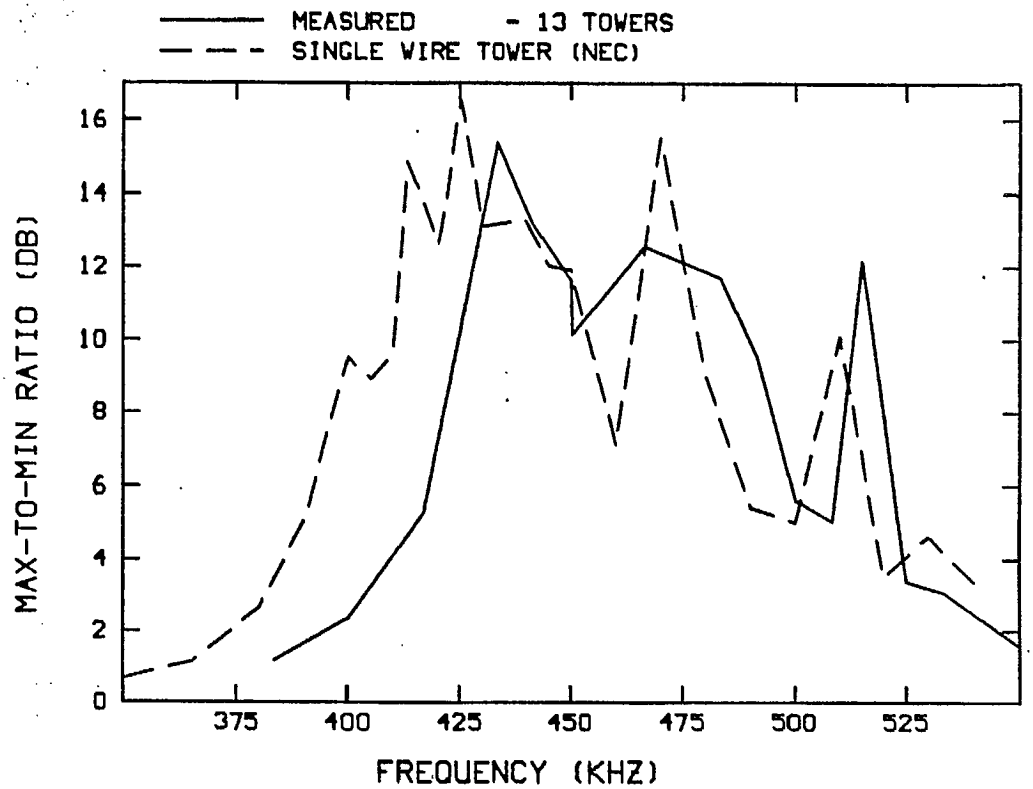

Fig. 3.4(b) - The max-to-min ratio enlarged in the one-wavelength loop resonance frequency band.

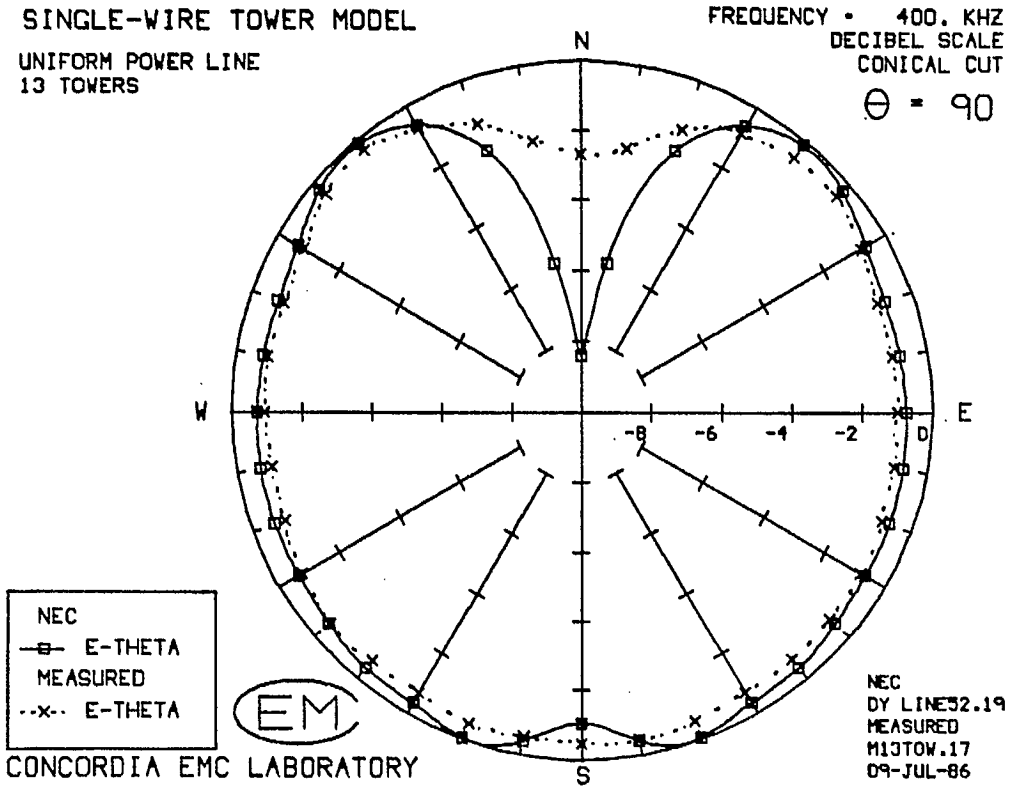

Fig. 3.5(a) - The azimuth pattern at 400 kHz with the "single-wire tower" model.

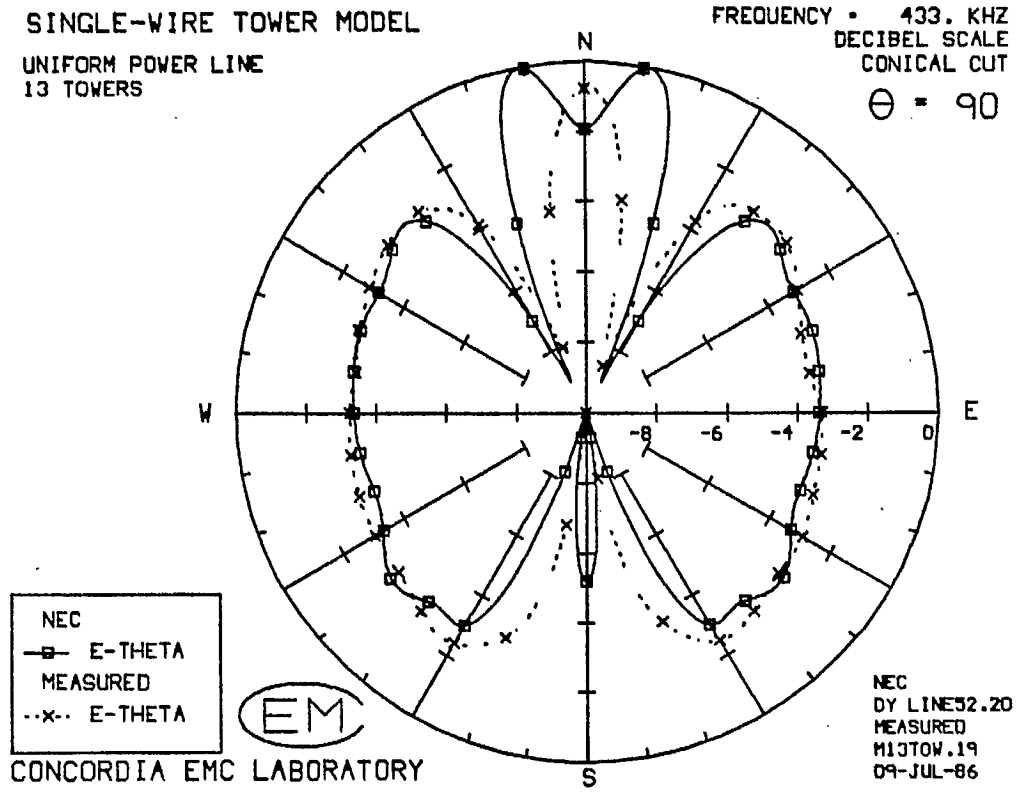

Fig. 3.5(b) - The azimuth pattern at 433.33 kHz with the "single-wire tower" model.

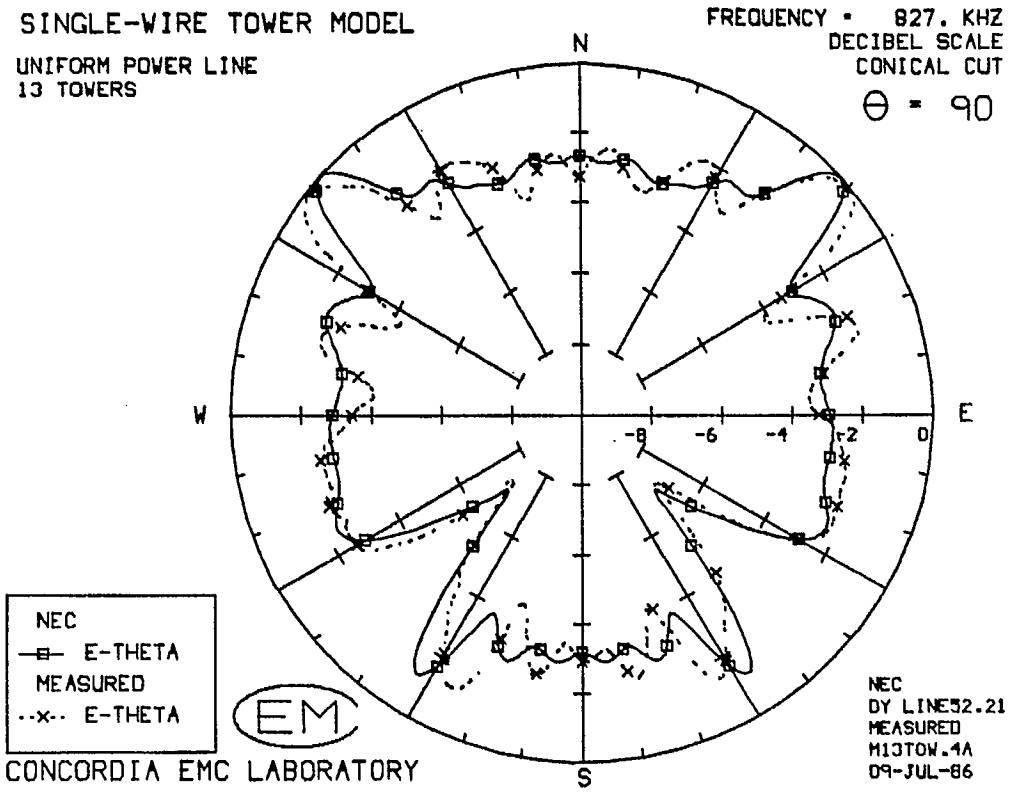

Fig. 3.6(a) - The azimuth pattern at 826.67 kHz with the "single-wire tower" model.

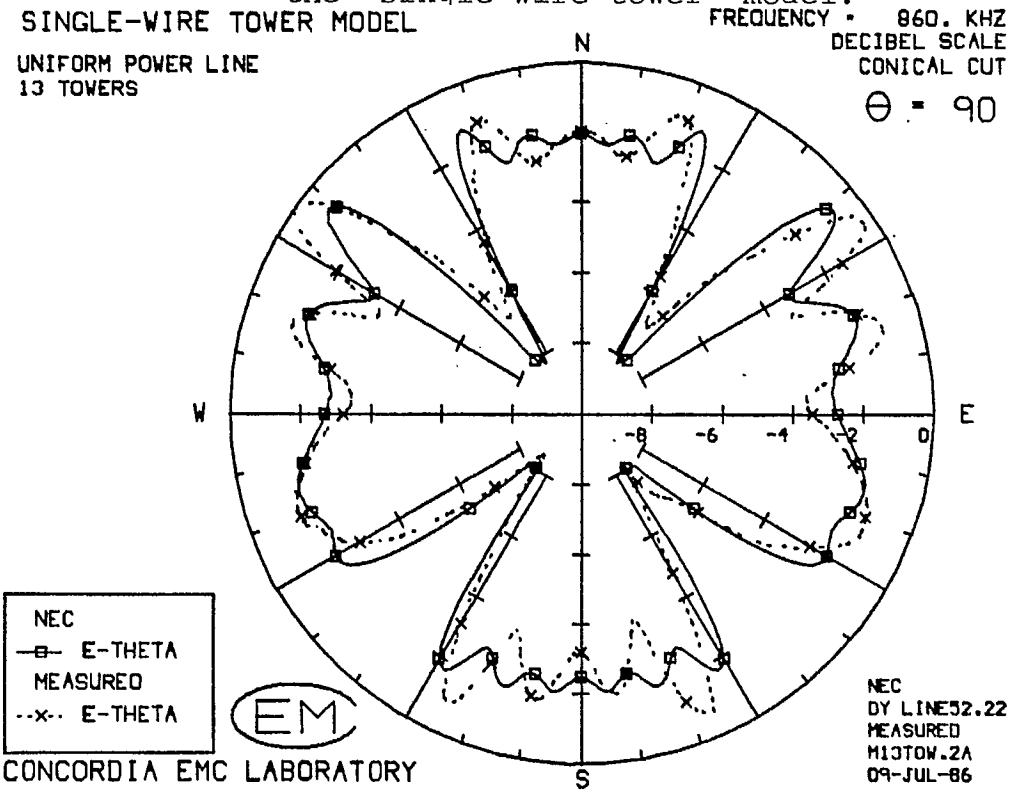

Fig. 3.6(b) - The azimuth pattern at 860 kHz with the "single-wire tower" model.

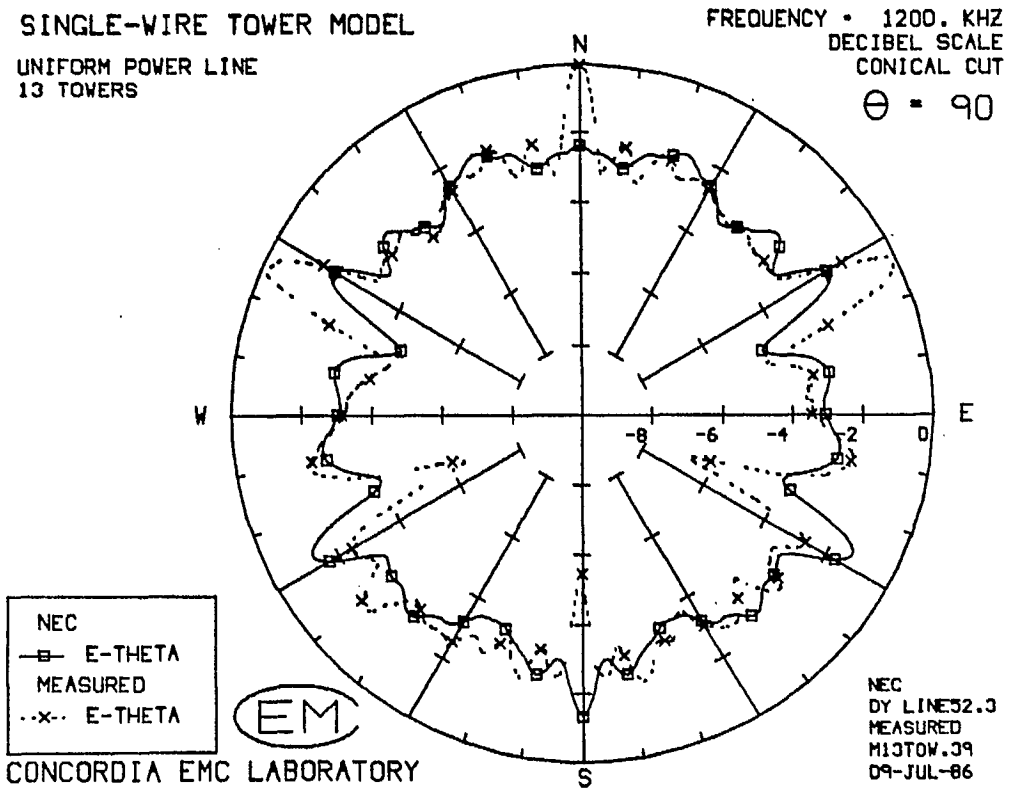

Fig. 3.7(a) - The azimuth pattern at 1200 kHz with the "single-wire tower" model.

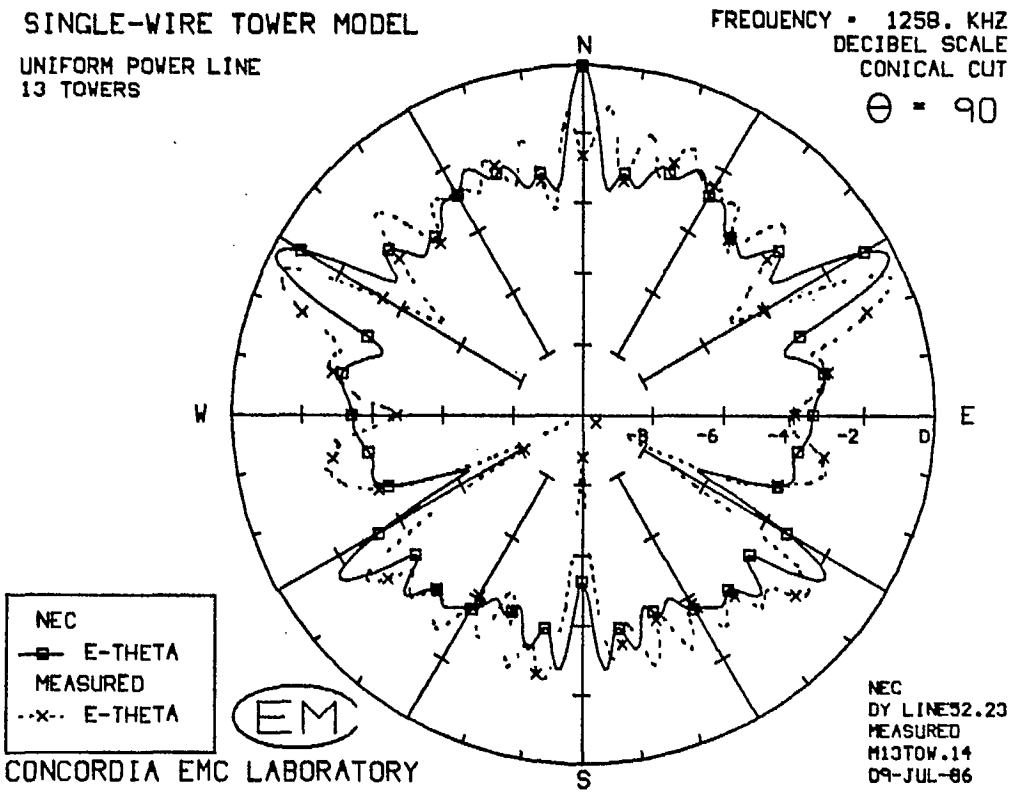

Fig. 3.7(b) - The azimuth pattern at 1258.33 kHz with the "single-wire tower" model.

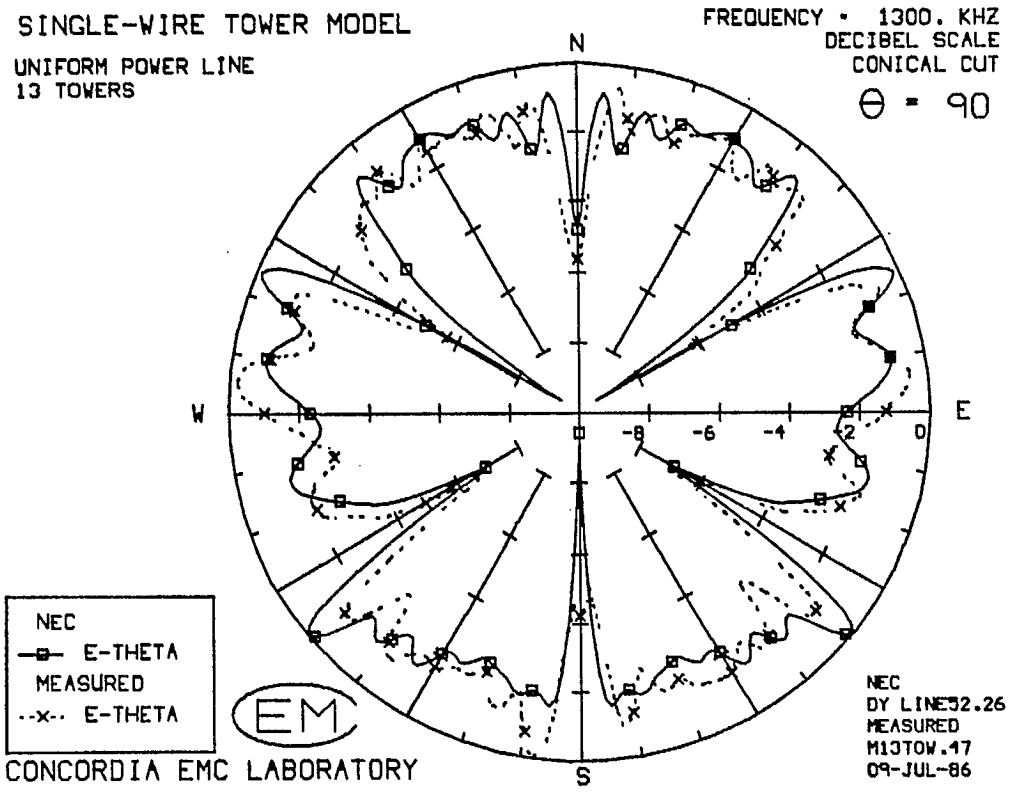

Fig. 3.7(c) - The azimuth pattern at 1300 kHz with the "single-wire tower" model.

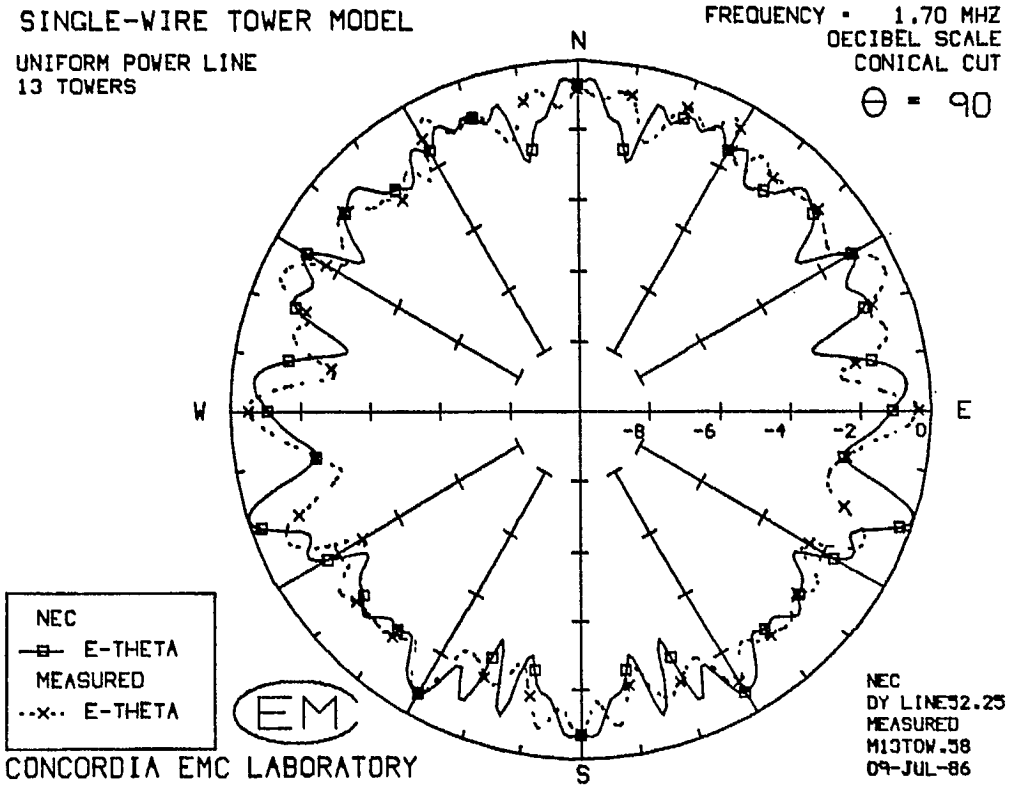

Fig. 3.8(a) - The azimuth pattern at 1700 kHz with the "single-wire tower" model.

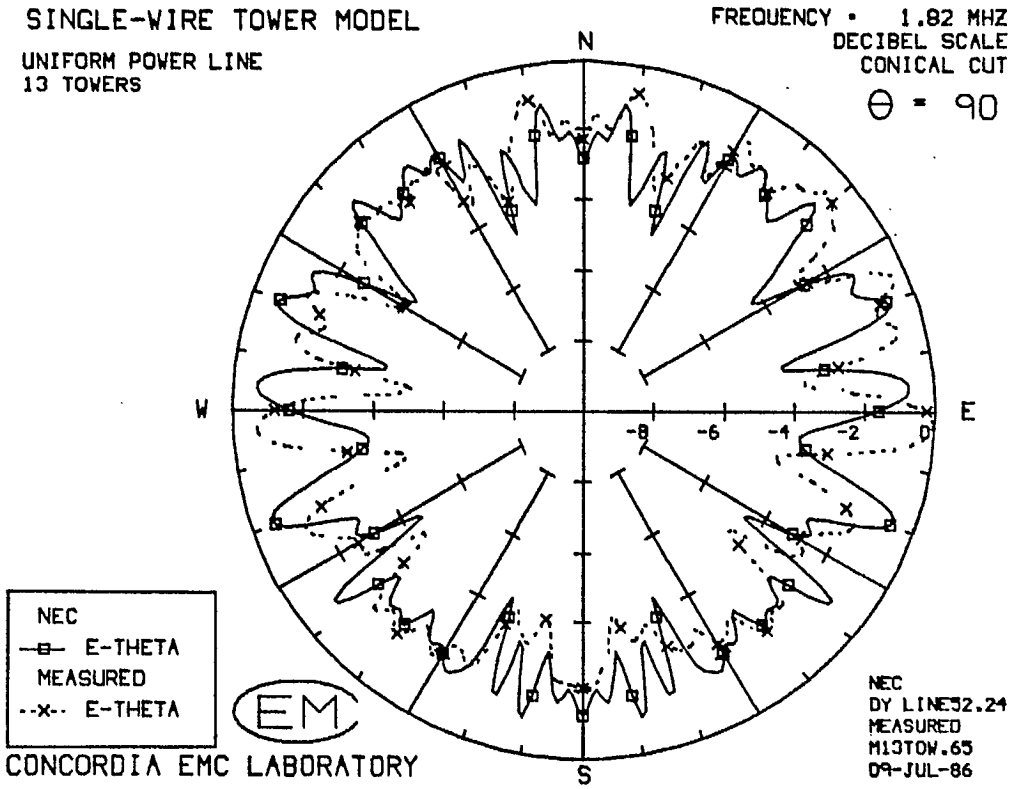

Fig. 3.8(b) - The azimuth pattern at 1816.67 kHz with the "single-wire tower" model.

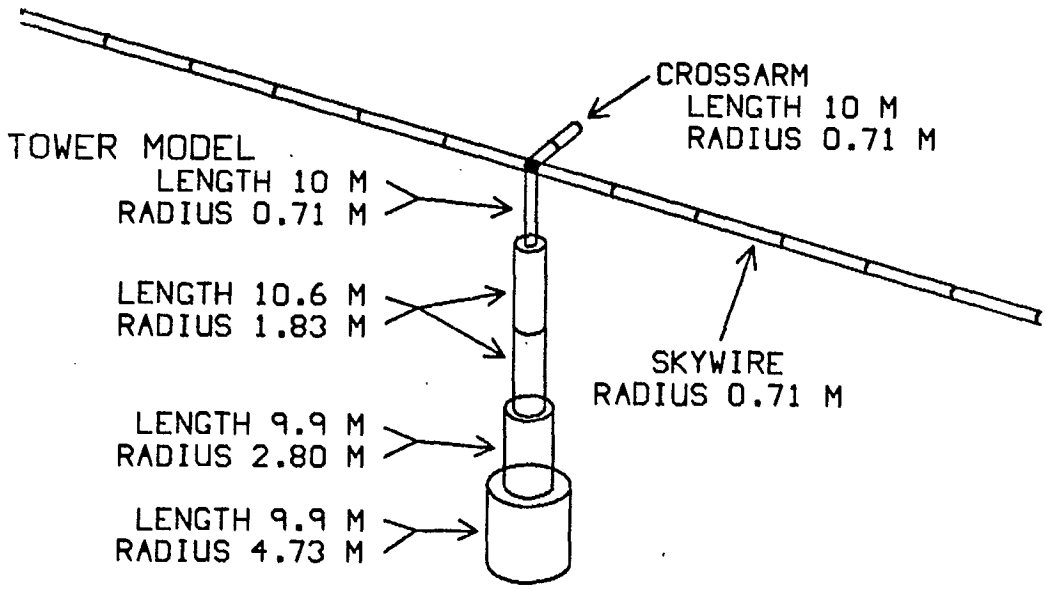

Fig. 3.9 - The "tapered tower" model, which uses a single skywire of equivalent radius 0.71 m, centered at the top of the tower, and a crossarm of length 10 m.

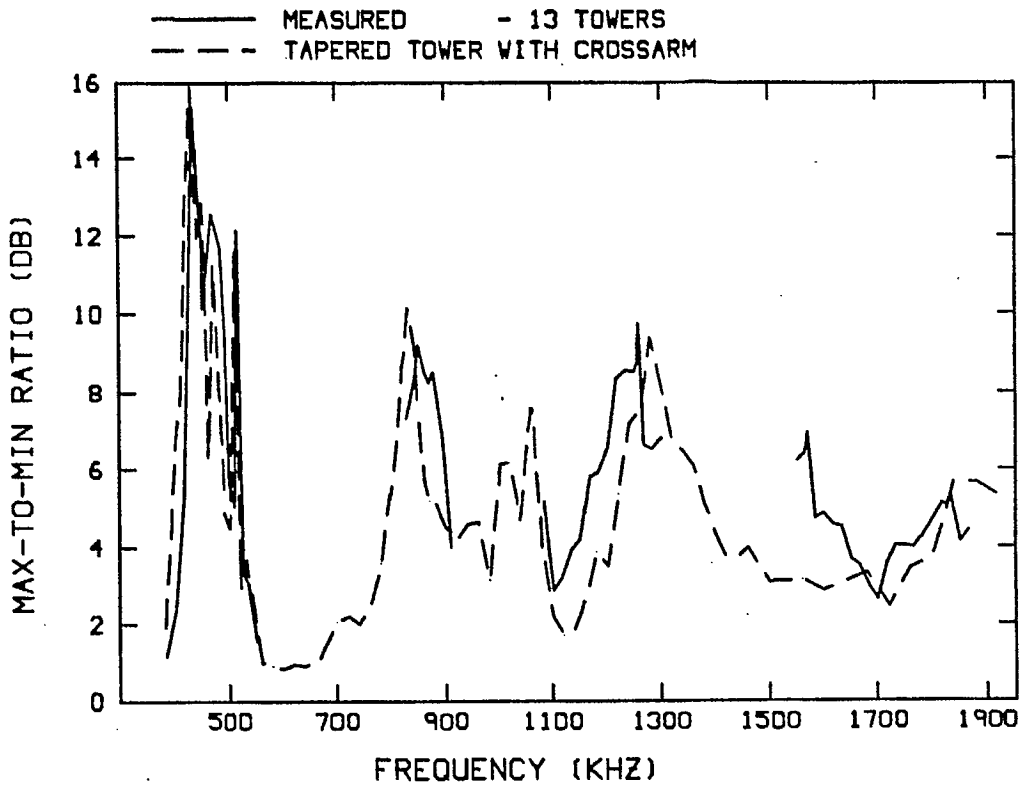

Fig. 3.10(a) - The max-to-min ratio as a function of the frequency for the "tapered tower" model.

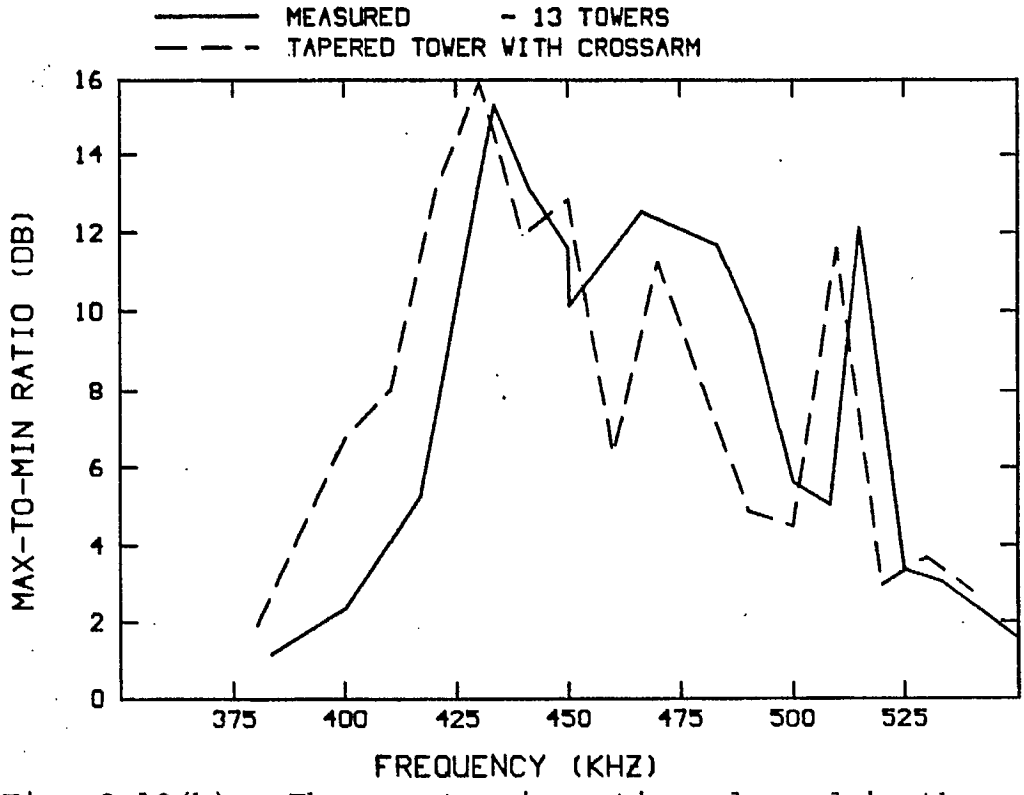

Fig. 3.10(b) - The max-to-min ratio enlarged in the one-wavelength loop resonance frequency band.

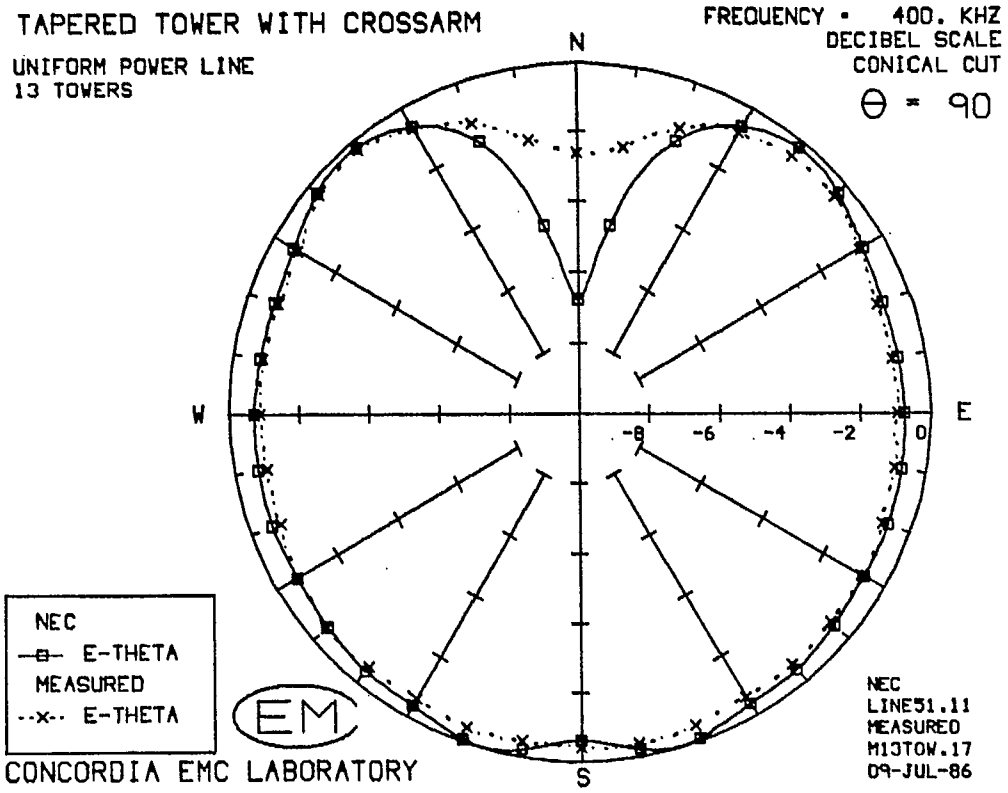

Fig. 3.11(a) - The azimuth pattern at 400 kHz with the "tapered tower" model.

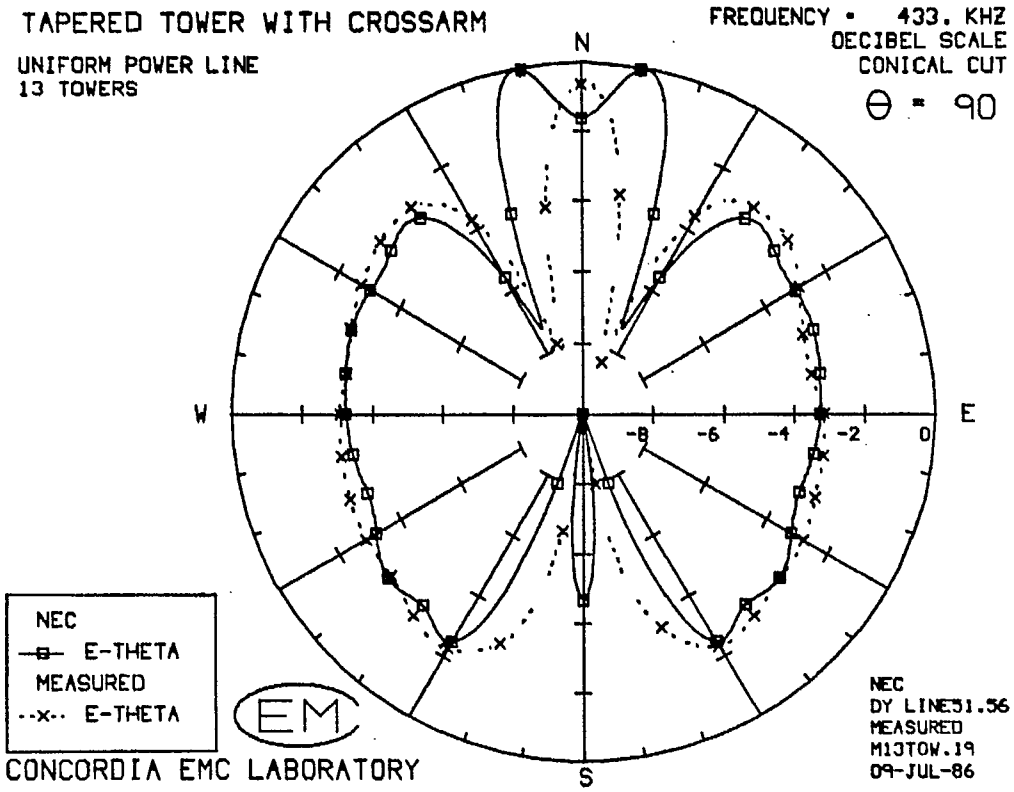

Fig. 3.11(b) - The azimuth pattern at 433.33 kHz with the "tapered tower" model.

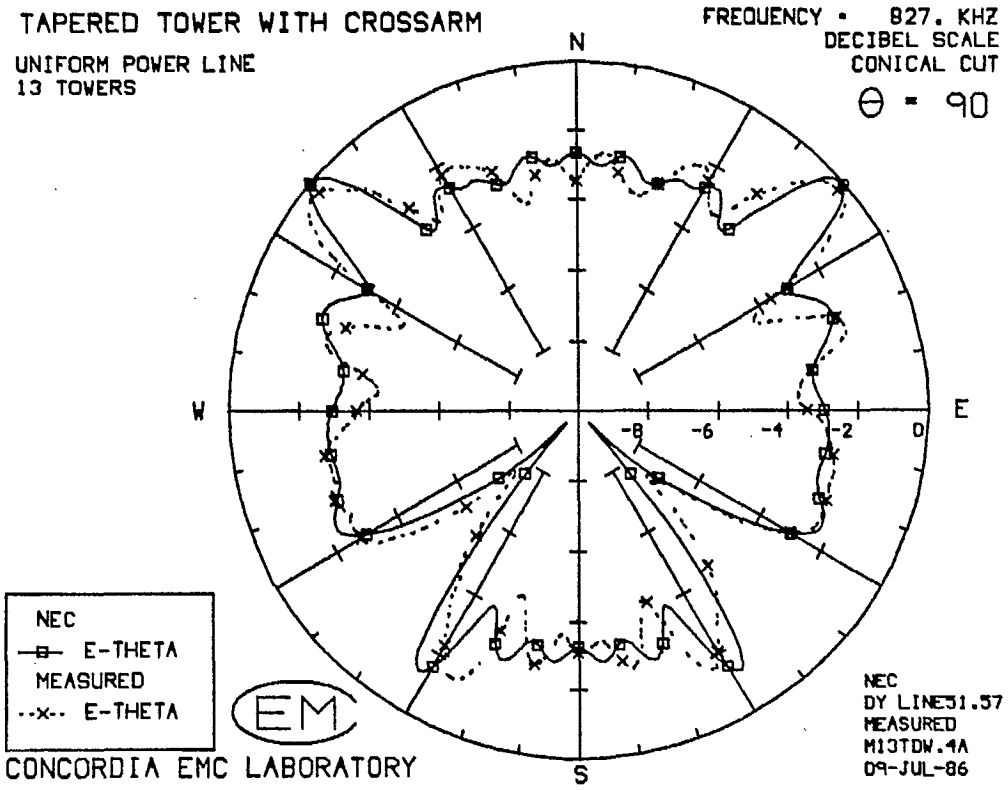

Fig. 3.12(a) - The azimuth pattern at 826.67 kHz with the "tapered tower" model.

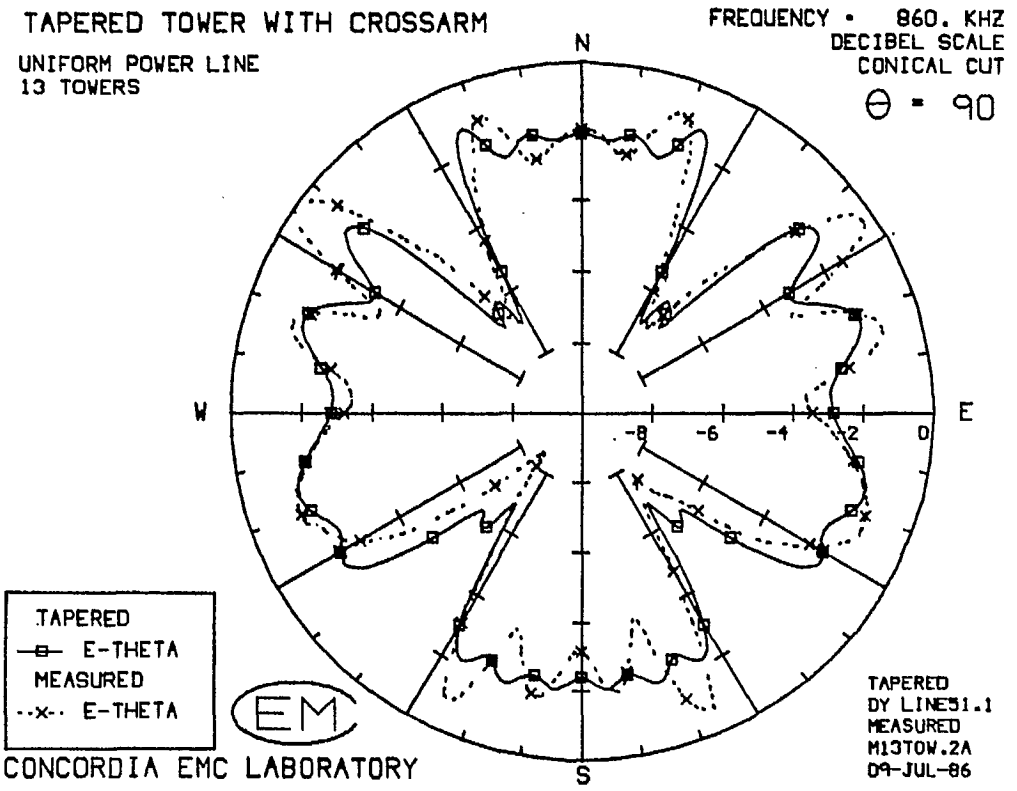

Fig. 3.12(b) - The azimuth pattern at 860 kHz with the "tapered tower" model.

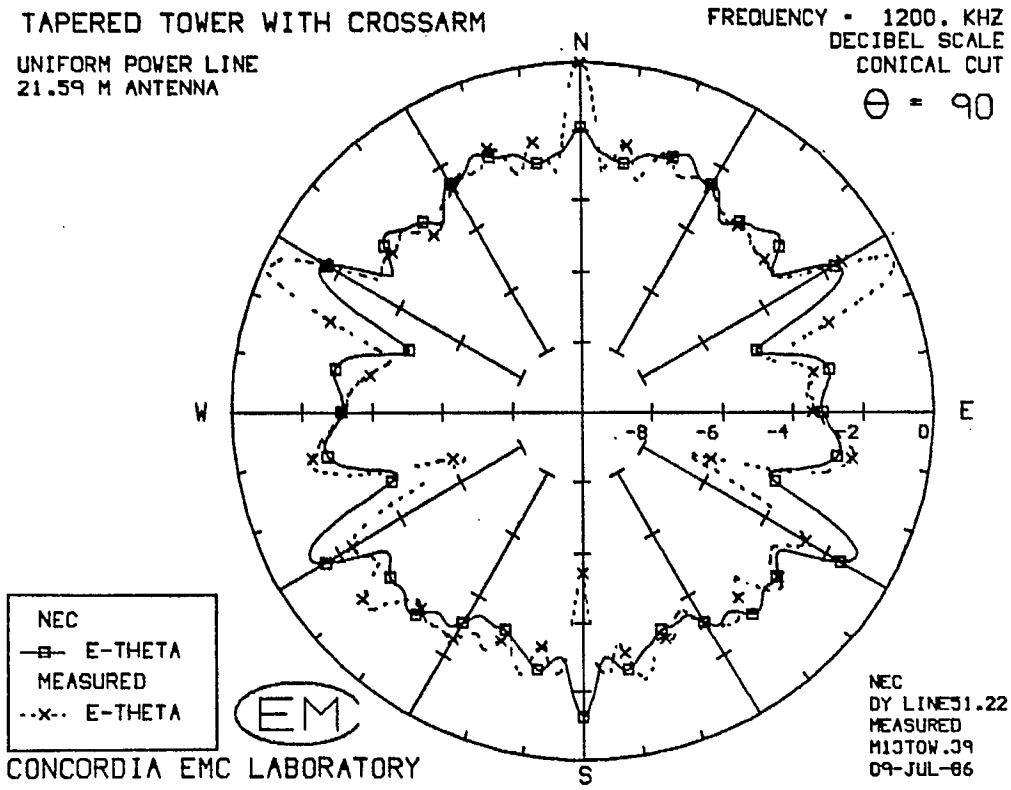

Fig. 3.13(a) - The azimuth pattern at 1200 kHz with the "tapered tower" model.

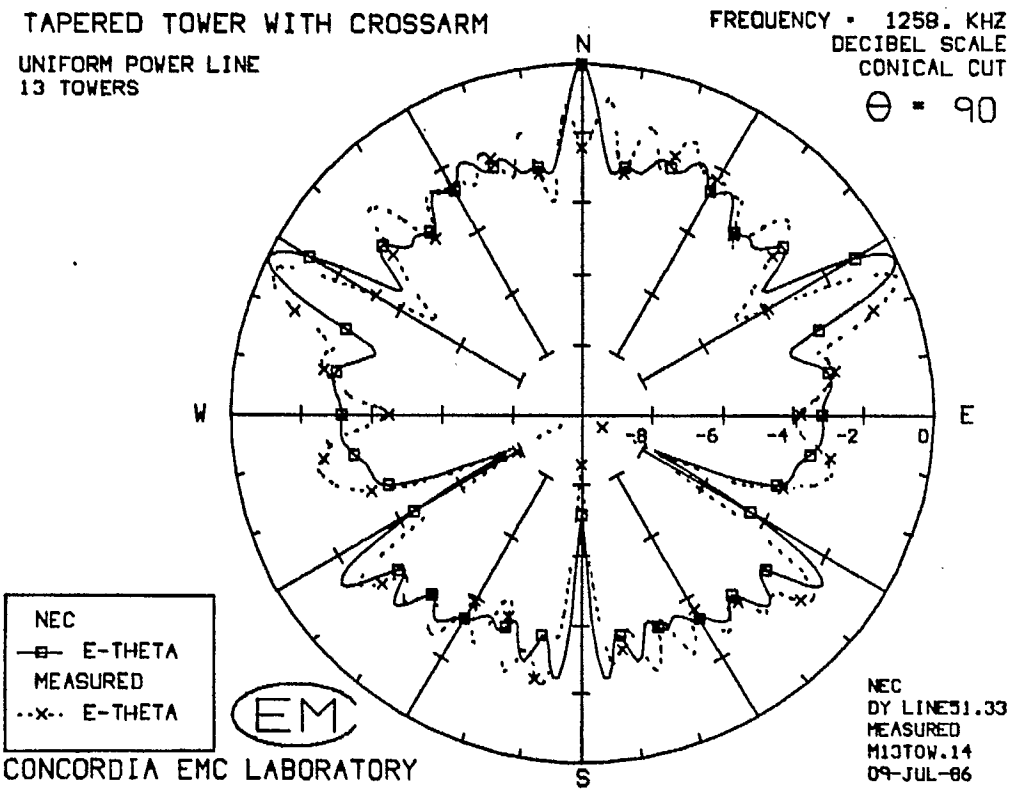

Fig. 3.13(b) - The azimuth pattern at 1258.33 kHz with the "tapered tower" model.

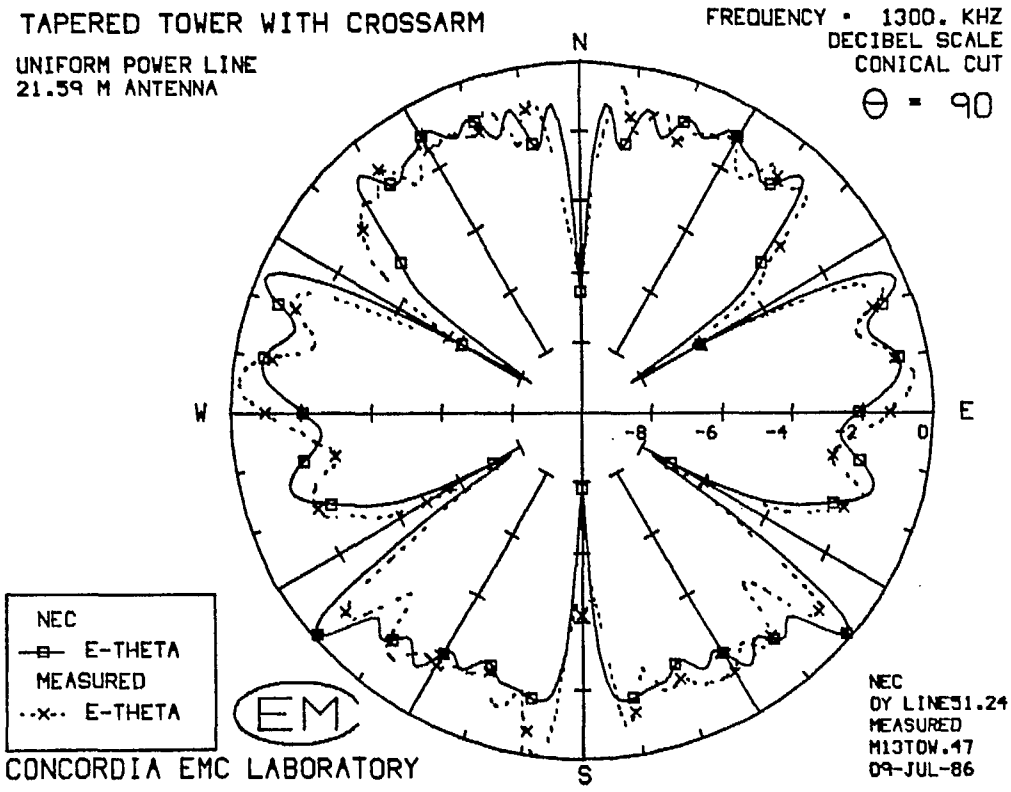

Fig. 3.13(c) - The azimuth pattern at 1300 kHz with the "tapered tower" model.

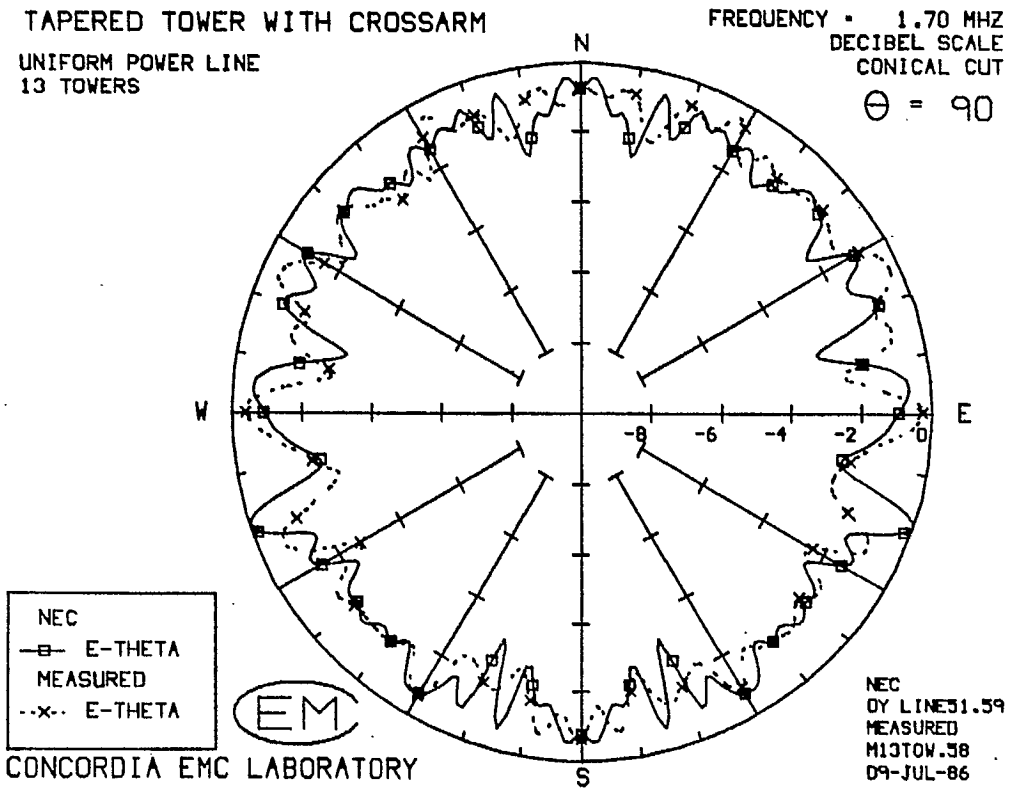

Fig. 3.14(a) - The azimuth pattern at 1700 kHz with the "tapered tower" model.

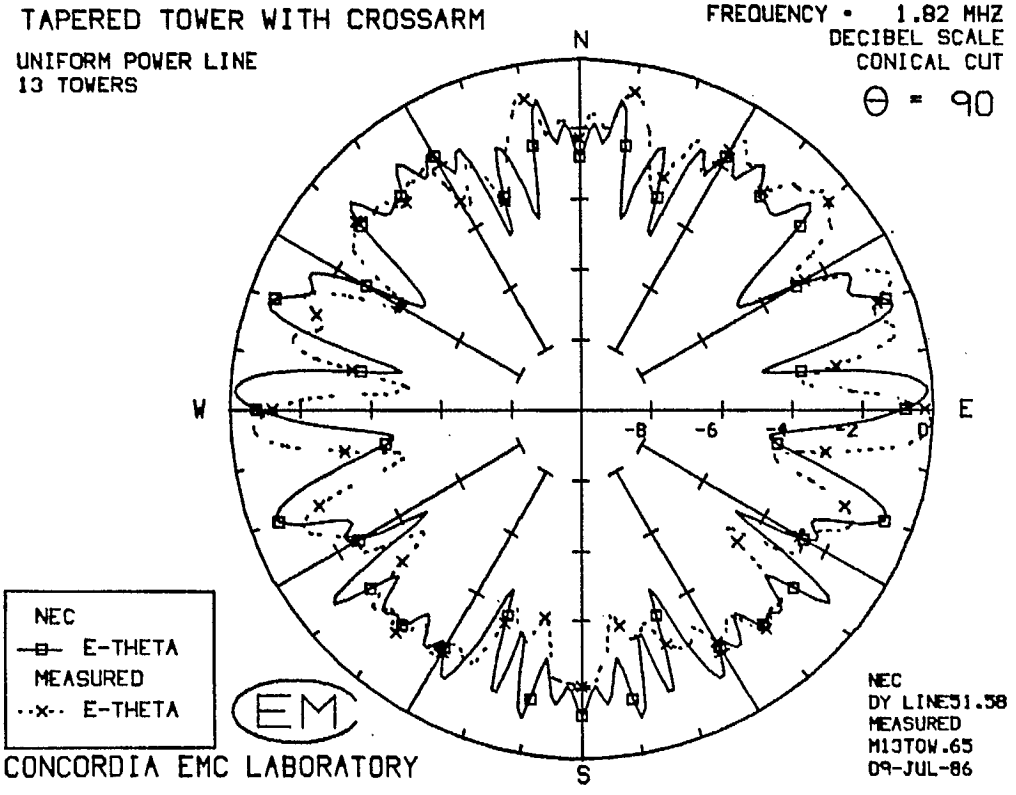

Fig. 3.14(b) - The azimuth pattern at 1816.67 kHz with the "tapered tower" model.

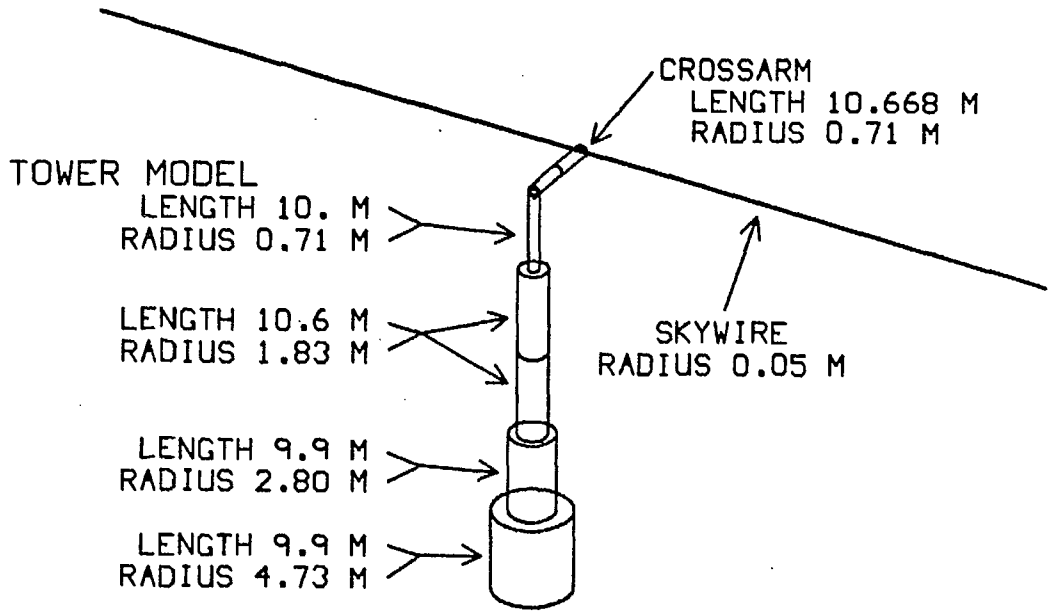

Fig. 3.15 - The "offset skywire" model uses a tapered tower, and has a single, thin skywire connected at the end of the crossarm.

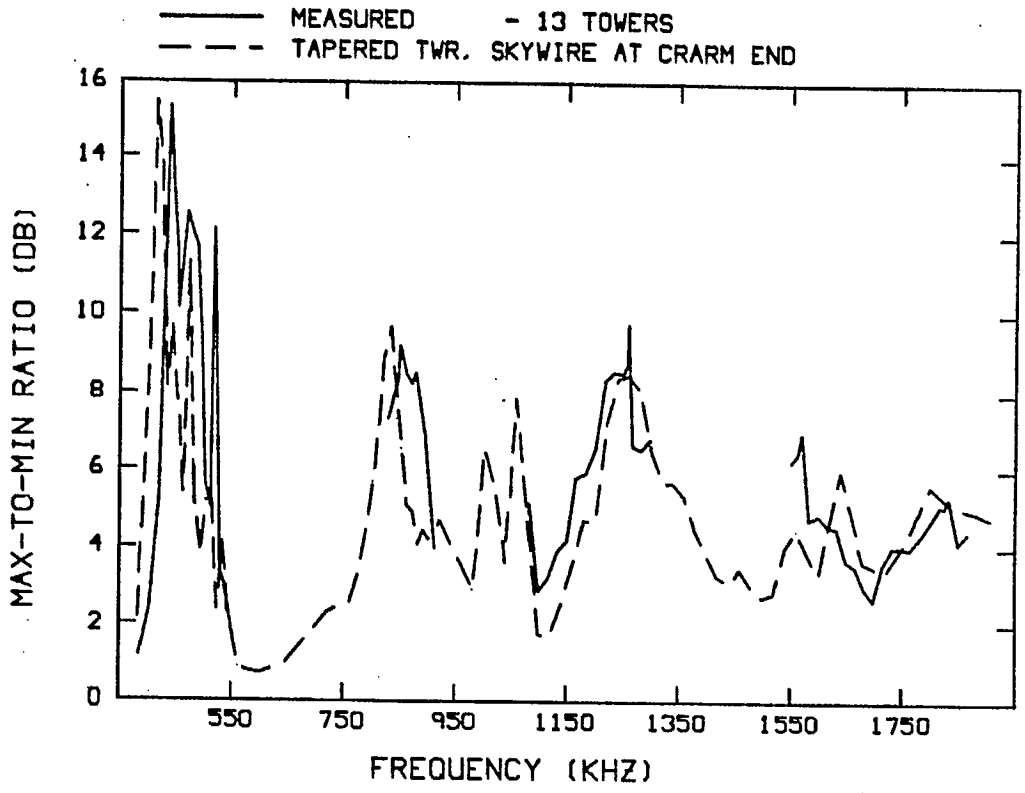

Fig. 3.16(a) - The max-to-min ratio as a function of the frequency for the "offset skywire" model.

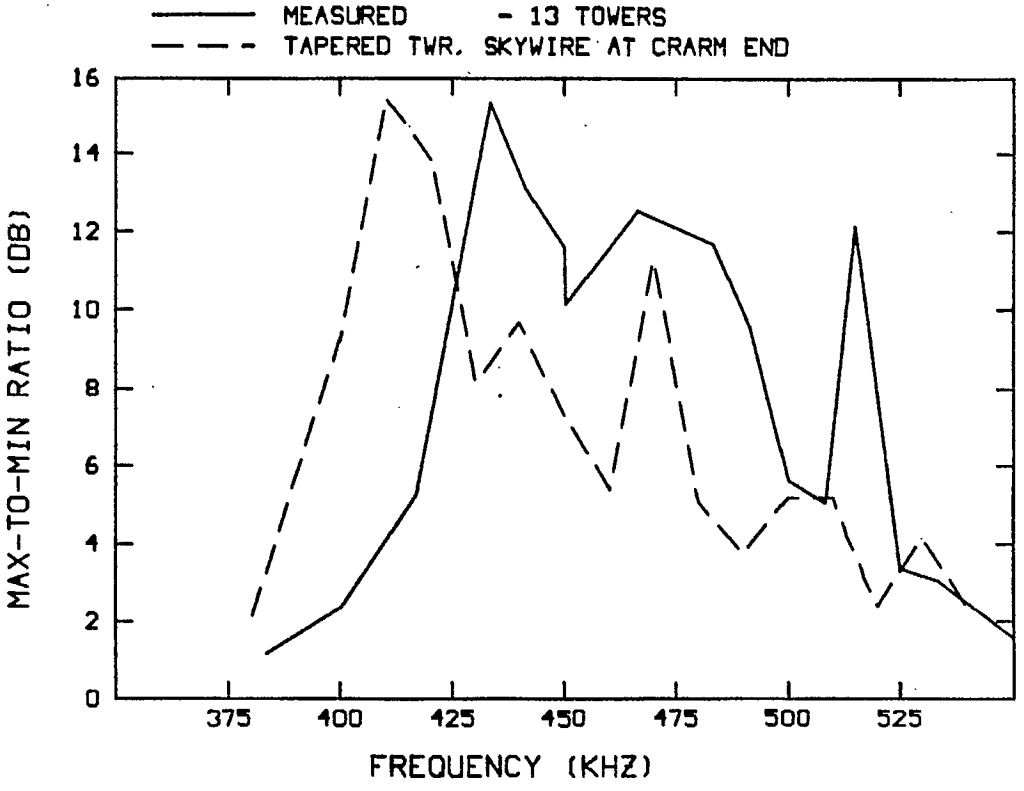

Fig. 3.16(b) - The max-to-min ratio enlarged in the one-wavelength loop resonance frequency band.

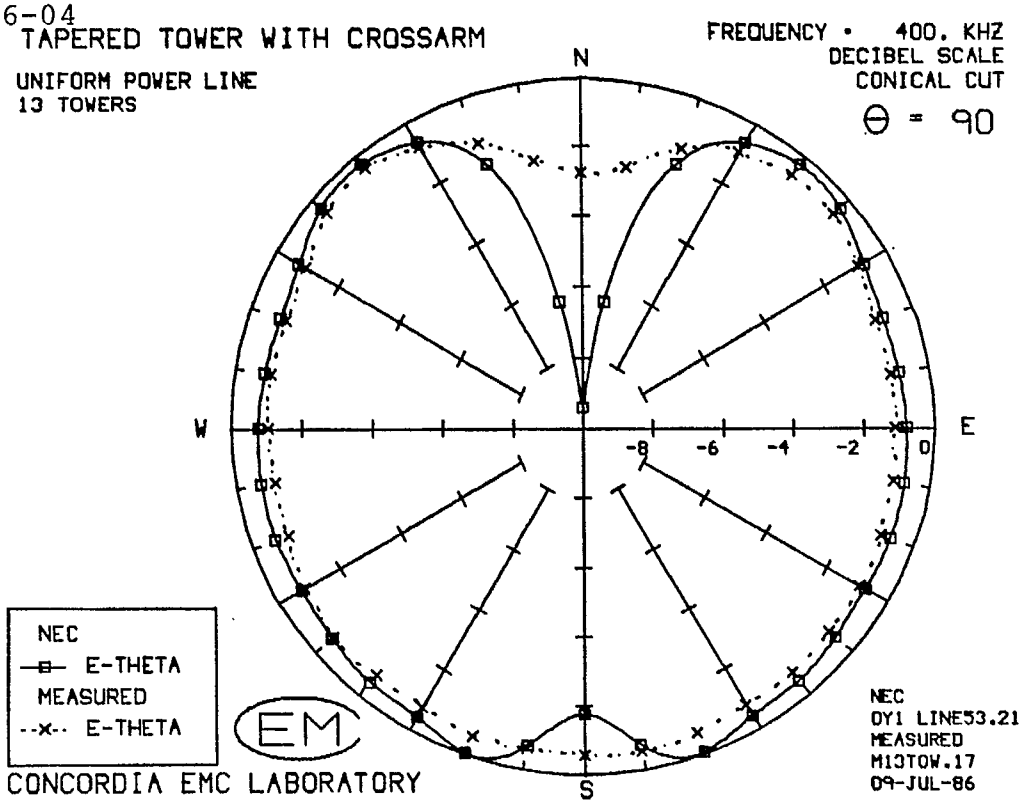

Fig. 3.17(a) - The azimuth pattern at 400 kHz with the "offset skywire" model.

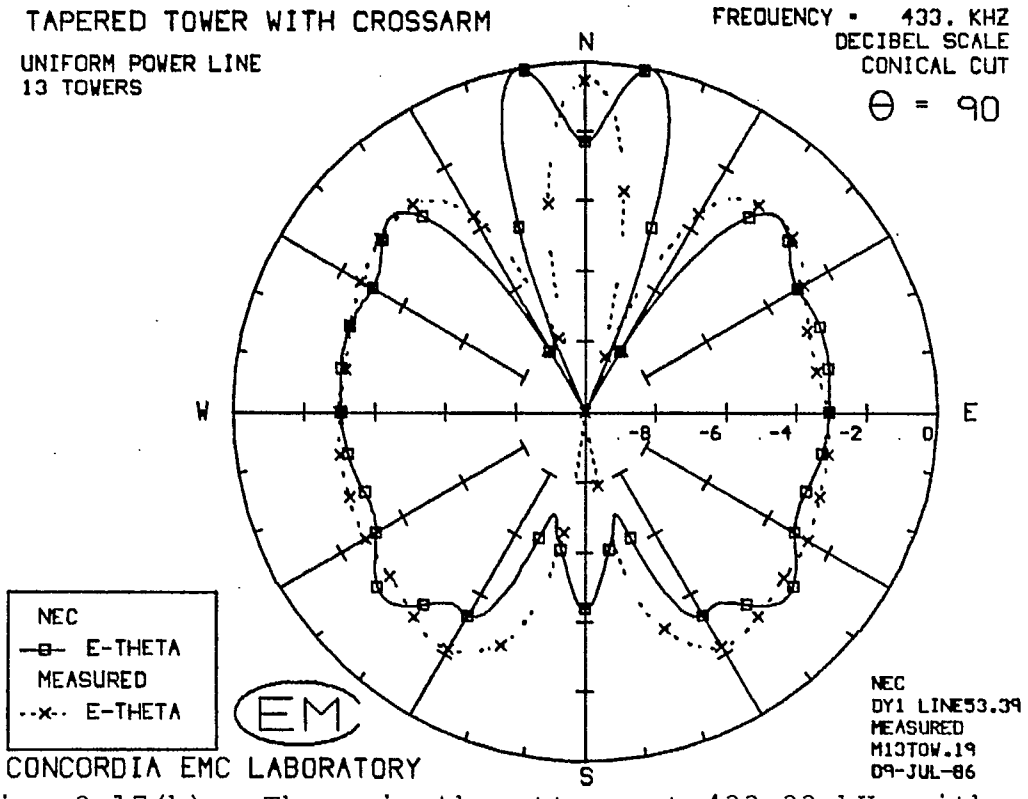

Fig. 3.17(b) - The azimuth pattern at 433.33 kHz with the "offset skywire" model.

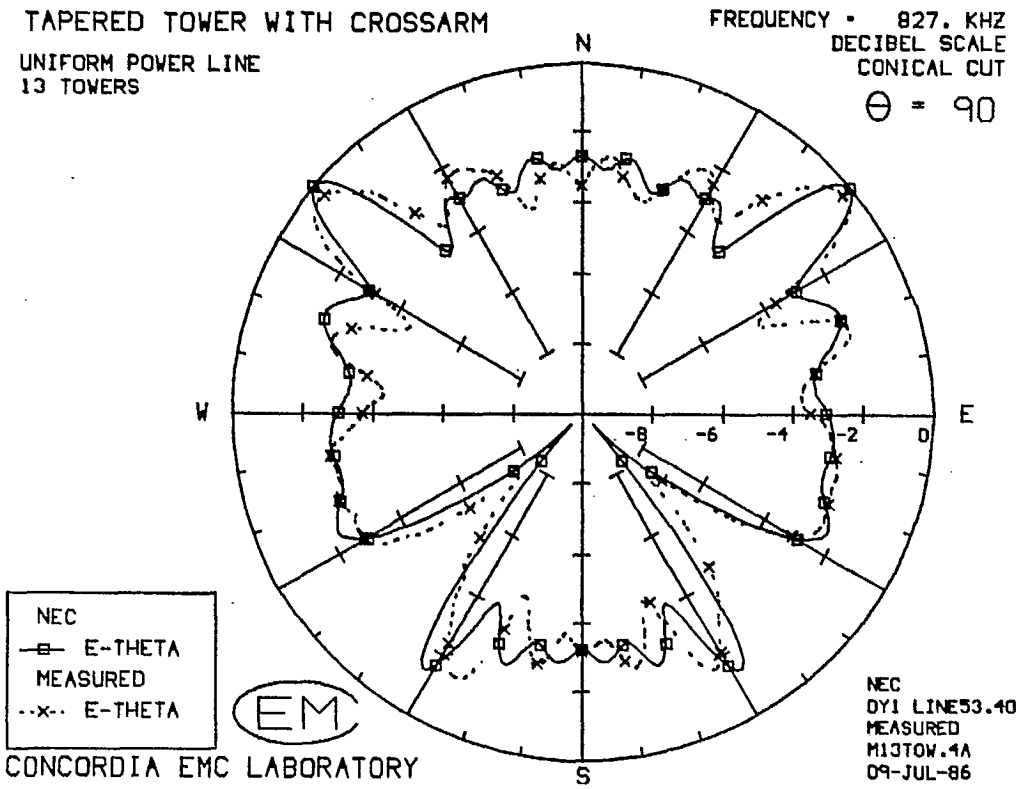

Fig. 3.18(a) - The azimuth pattern at 826.67 kHz with the "offset skywire" model.

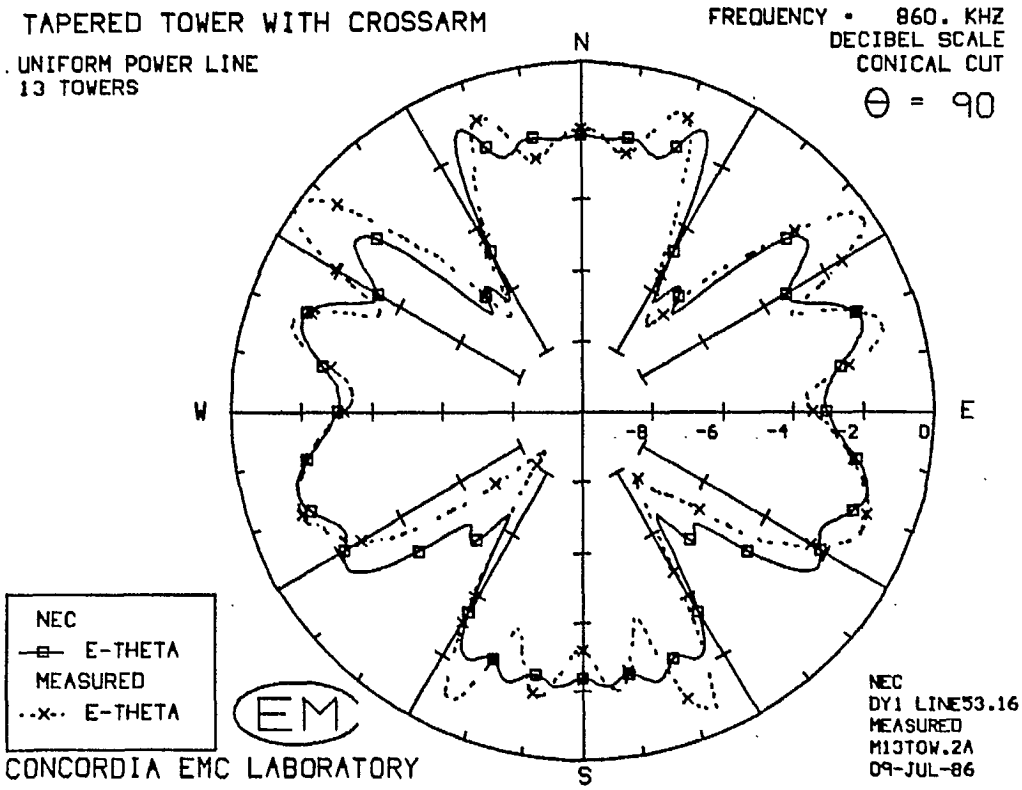

Fig. 3.18(b) - The azimuth pattern at 860 kHz with the "offset skywire" model.

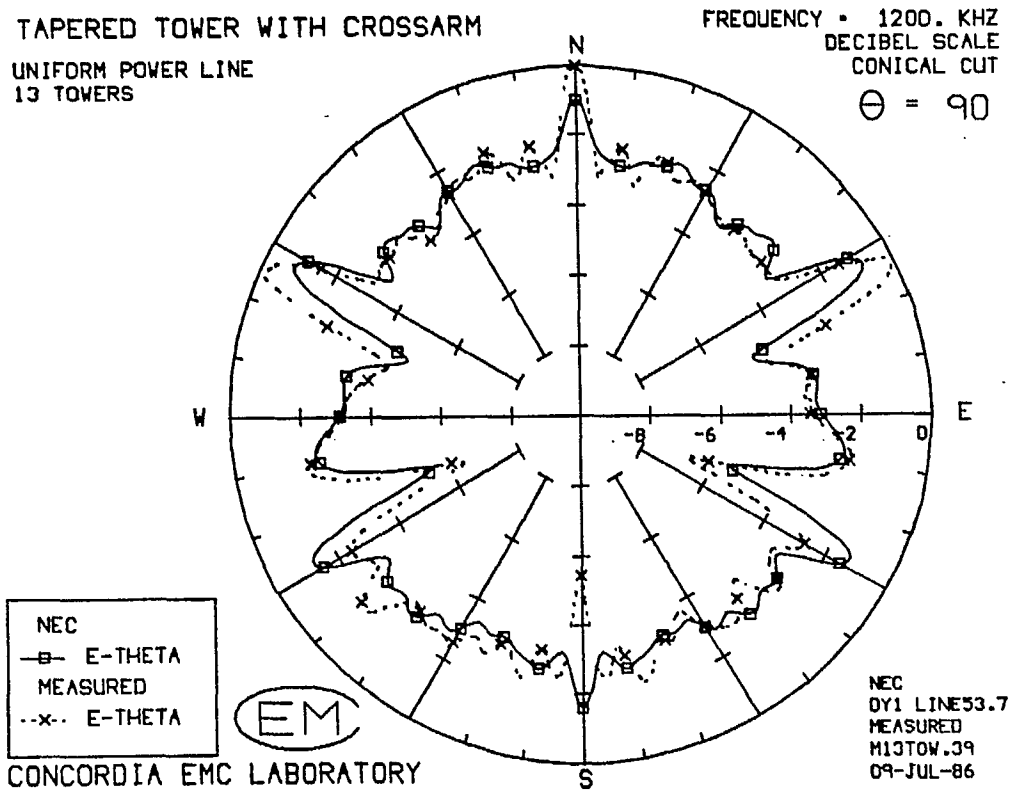

Fig. 3.19(a) - The azimuth pattern at 1200 kHz with the "offset skywire" model.

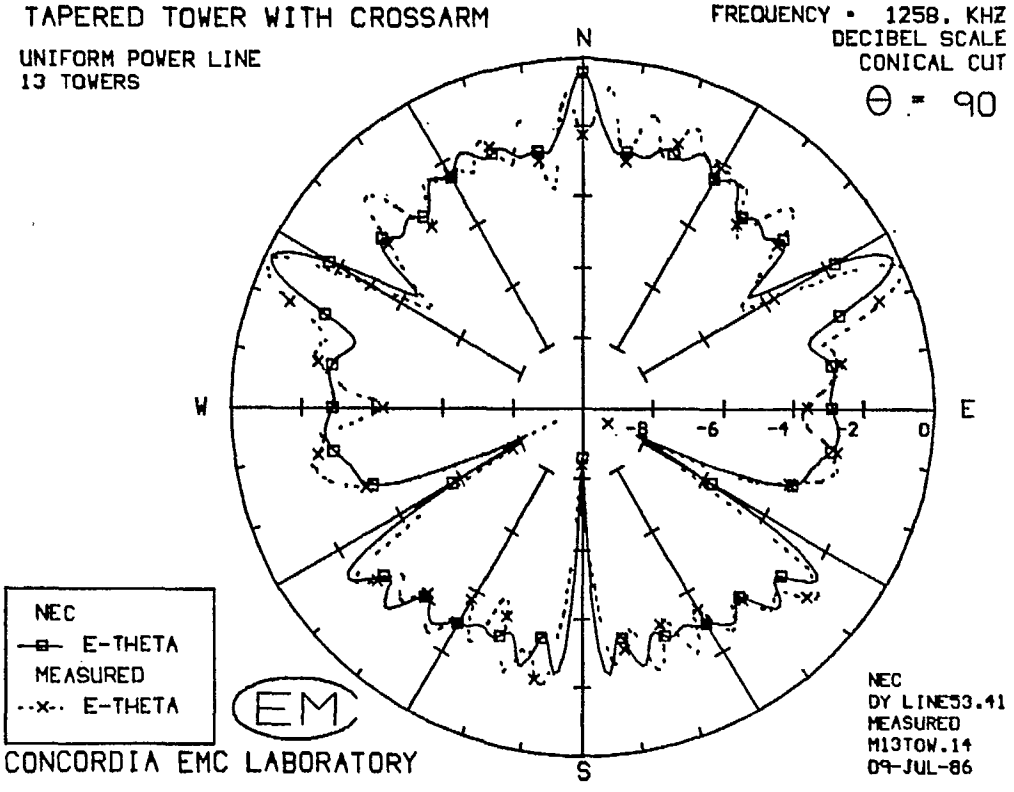

Fig. 3.19(b) - The azimuth pattern at 1258.33 kHz with the "offset skywire" model.

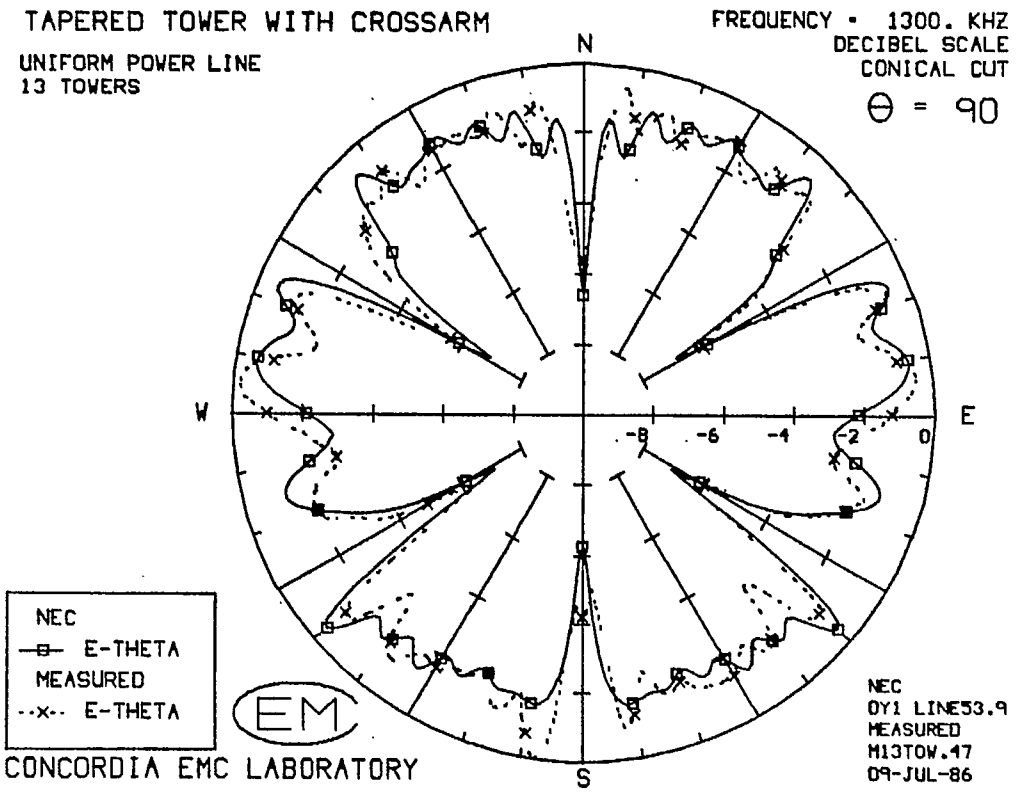

Fig. 3.19(c) - The azimuth pattern at 1300 kHz with the "offset skywire" model.

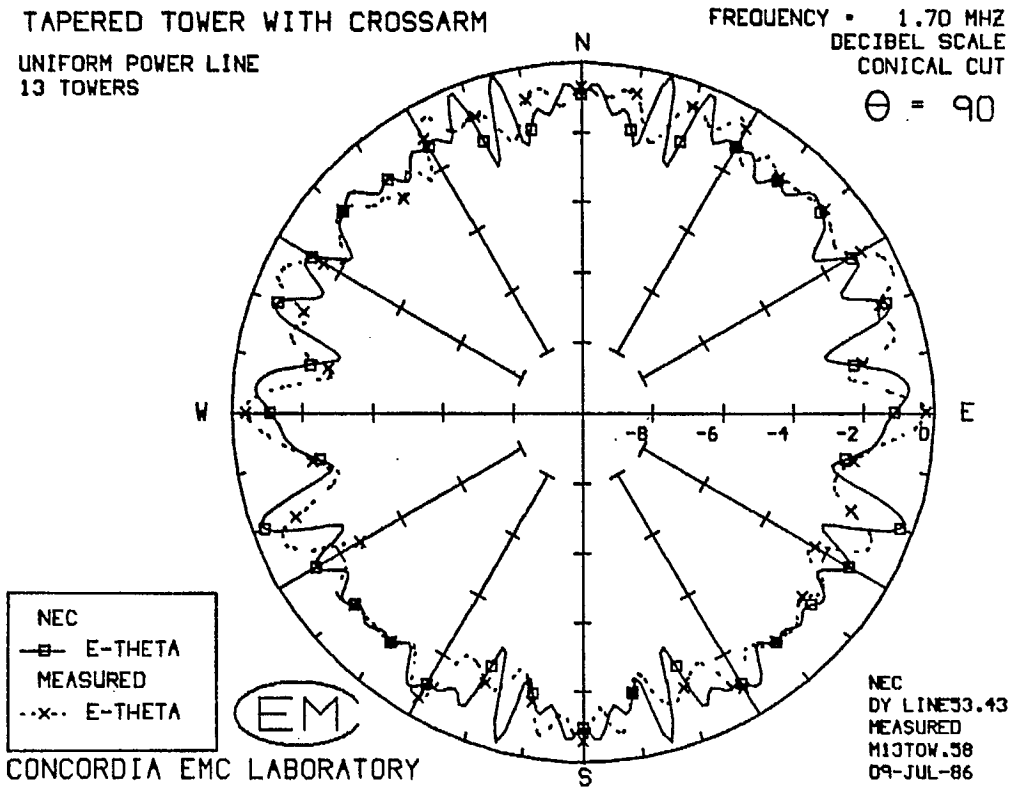

Fig. 3.20(a) - The azimuth pattern at 1700 kHz with the "offset skywire" model.

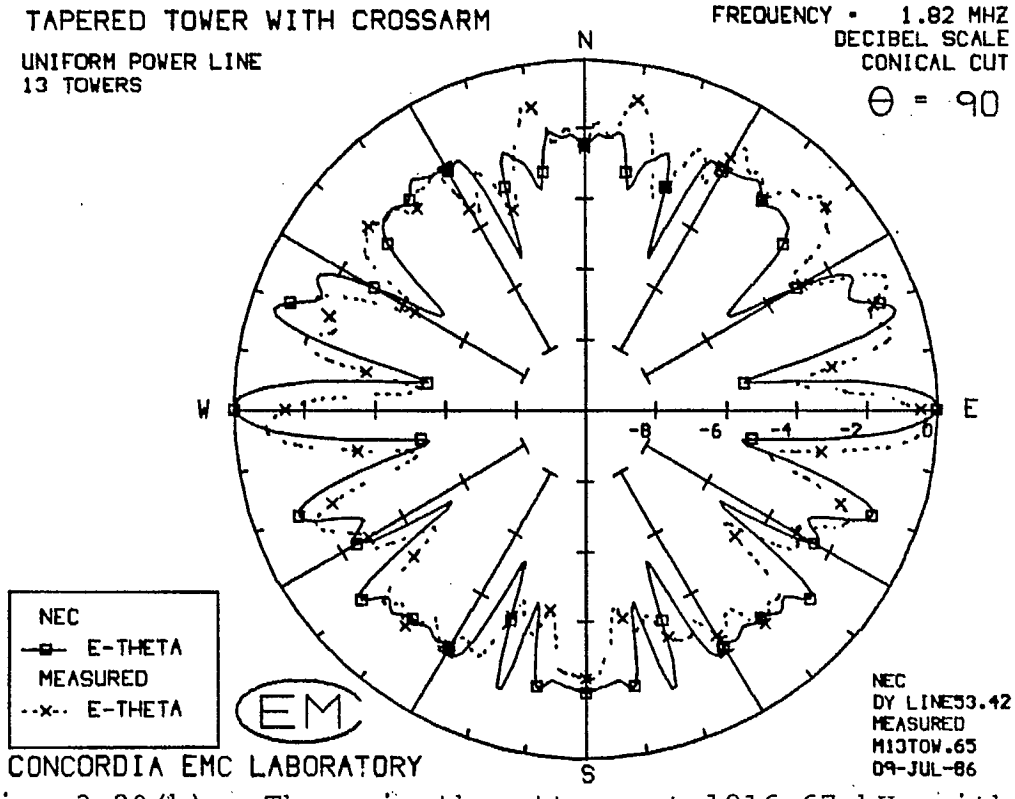

Fig. 3.20(b) - The azimuth pattern at 1816.67 kHz with the "offset skywire" model.

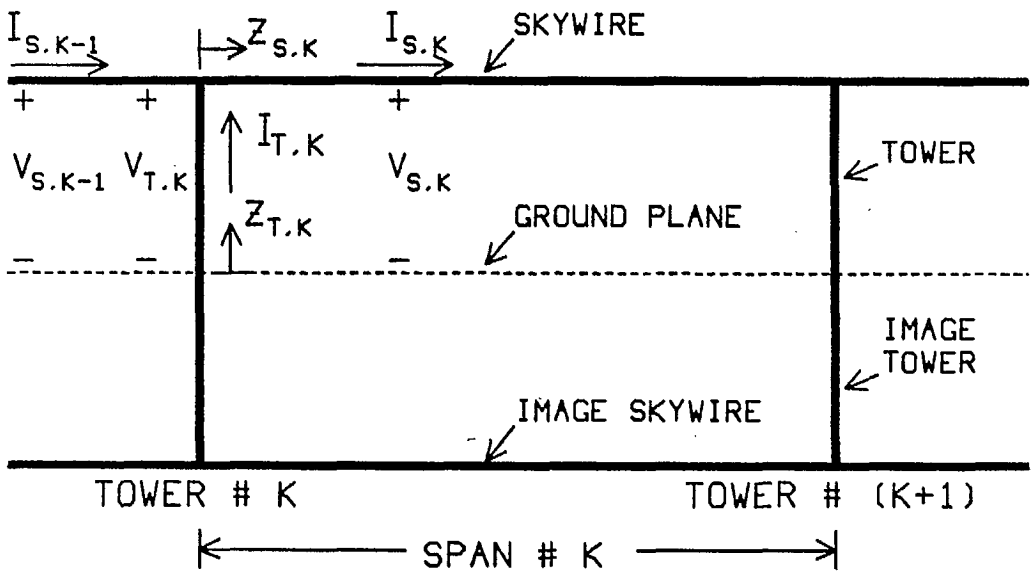

Fig. 4.1 - A typical span for analysis by the AMPL program.

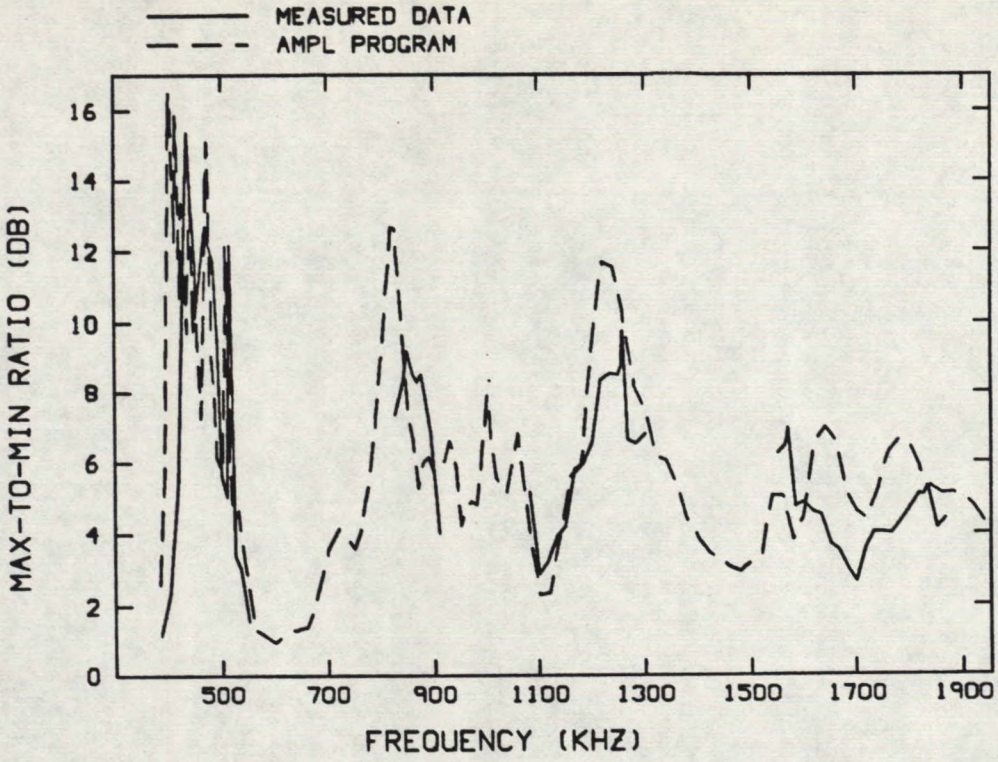

Fig. 4.2(a) - A comparison of the max-to-min ratio of the azimuth pattern of the 13 tower power line of Fig. 3.1 computed with AMPL with the max-to-min ratio of the measured patterns.

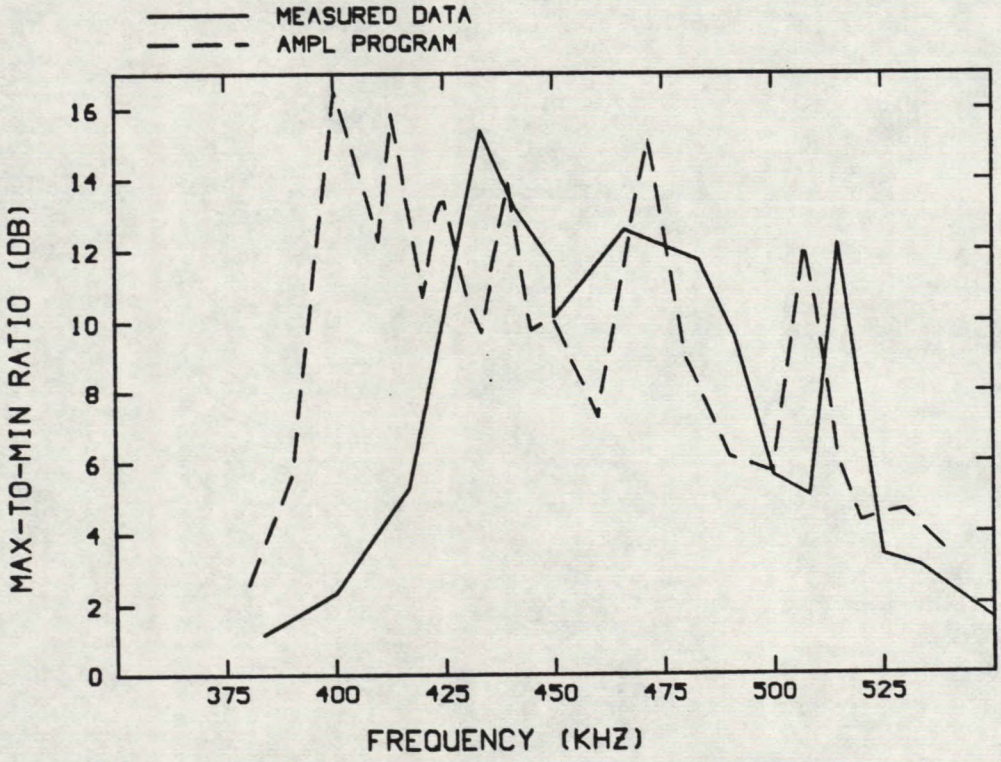

Fig. 4.2(b) - AMPL vs. the measured data in the one-wavelength frequency range.

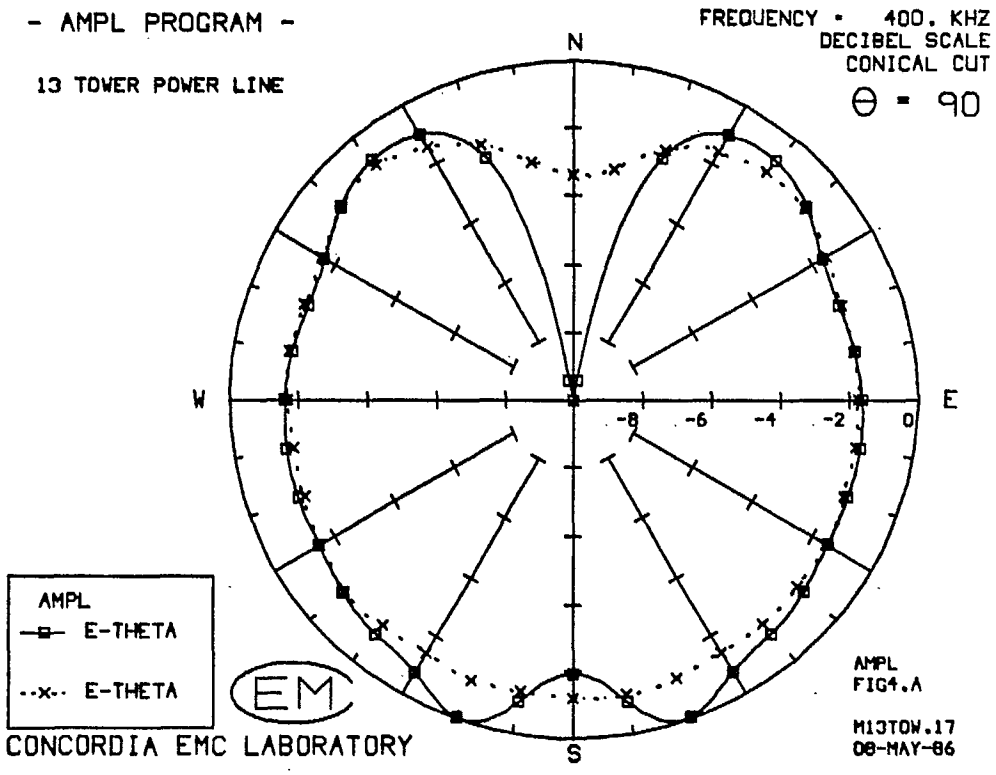

Fig. 4.3 - AMPL's pattern compared with the measured pattern at 400 kHz.

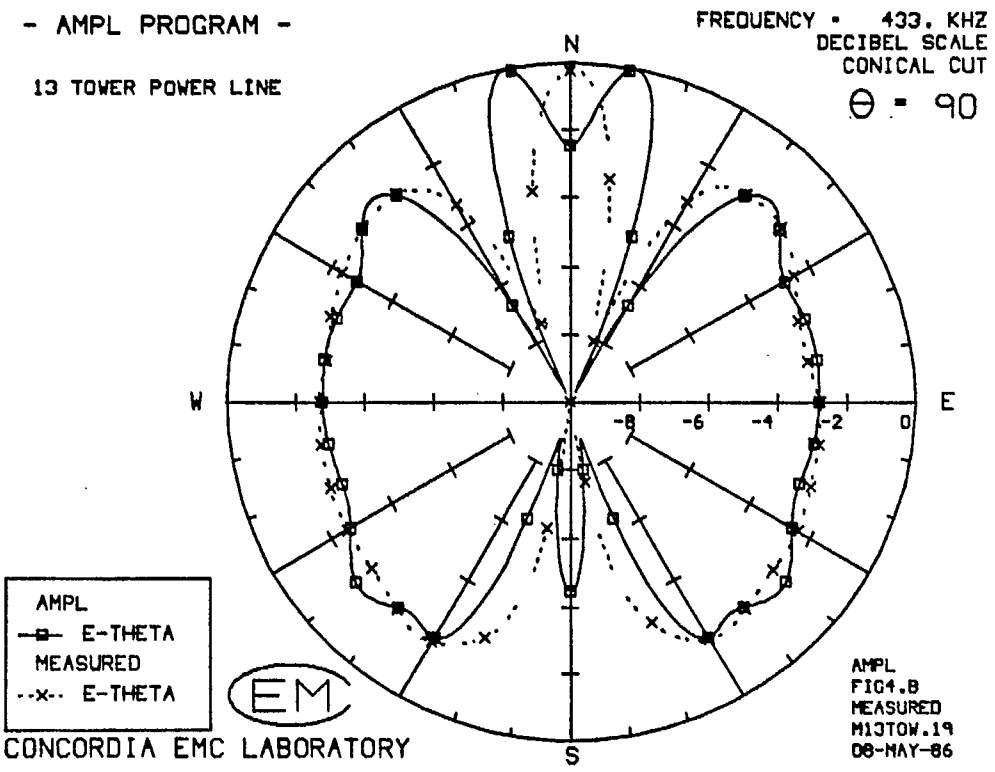

Fig. 4.4 - AMPL's pattern compared with the measured pattern at 433.33 kHz.

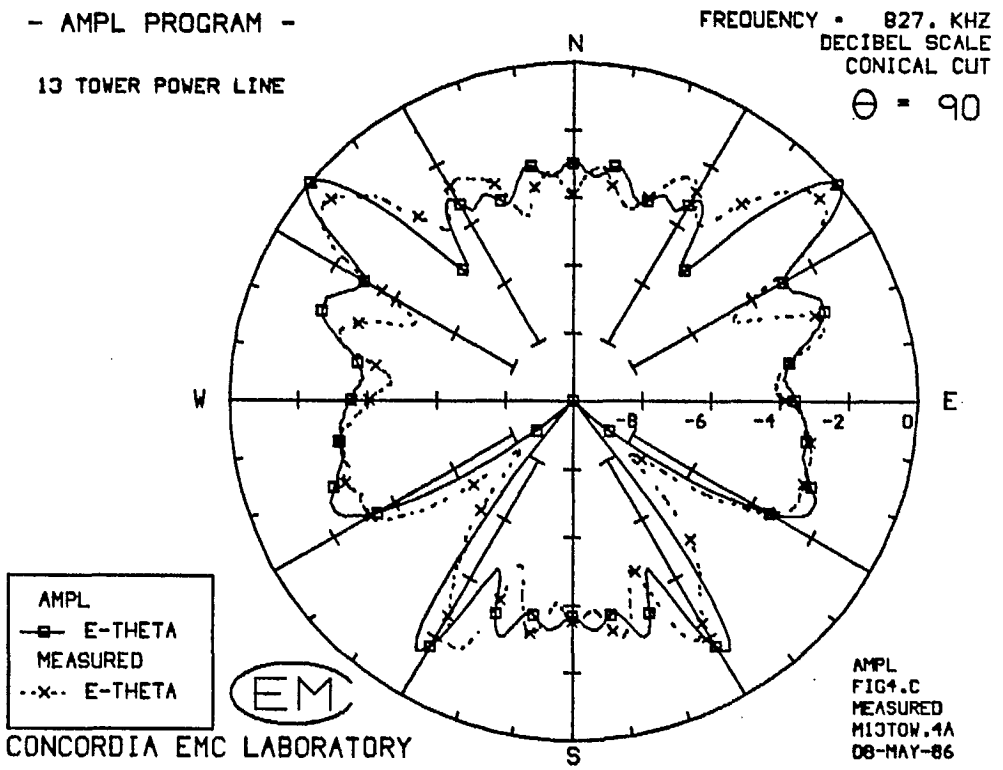

Fig. 4.5 - AMPL's pattern compared with the measured pattern at 826.67 kHz.

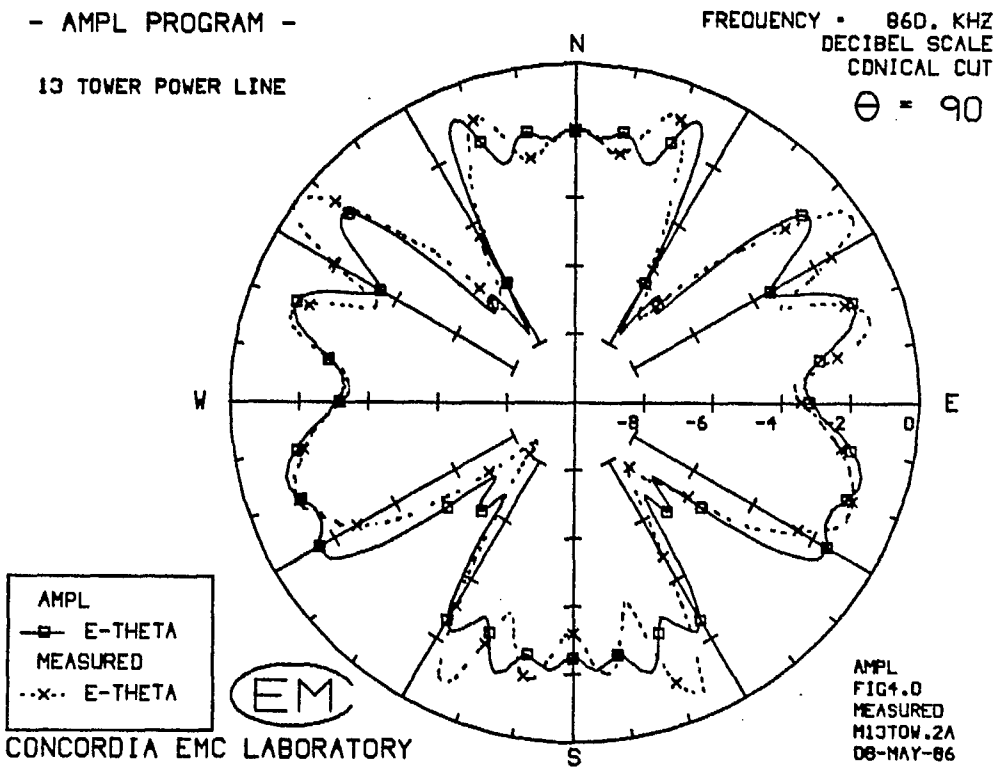

Fig. 4.6 - AMPL's pattern compared with the measured pattern at 860 kHz.

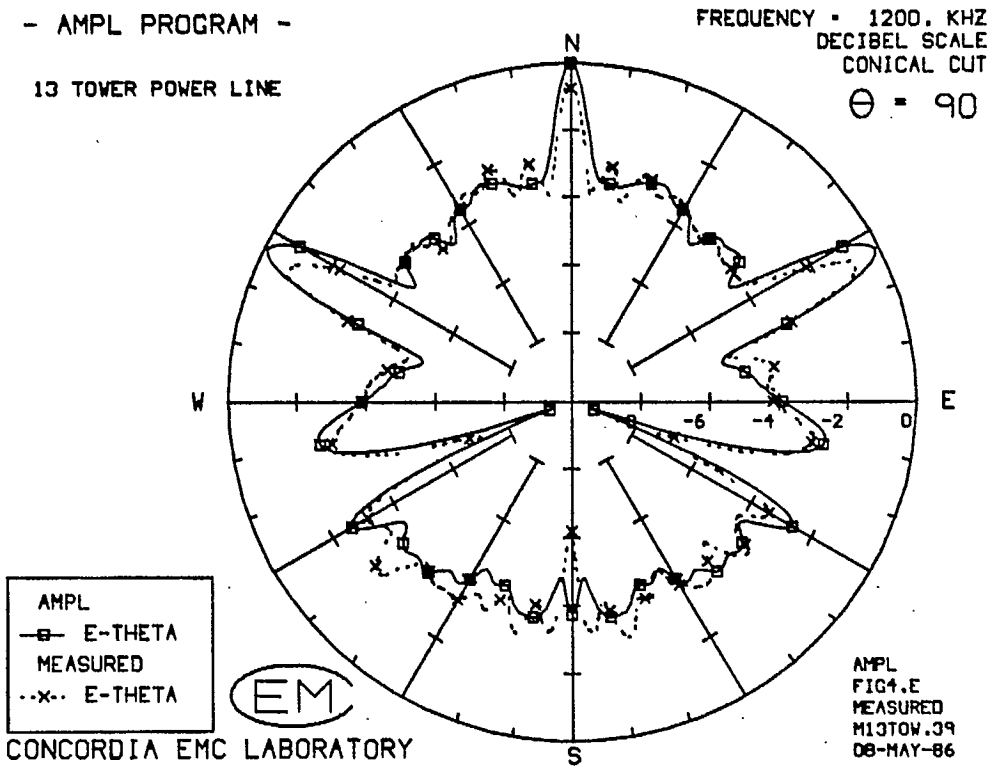

Fig. 4.7 - AMPL's pattern compared with the measured pattern at 1200 kHz.

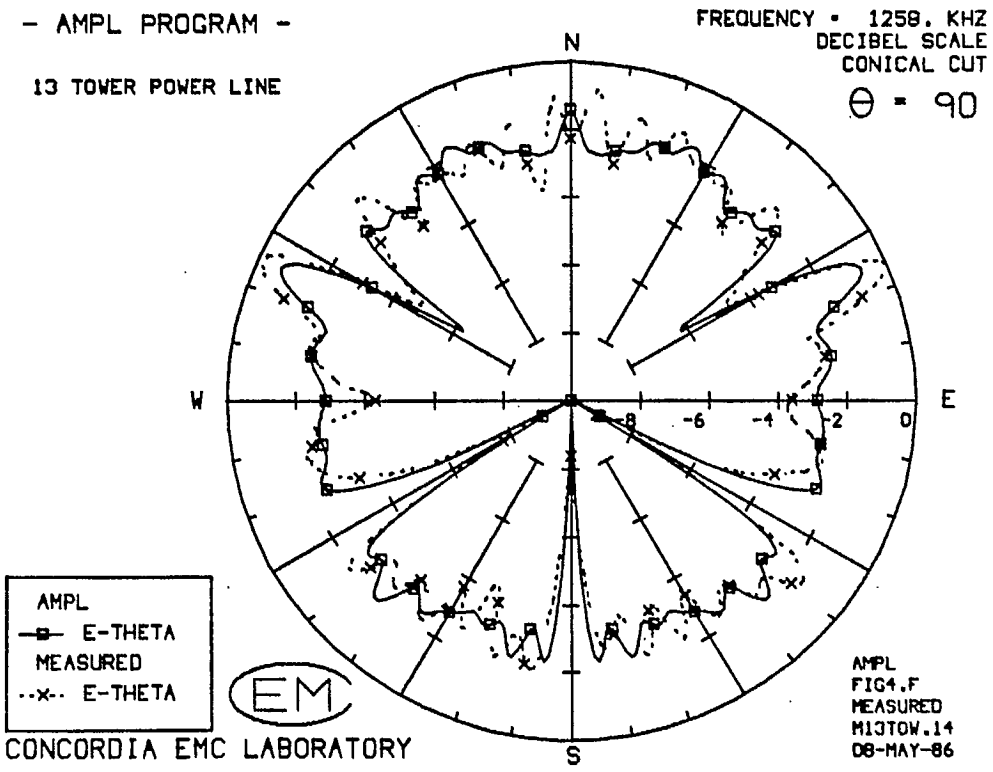

Fig. 4.8 - AMPL's pattern compared with the measured pattern at 1258.33 kHz.

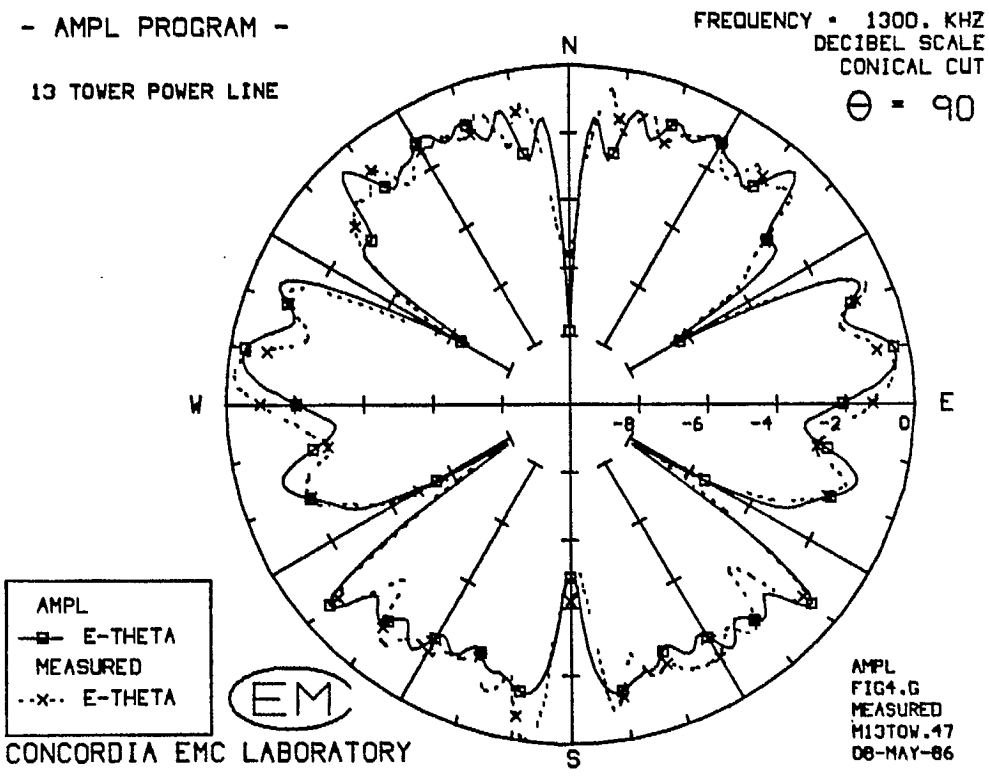

Fig. 4.9 - AMPL's pattern compared with the measured pattern at 1300 kHz.

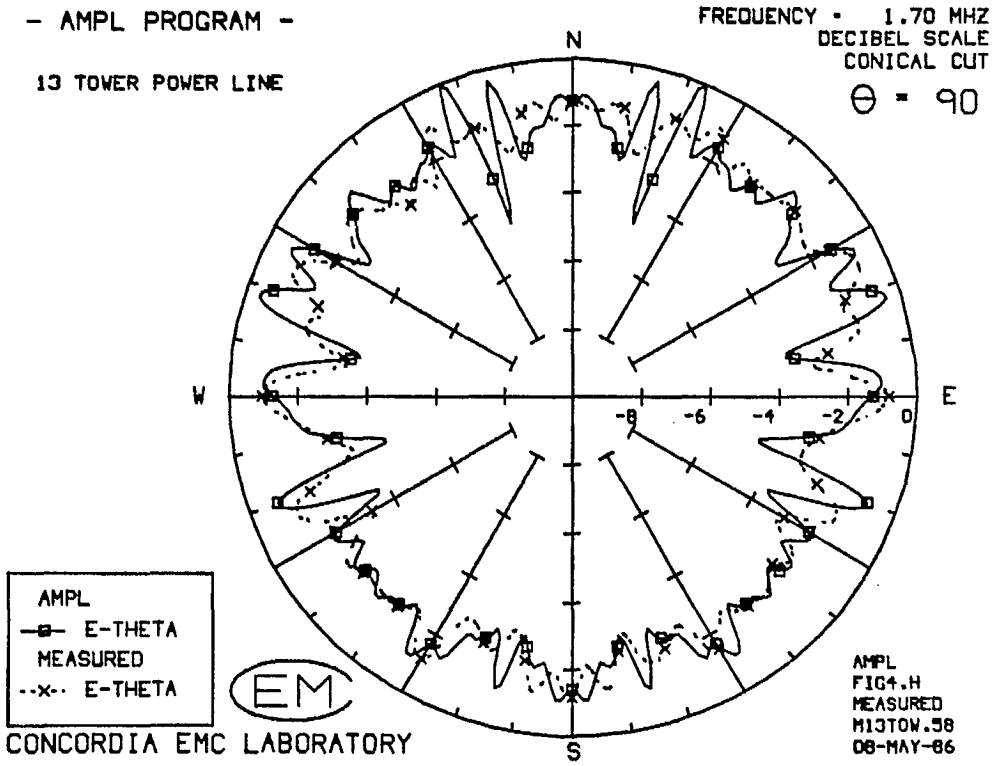

Fig. 4.10 - AMPL's pattern compared with the measured pattern at 1700 kHz.

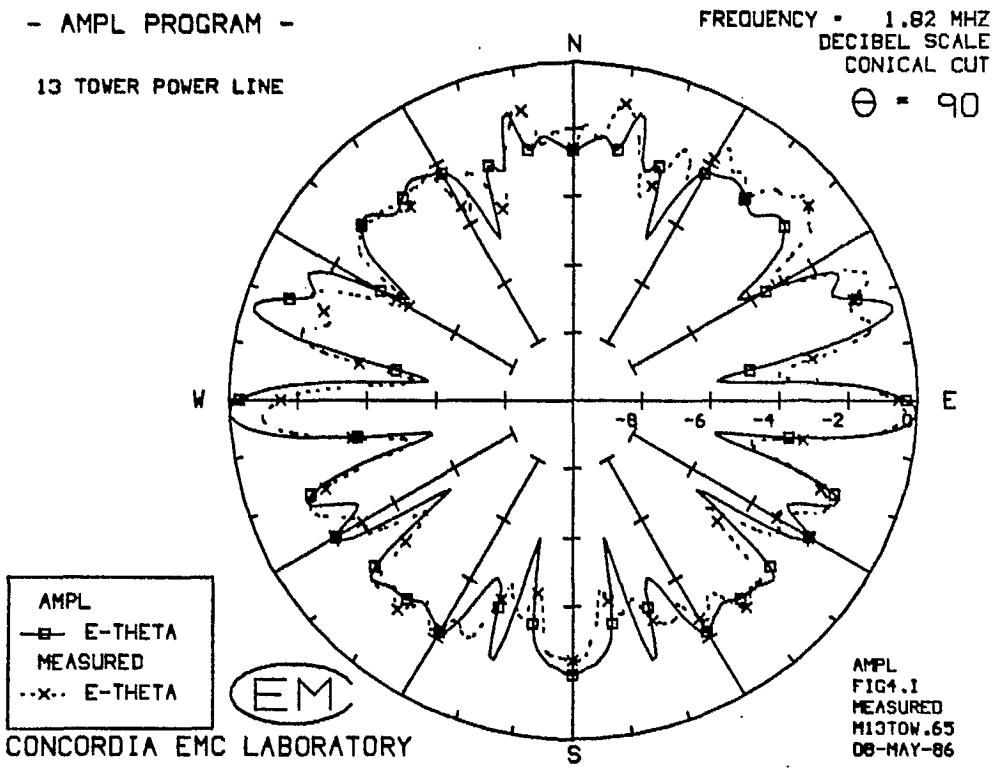

Fig. 4.11 - AMPL's pattern compared with the measured pattern at 1816.67 kHz.

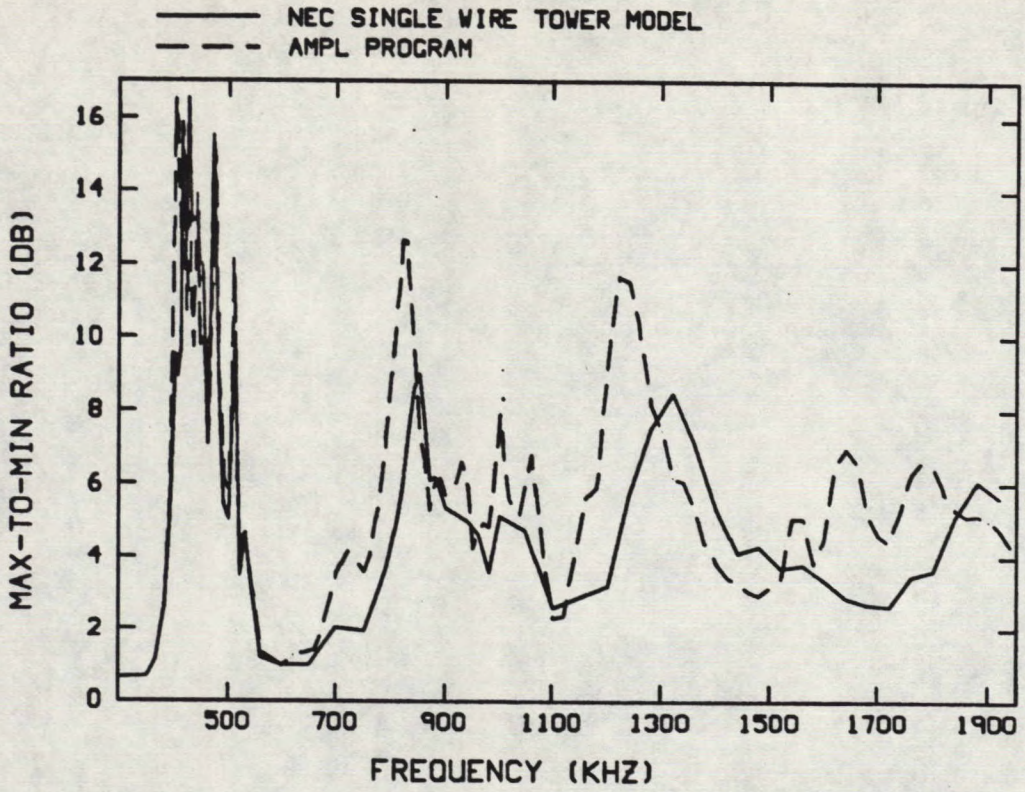

Fig. 4.12(a) - A comparison of the max-to-min ratio of the azimuth pattern of the 13 tower power line of Fig. 3.1 computed with AMPL with that computed with NEC and the "single-wire tower" model.

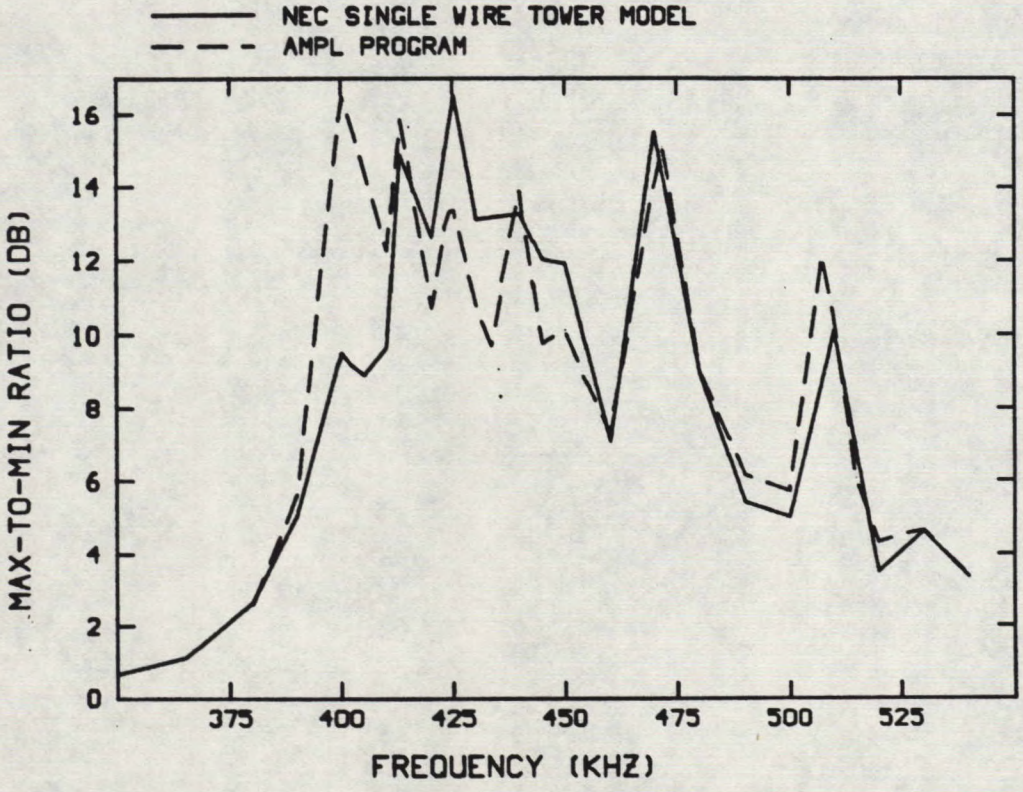

Fig. 4.12(b) - AMPL vs. the "single-wire tower" model in the one-wavelength resonance frequency range.

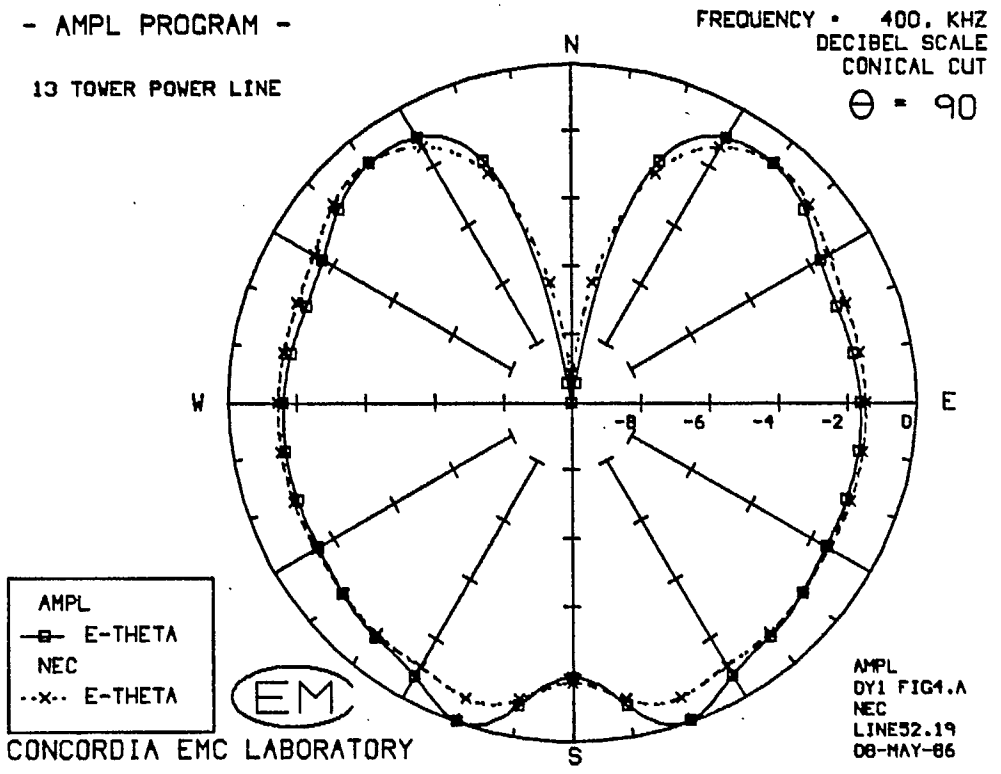

Fig. 4.13(a) - AMPL's pattern compared with the "single-wire tower" model's pattern at 400 kHz.

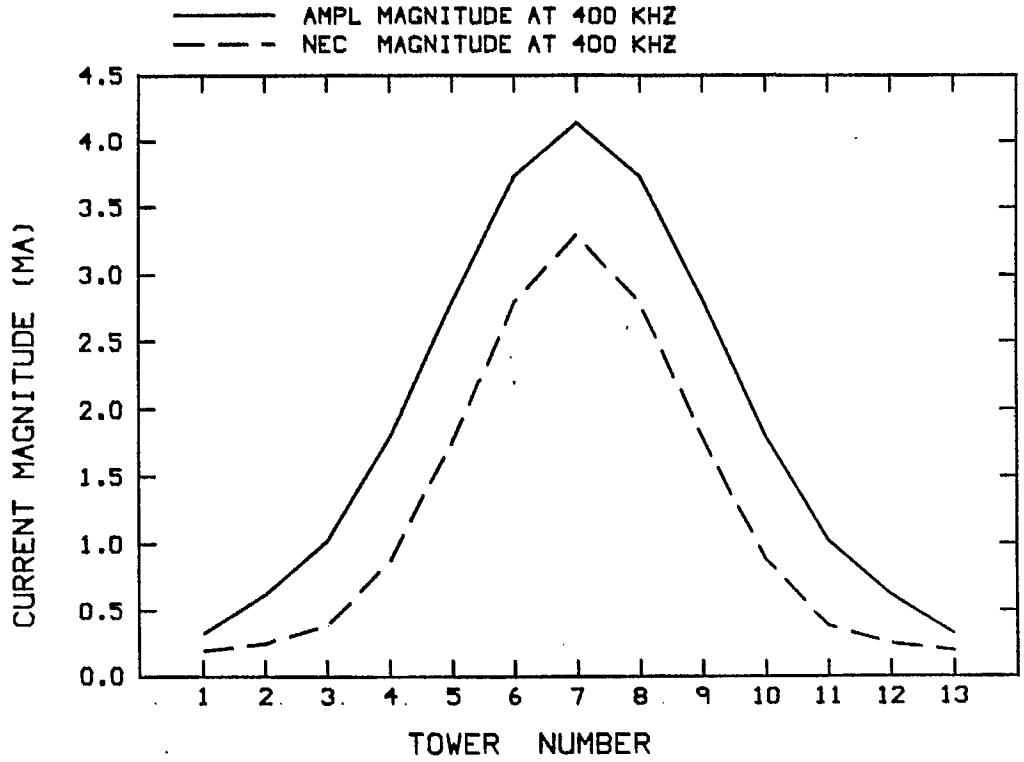

Fig. 4.13(b) - The tower base currents at 400 kHz as predicted by AMPL compared with those computed with NEC and the "single-wire tower" model.

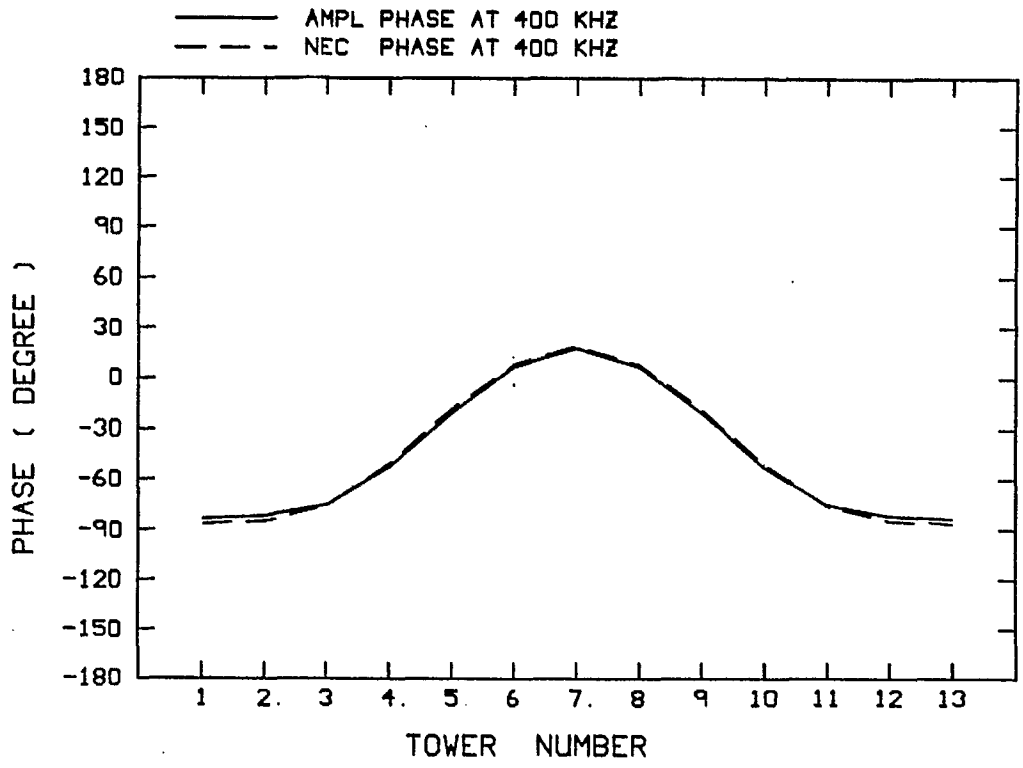

Fig. 4.13(c) - The tower base current phases at 400 kHz.

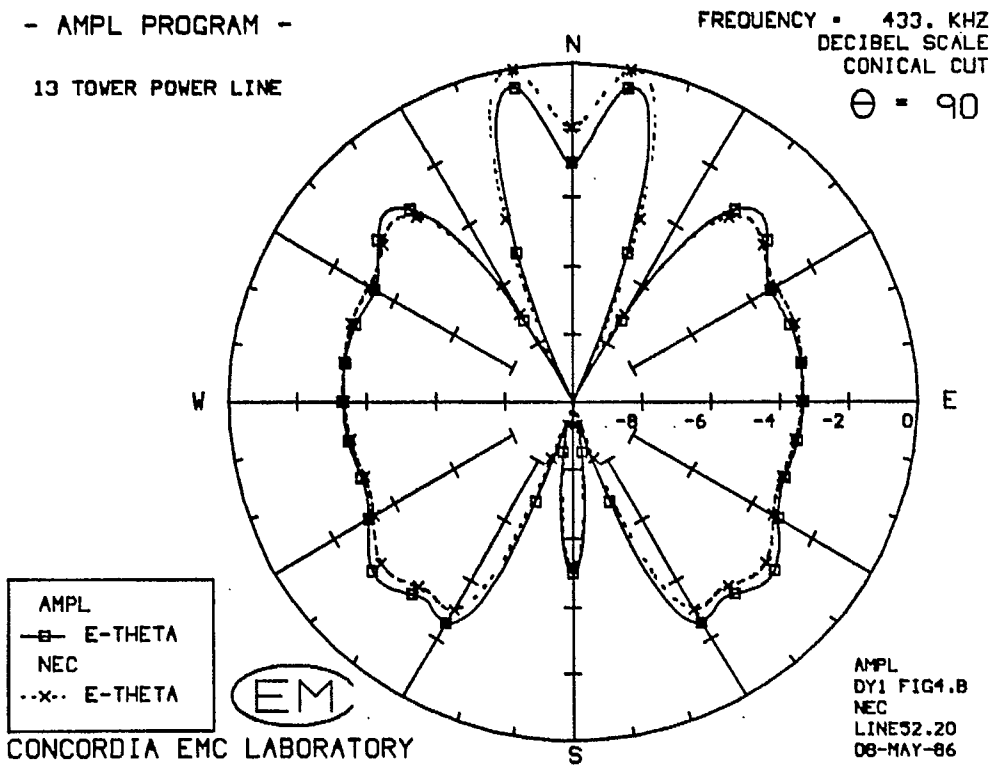

Fig. 4.14(a) - AMPL's pattern compared with the "single-wire tower" model's pattern at 433.33 kHz.

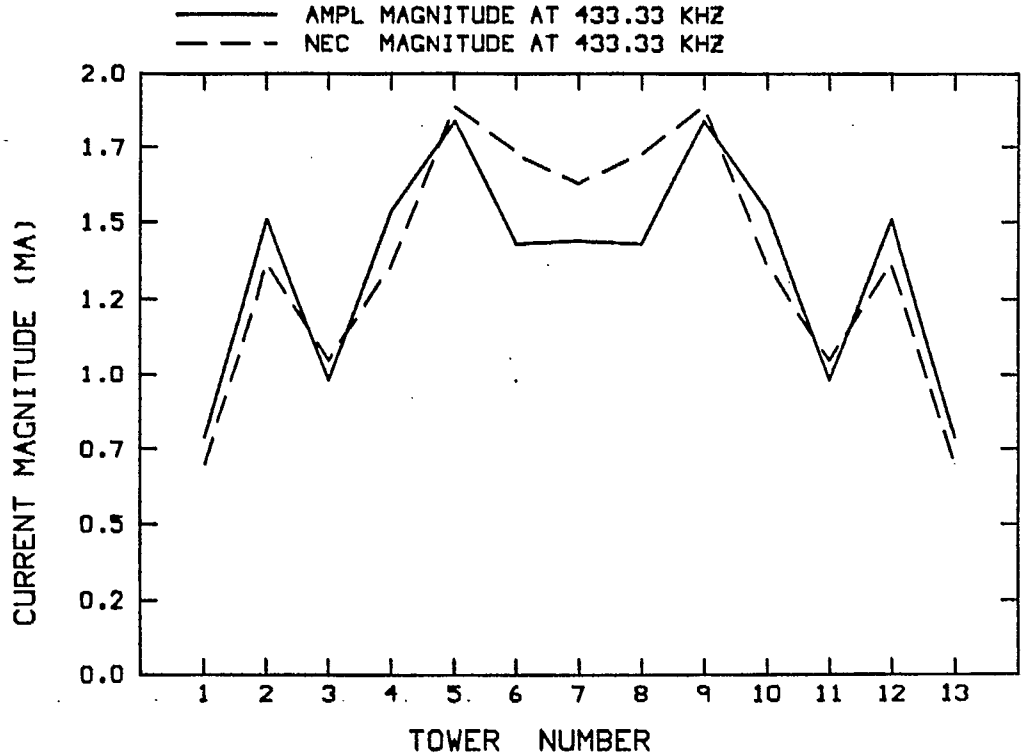

Fig. 4.14(b) - The tower base currents magnitudes at 433.33 kHz.

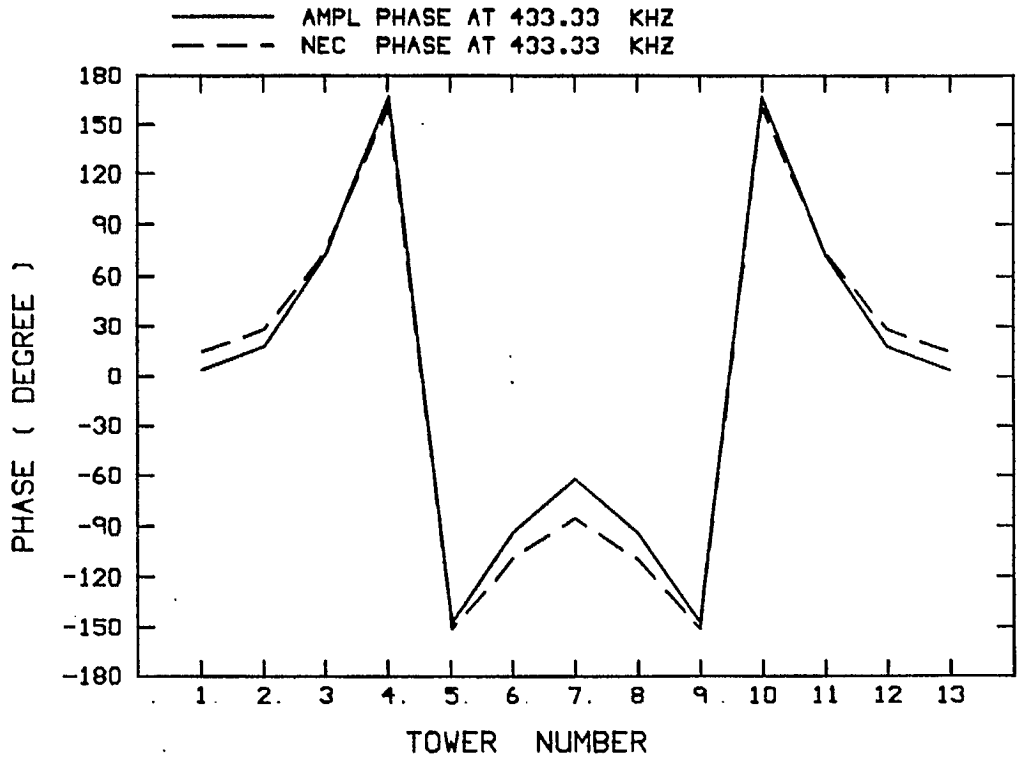

Fig. 4.14(c) - The tower base current phases at 433.33 kHz.

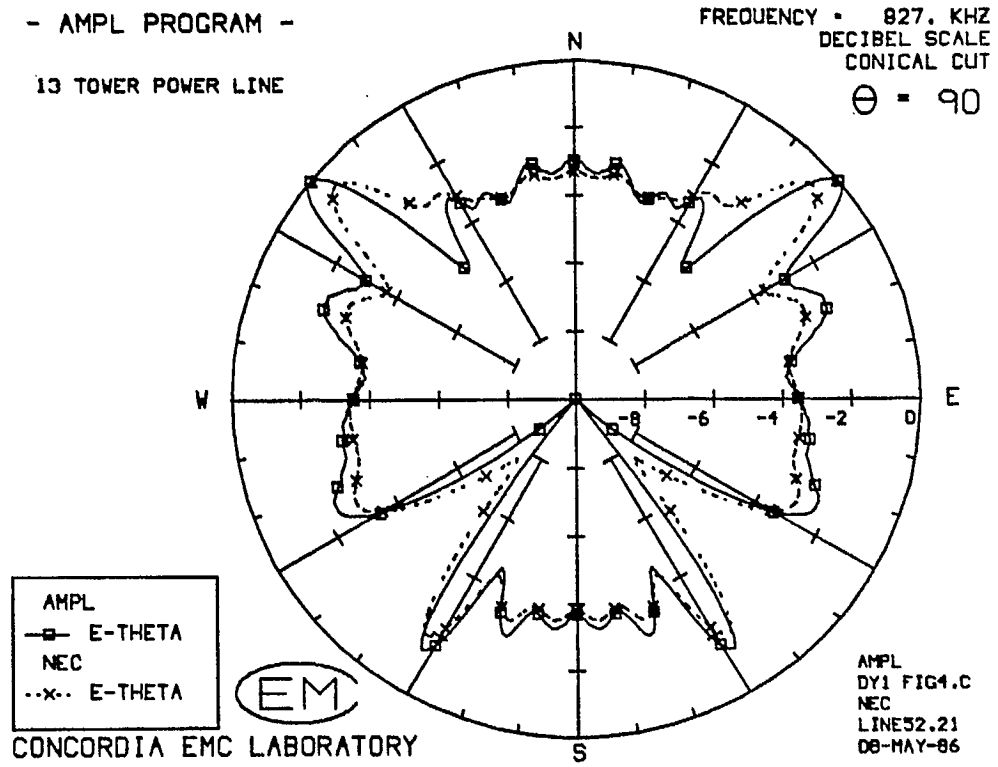

Fig. 4.15(a) - AMPL's pattern compared with the "single-wire tower" model's pattern at 826.67 kHz.

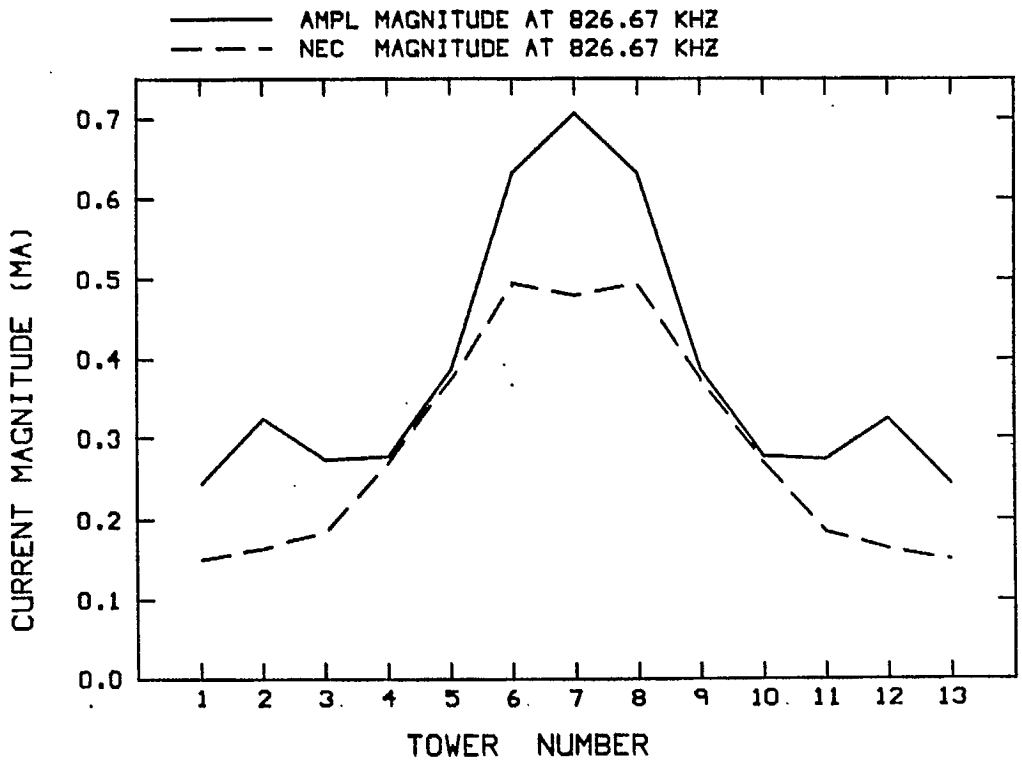

Fig. 4.15(b) - The tower base currents magnitudes at 826.67 kHz.

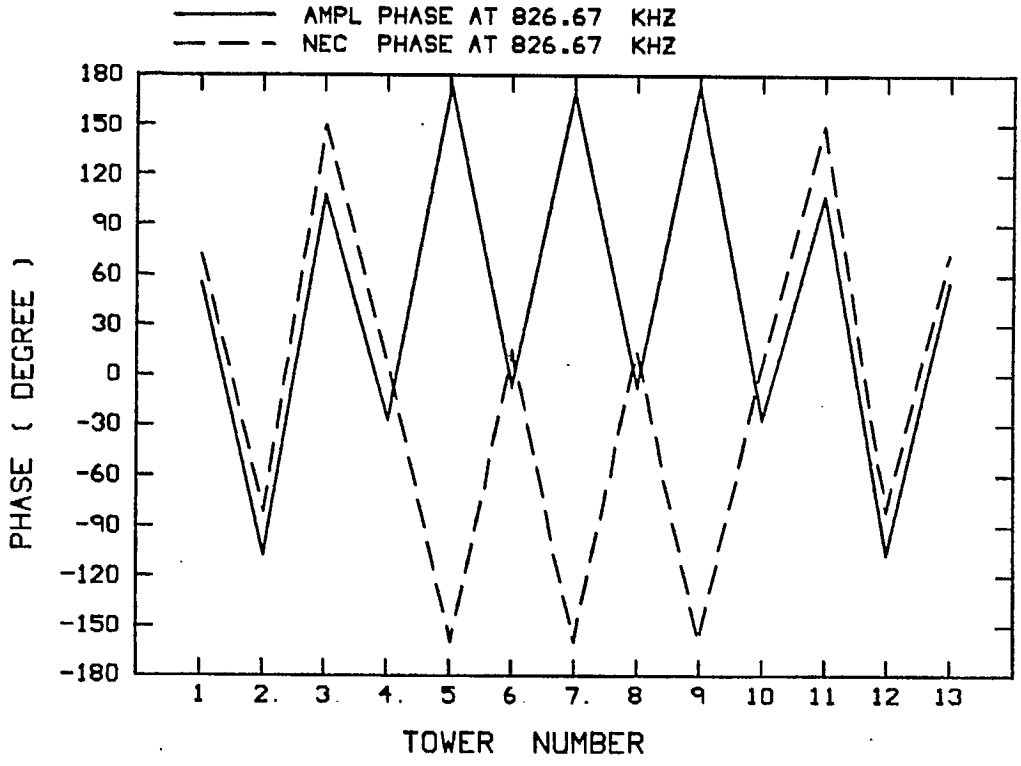

Fig. 4.15(c) - The tower base current phases at 826.67 kHz.

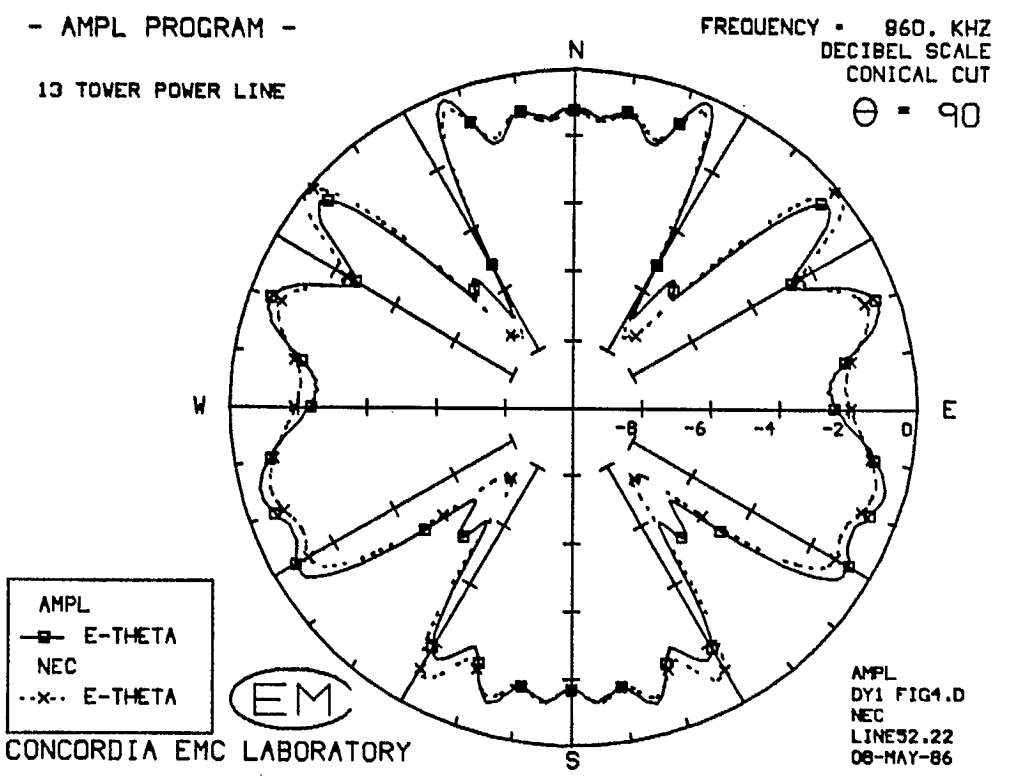

Fig. 4.16(a) - AMPL's pattern compared with the "single-wire tower" model's pattern at 860 kHz.

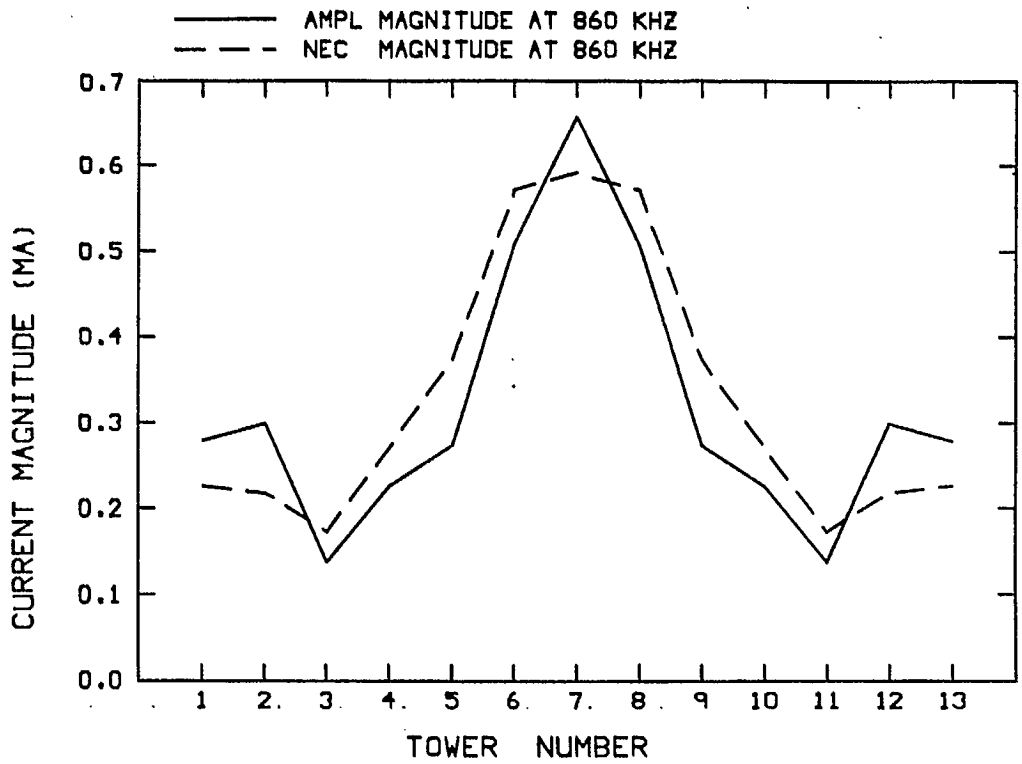

Fig. 4.16(b) - The tower base currents magnitudes at 860 kHz.

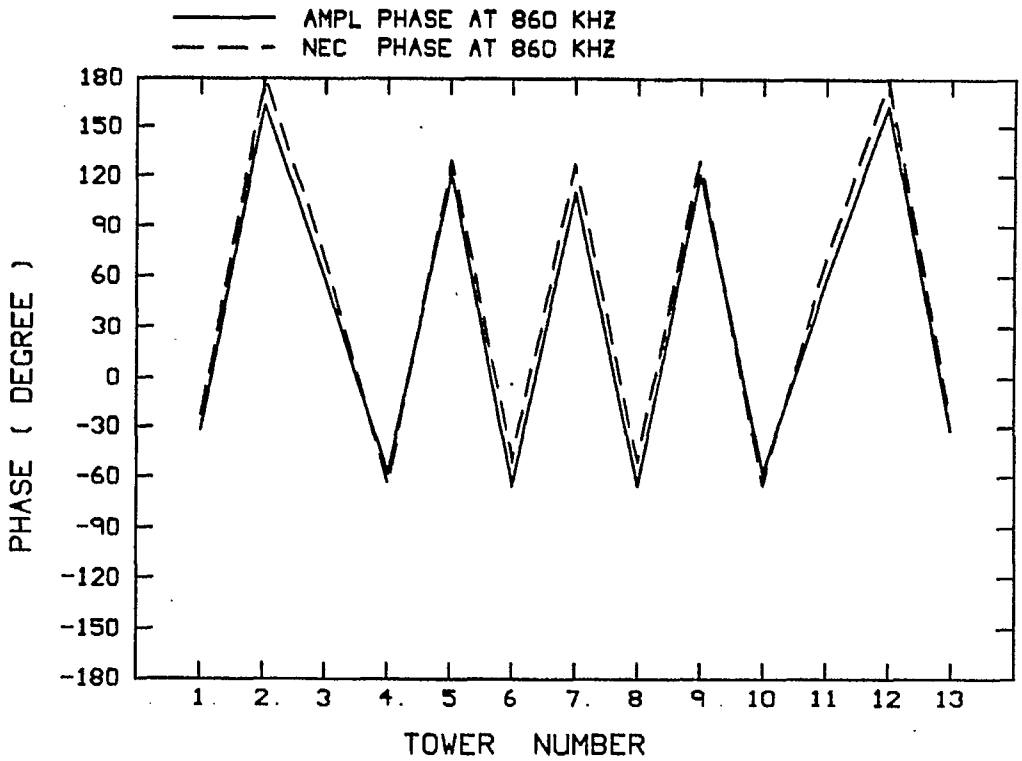

Fig. 4.16(c) - The tower base current phases at 860 kHz.

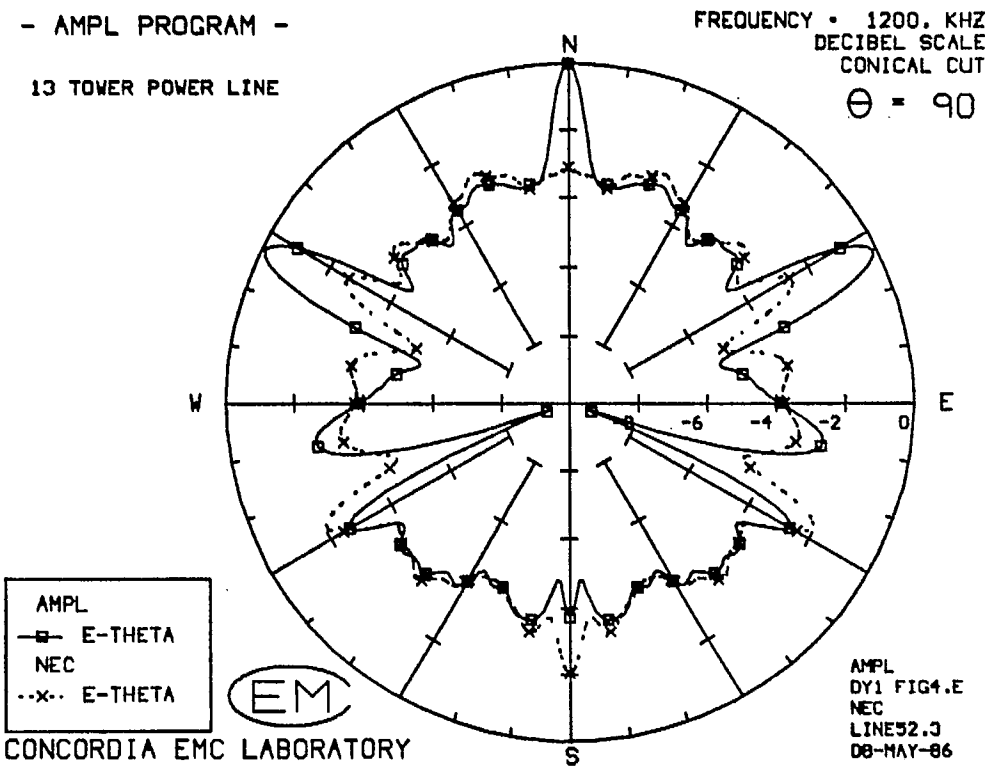

Fig. 4.17(a) - AMPL's pattern compared with the "single-wire tower" model's pattern at 1200 kHz.

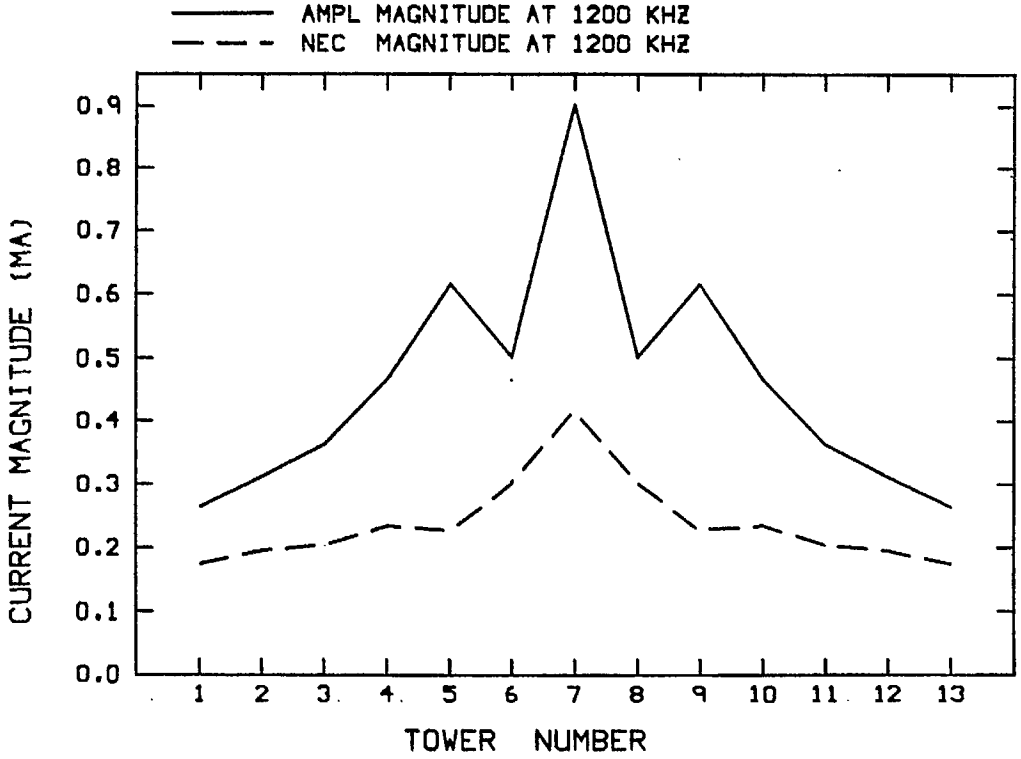

Fig. 4.17(b) - The tower base currents magnitudes at 1200 kHz.

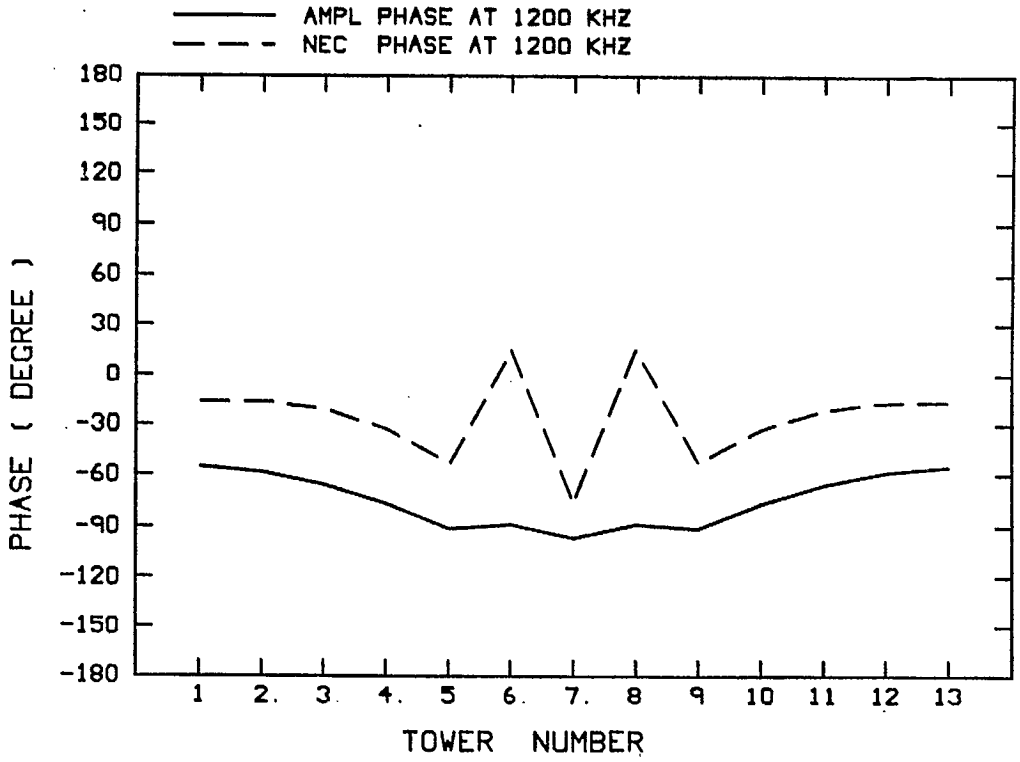

Fig. 4.17(c) - The tower base current phases at 1200 kHz.

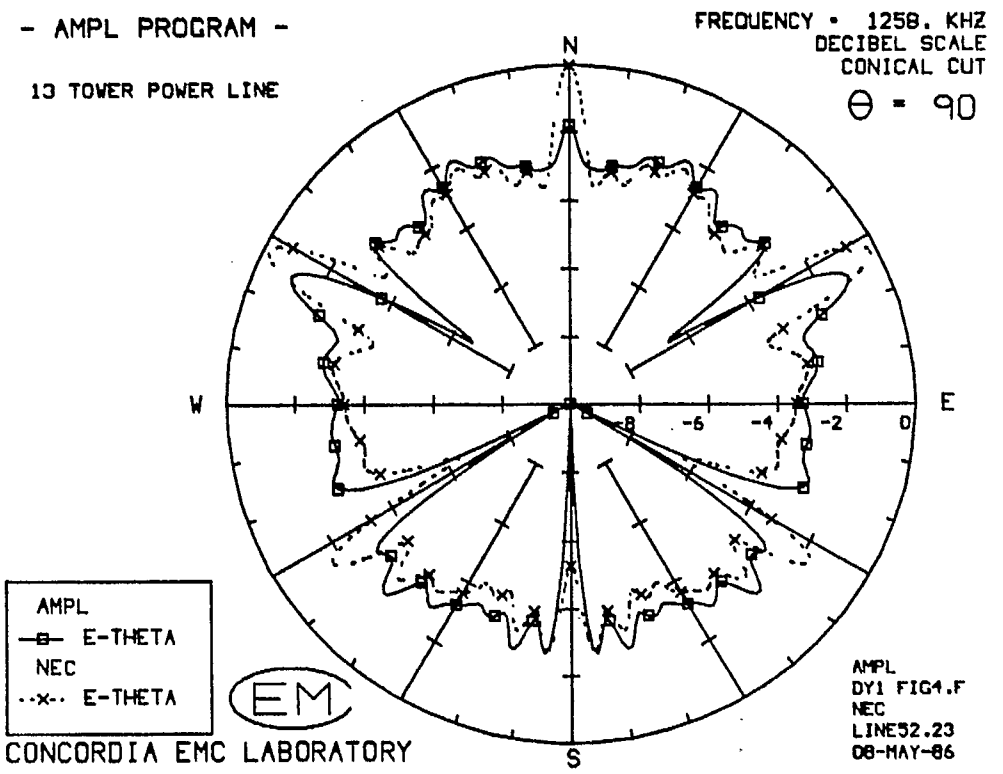

Fig. 4.18(a) - AMPL's pattern compared with the "single-wire tower" model's pattern at 1258.33 kHz.

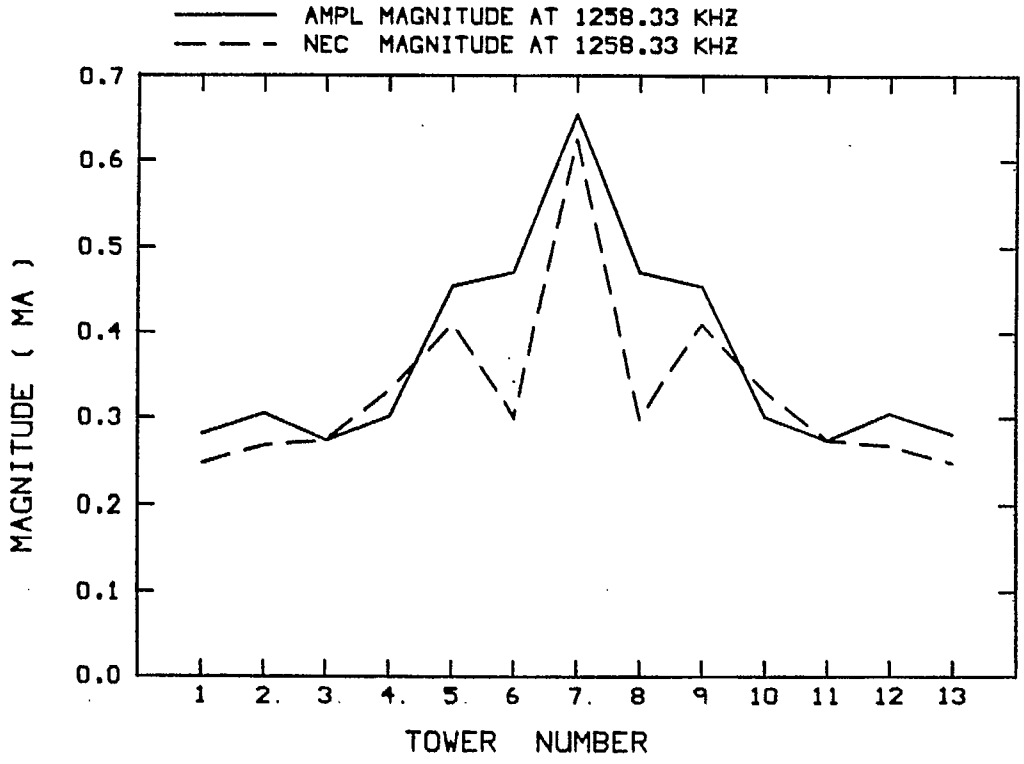

Fig. 4.18(b) - The tower base currents magnitudes at 1258.33 kHz.

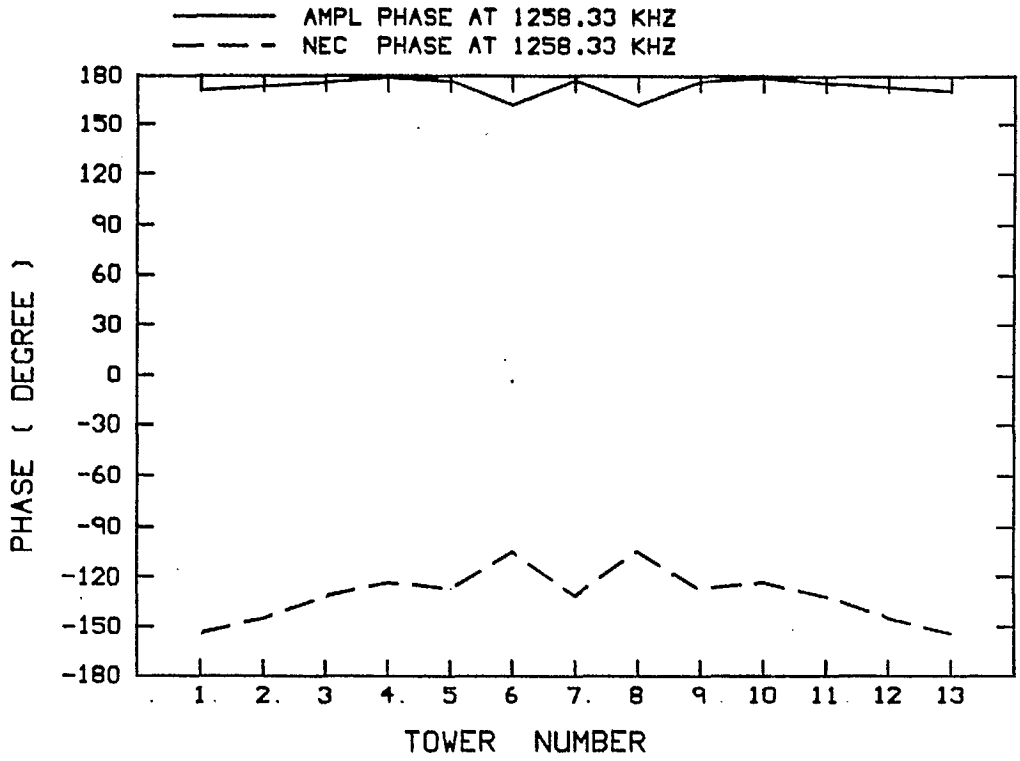

Fig. 4.18(c) - The tower base current phases at 1258.33 kHz.

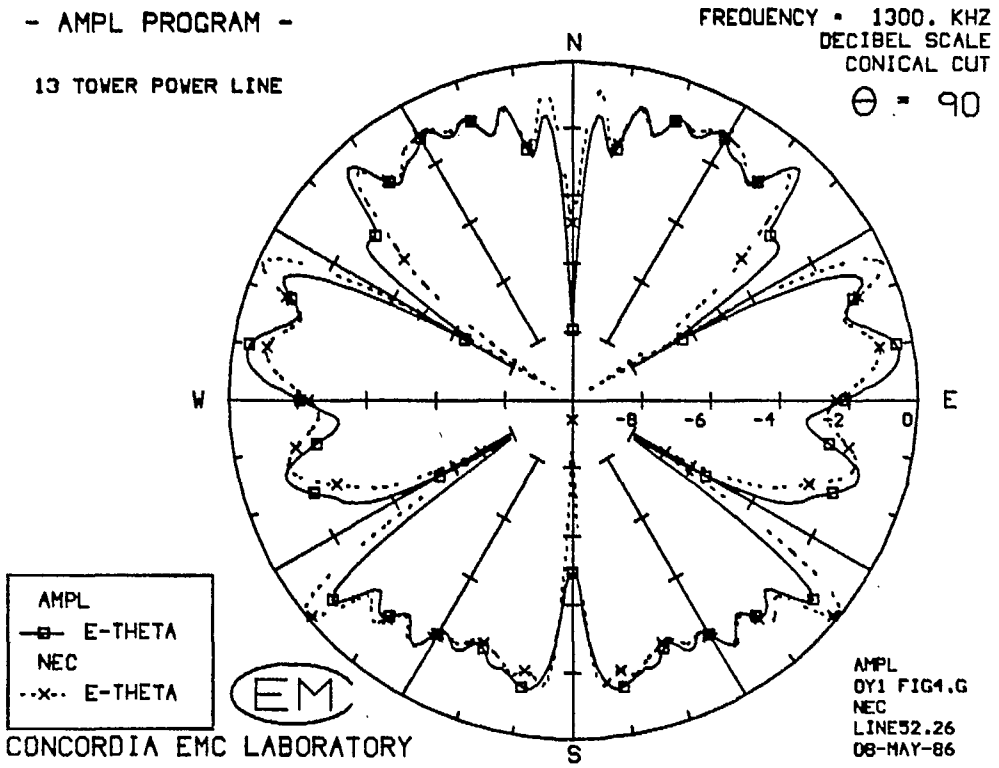

Fig. 4.19(a) - AMPL's pattern compared with the "single-wire tower" model's pattern at 1300 kHz.

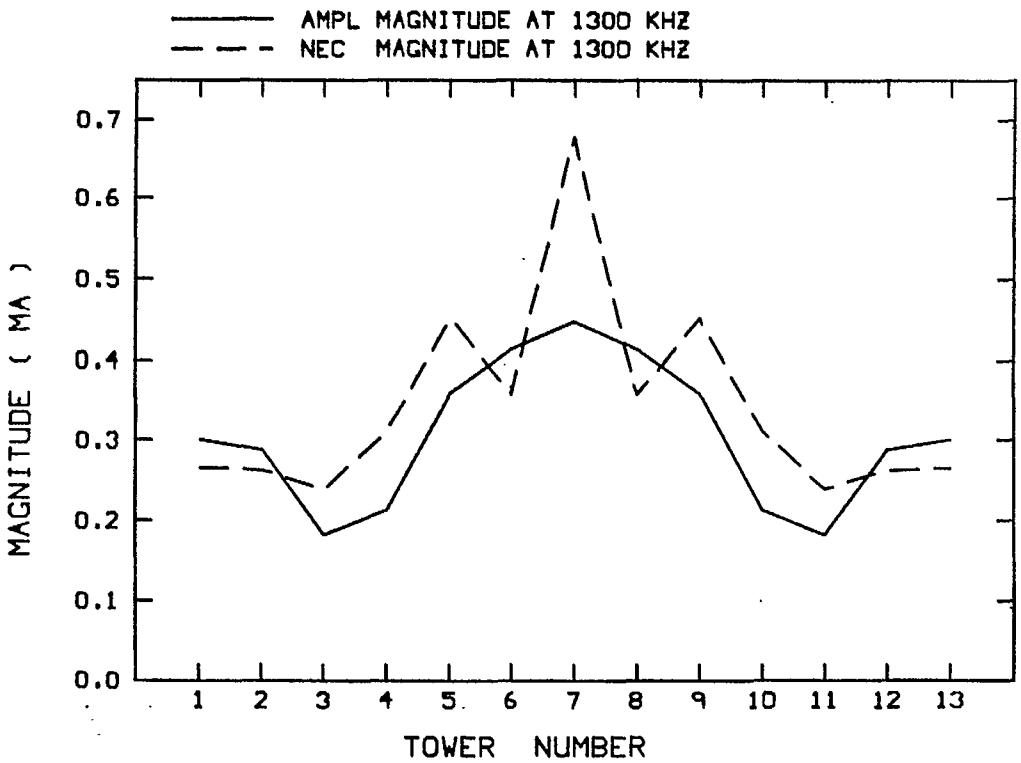

Fig. 4.19(b) - The tower base currents magnitudes at 1300 kHz.

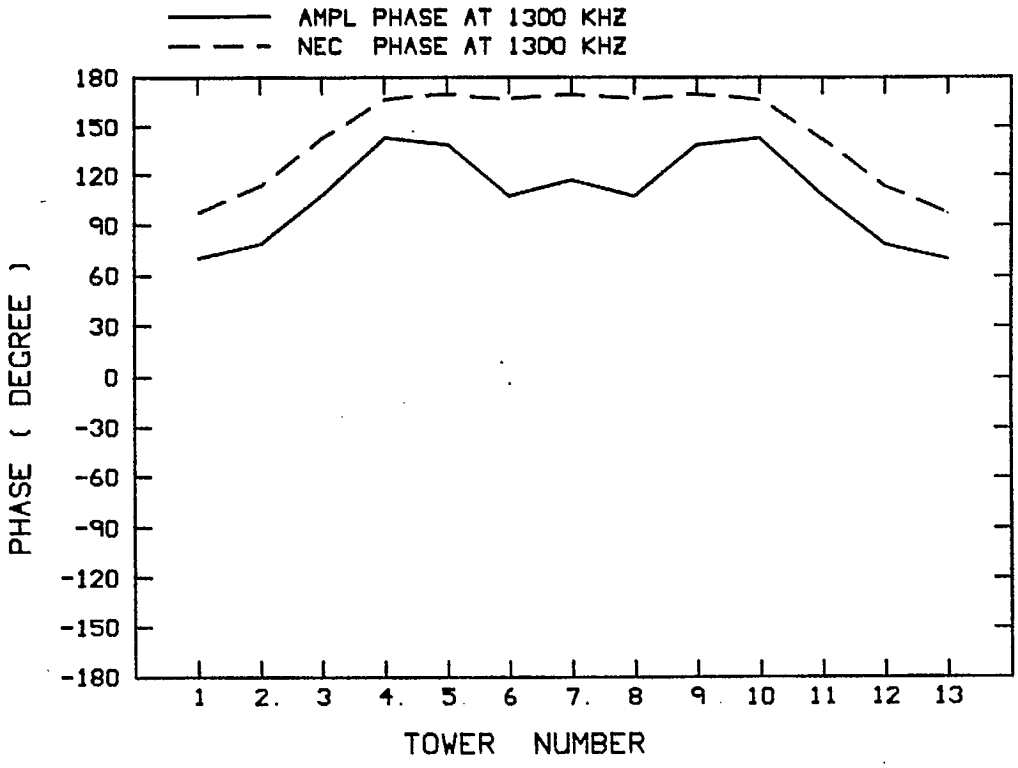

Fig. 4.19(c) - The tower base current phases at 1300 kHz.

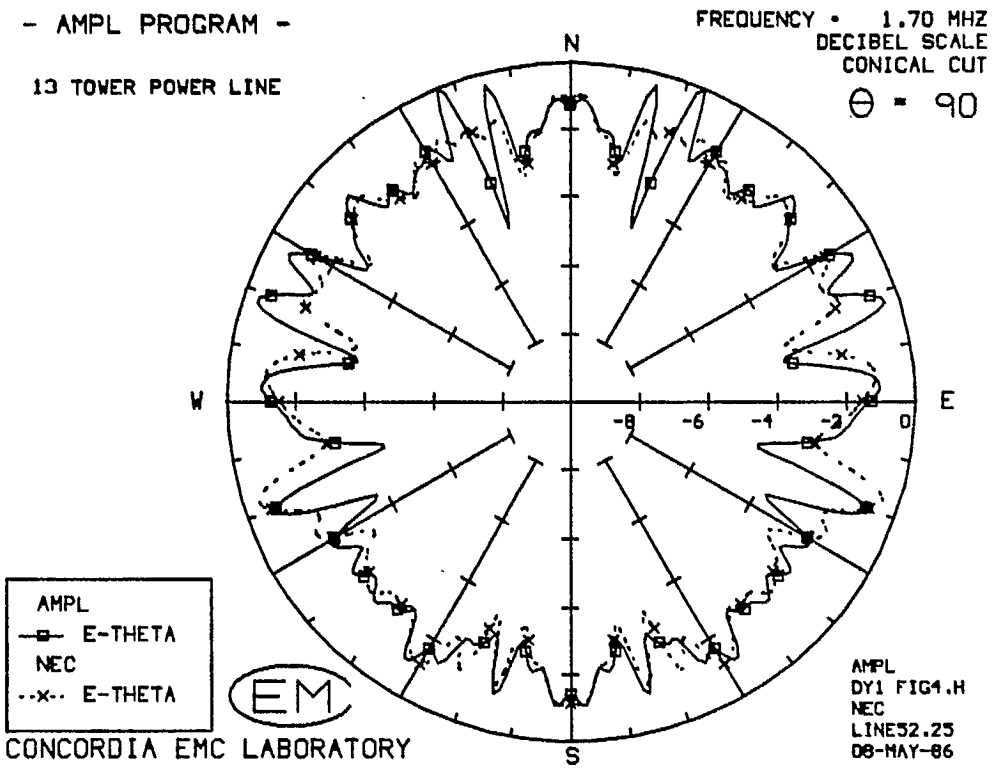

Fig. 4.20(a) - AMPL's pattern compared with the "single-wire tower" model's pattern at 1700 kHz.

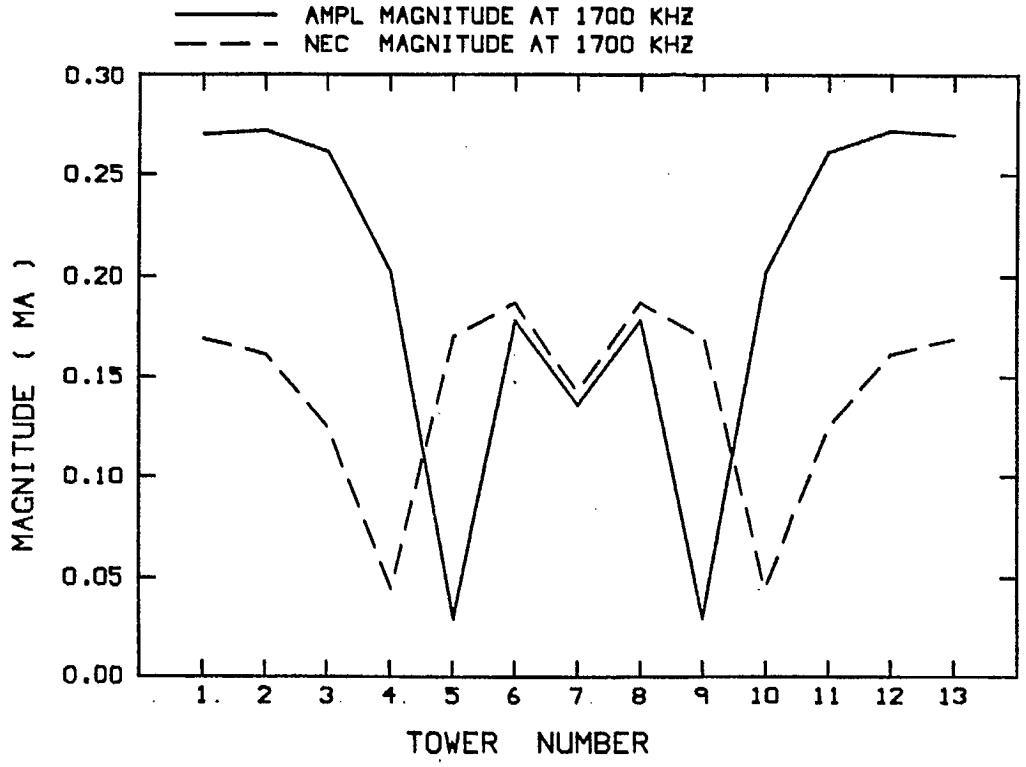

Fig. 4.20(b) - The tower base currents magnitudes at 1700 kHz.

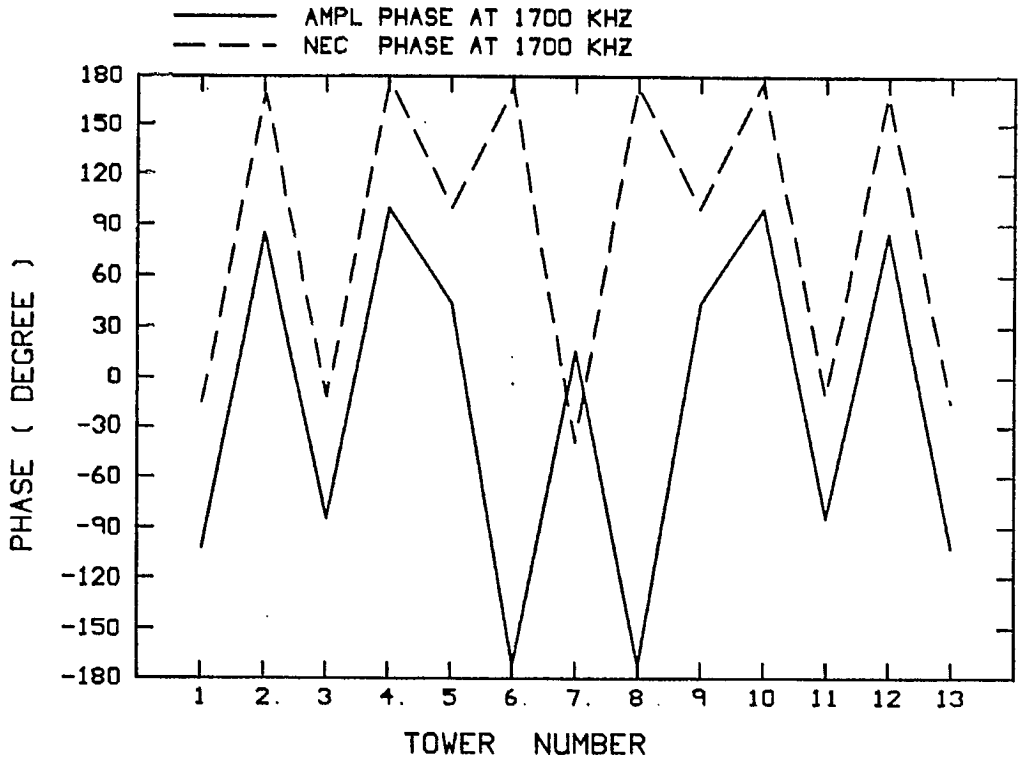

Fig. 4.20(c) - The tower base current phases at 1700 kHz.

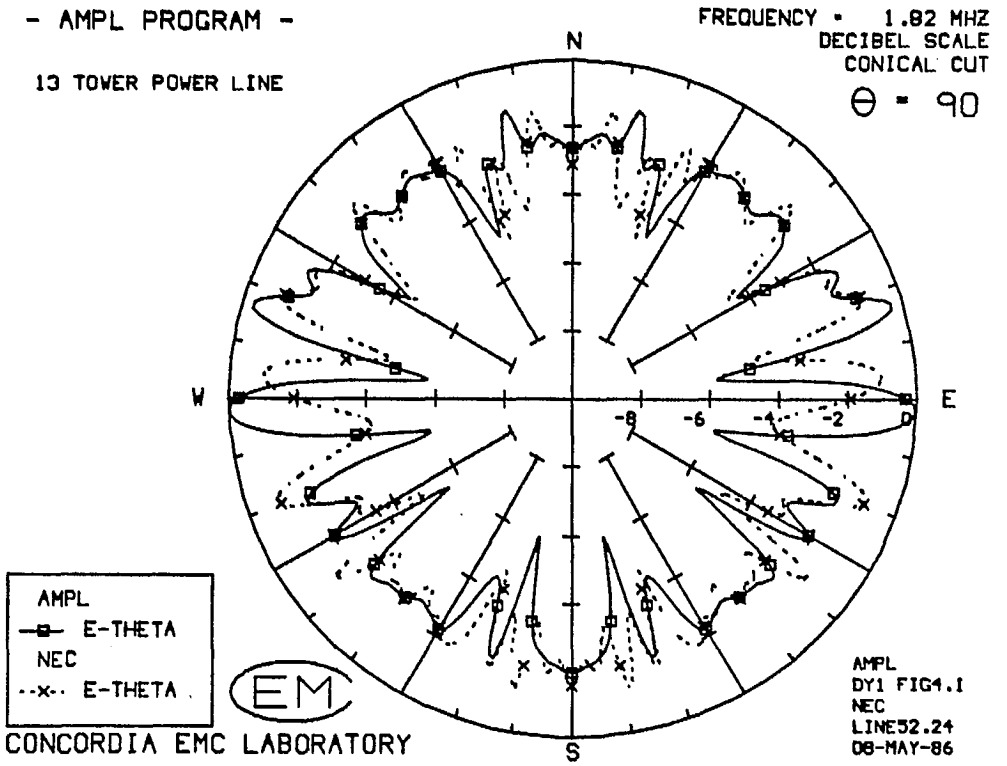

Fig. 4.21(a) - AMPL's pattern compared with the "single-wire tower" model's pattern at 1860 kHz.

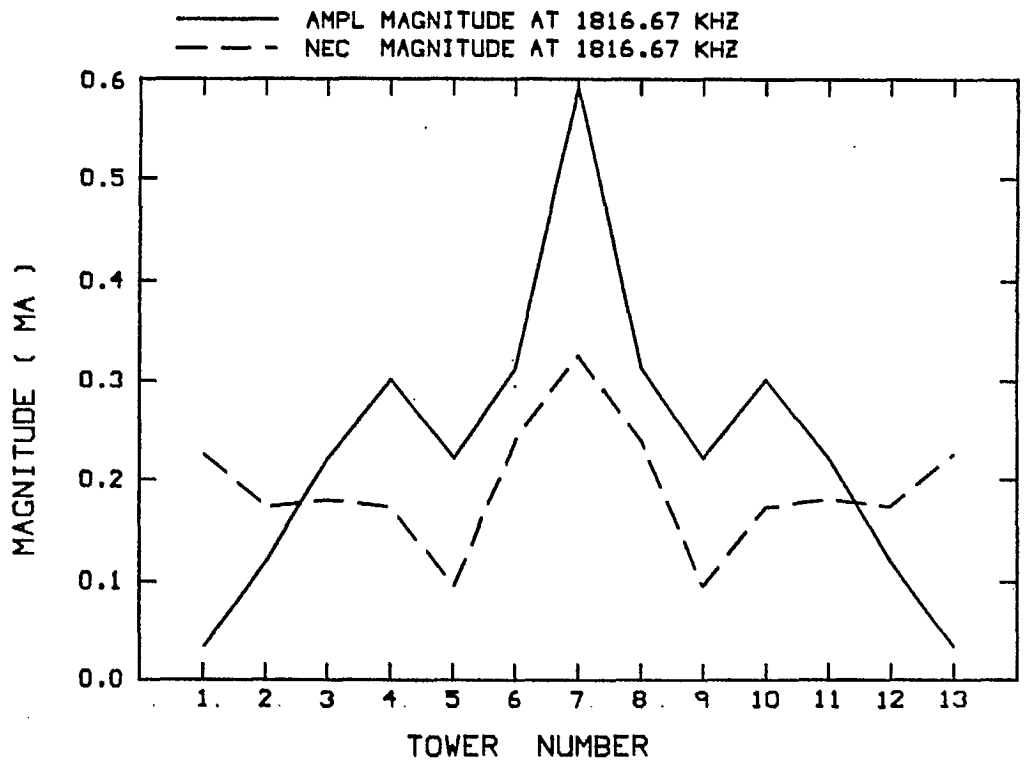

Fig. 4.21(b) - The tower base currents magnitudes at 1816.67 kHz.

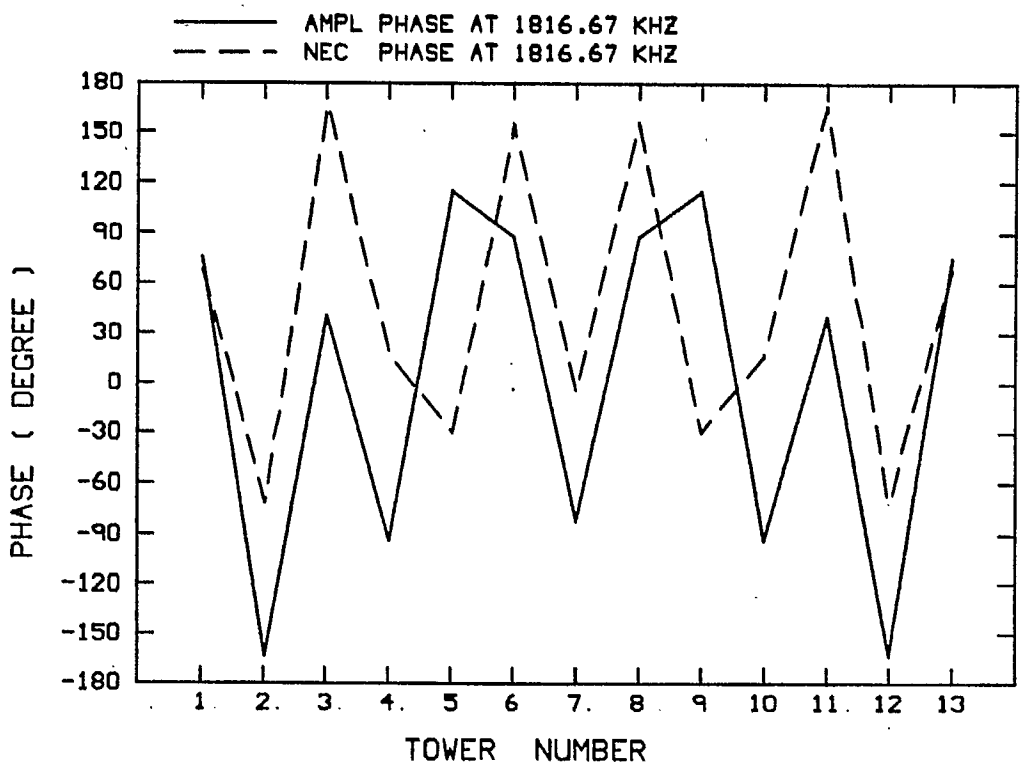

Fig. 4.21(c) - The tower base current phases at 1816.67 kHz.

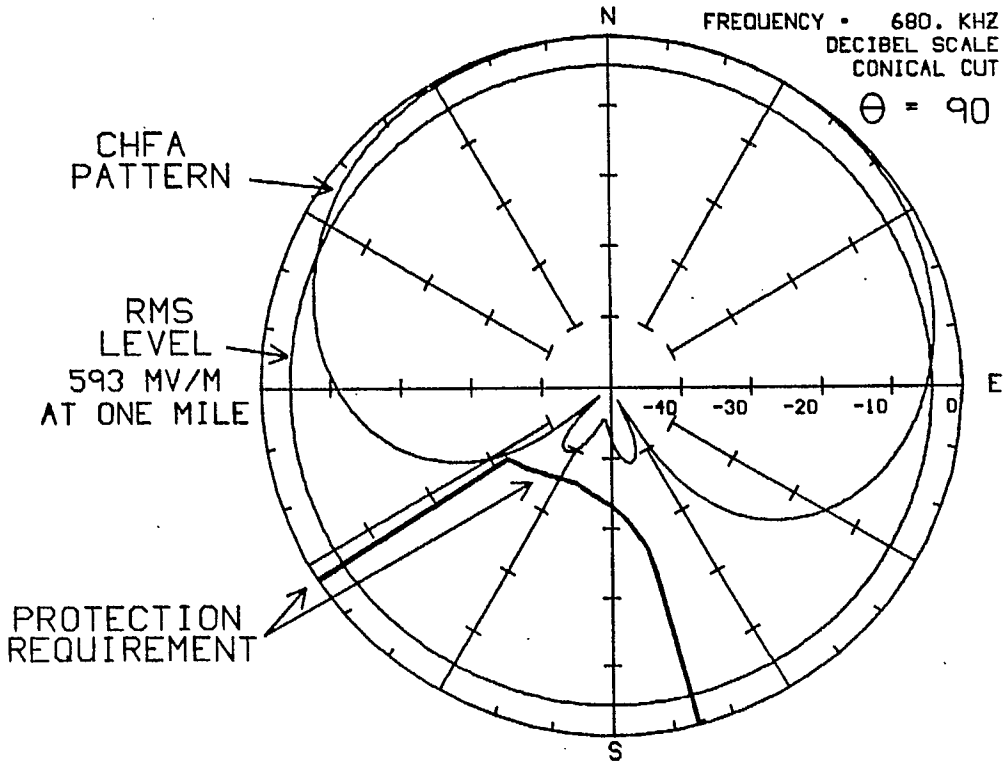

Fig. 5.1(a) - The CHFA antenna array's azimuth pattern.

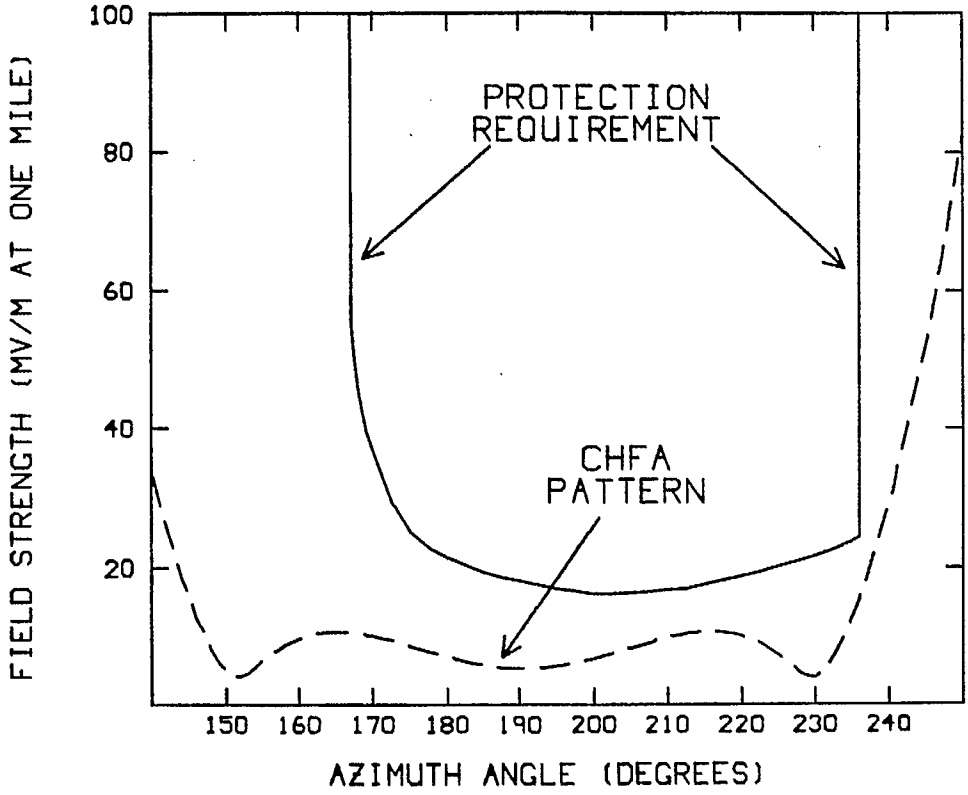

Fig. 5.1(b) - The field strength in the pattern minimum in comparison to the protection requirement.

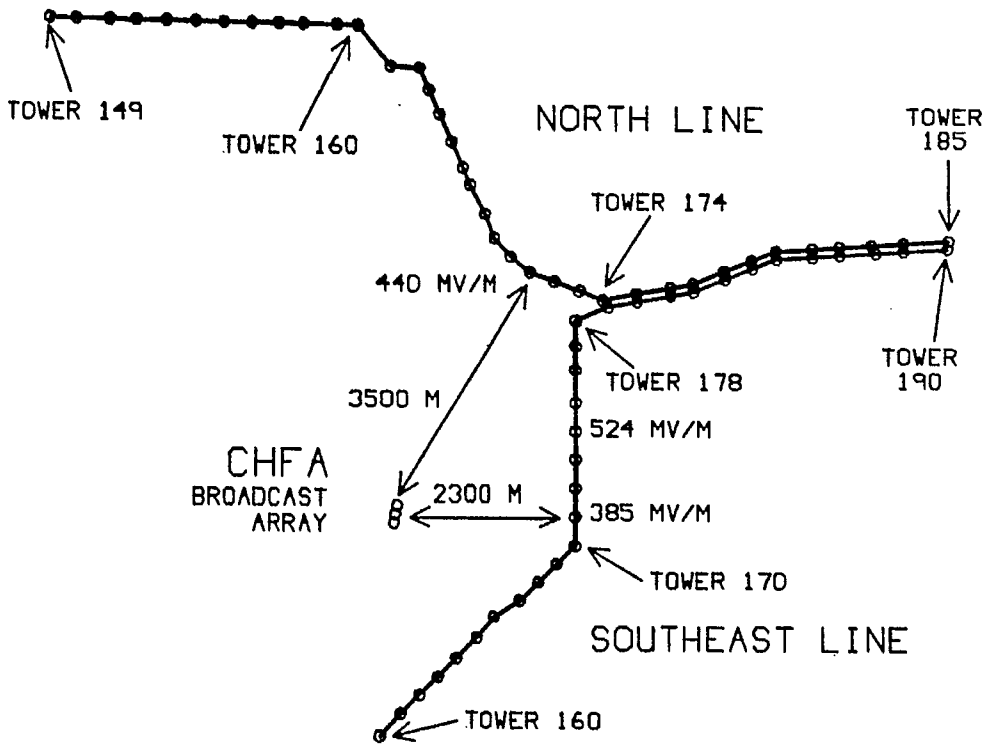

Fig. 5.2 - The power lines near the CHFA antenna array.

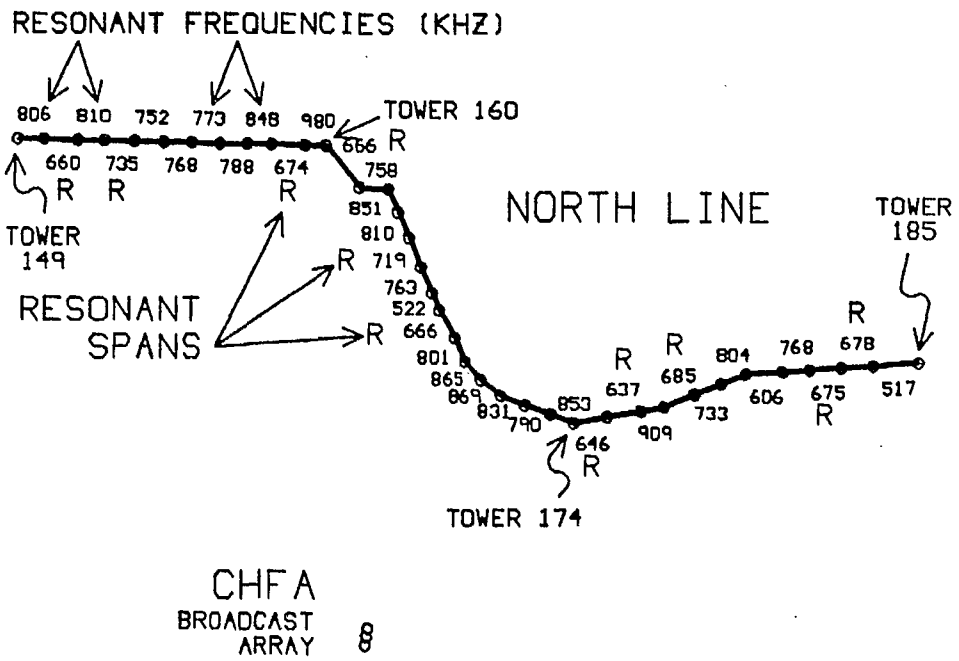

Fig. 5.3 - The resonant frequencies of the spans of the "north" power line. Those marked "R" are resonant within 60 kHz of CHFA's frequency of 680 kHz.

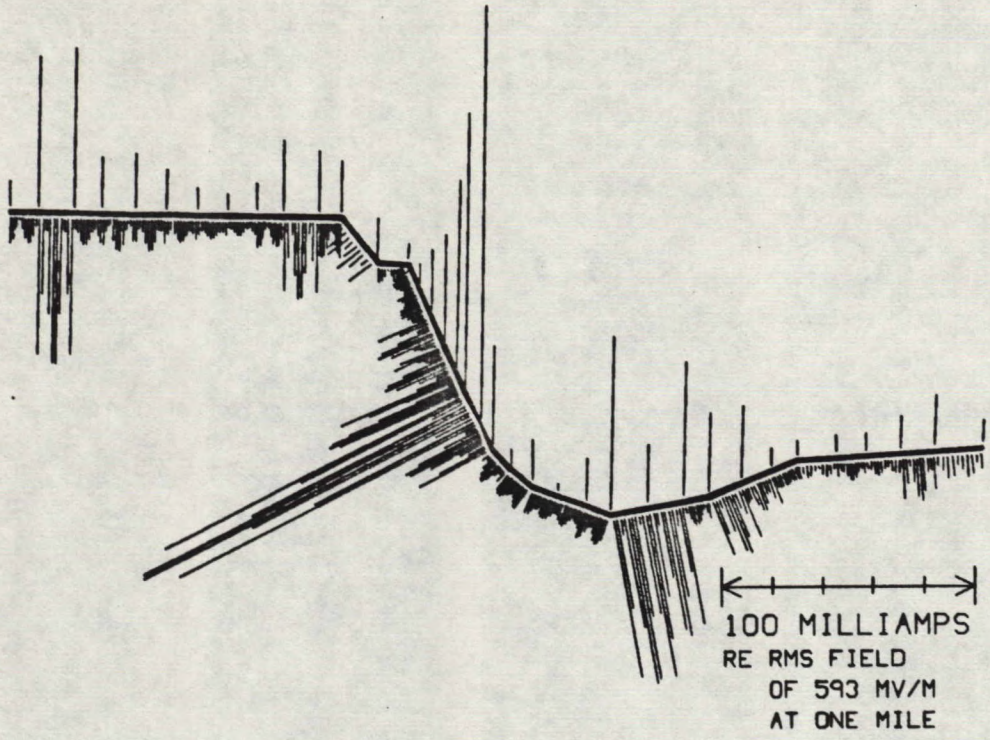

Fig. 5.4 - A schematic representation of the RF current flow on the "north" power line, using "perfect" ground conductivity. The tower currents are shown above the power line route, and the skywire currents are shown below.

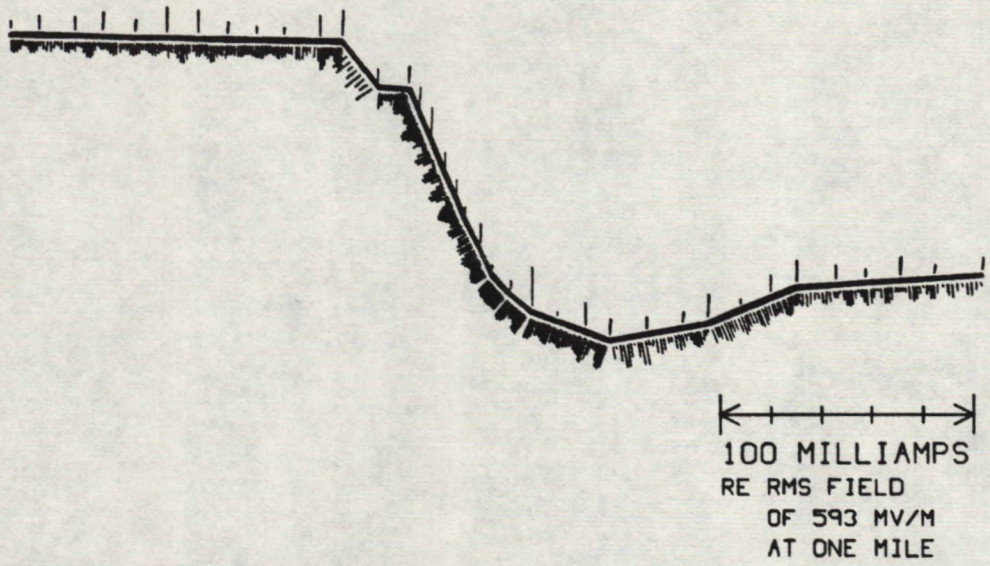

Fig. 5.5 - The RF current flow on the towers and skywires of the "north" power line, when selected towers are isolated from the overhead skywire.

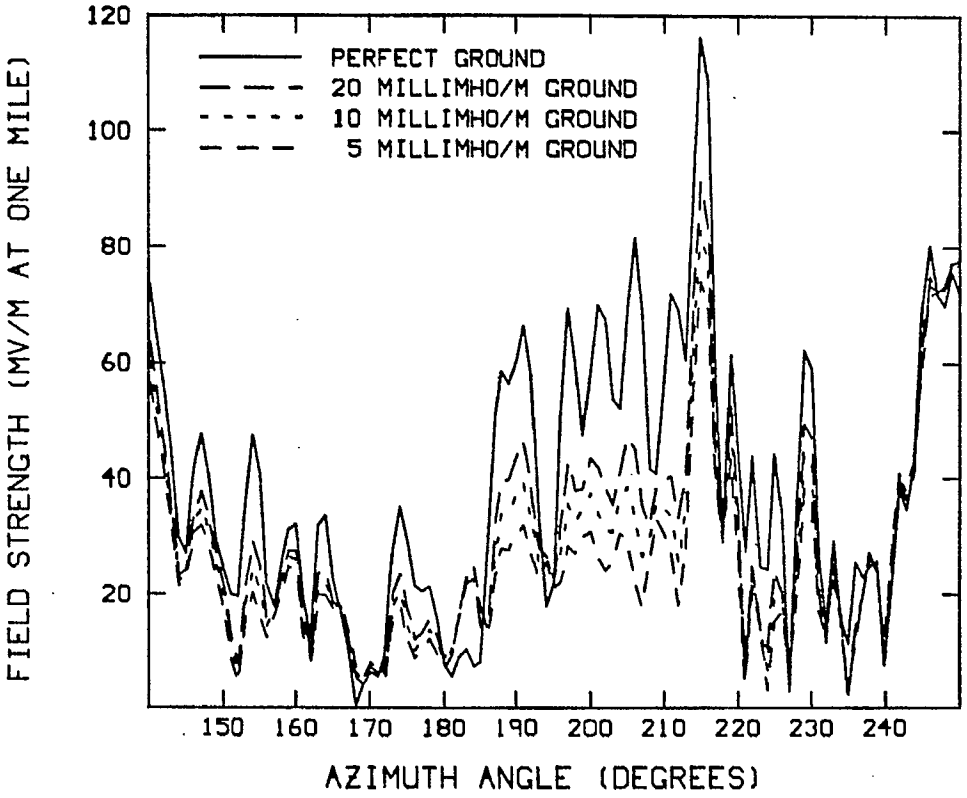

Fig. 5.6(a) - A comparison of the field strength in the CHFA pattern minimum for "perfect" ground, and for three representative ground conductivities.

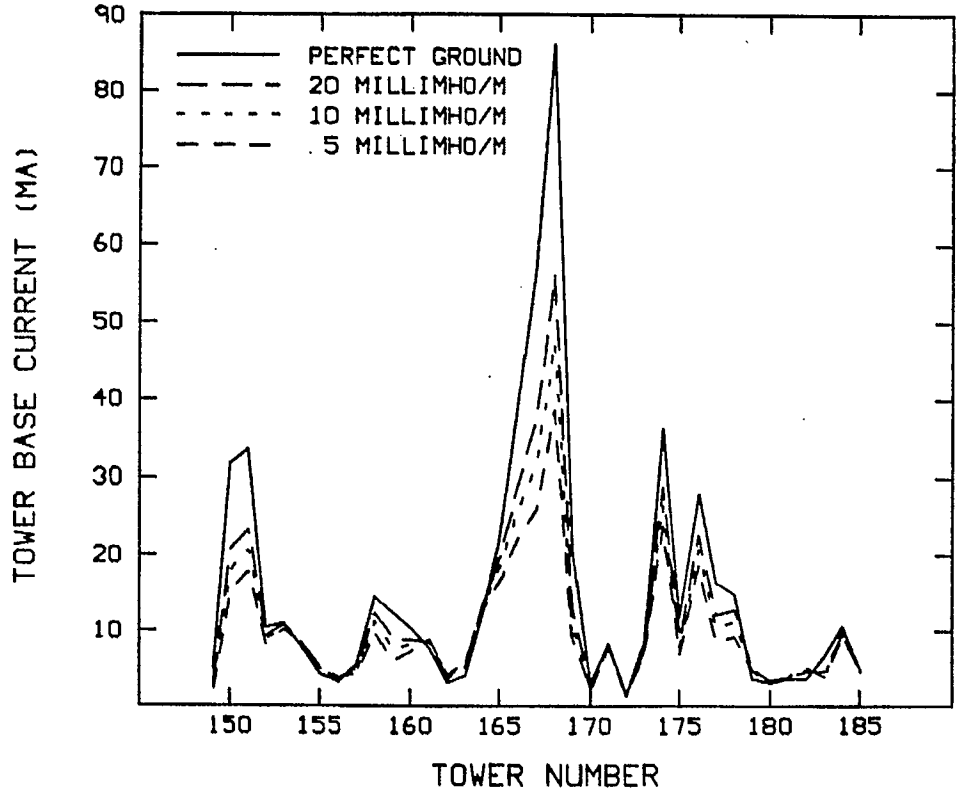

Fig. 5.6(b) - A comparison of the tower base currents on the "north" power line with "perfect" ground, and with three representative ground conductivities.

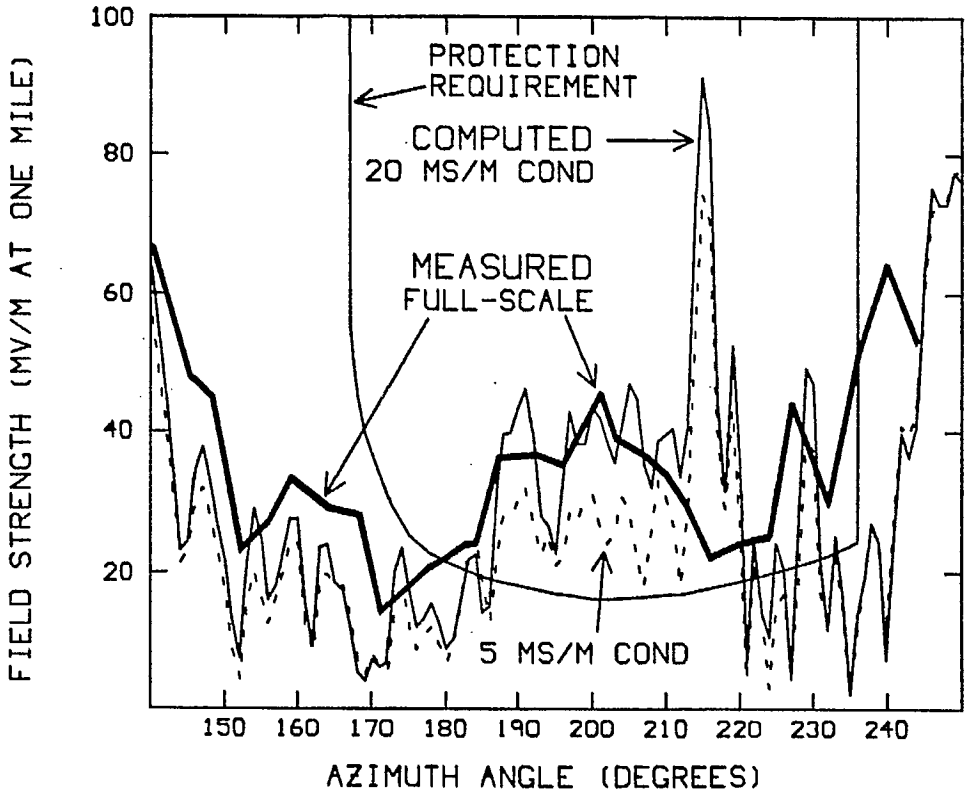

Fig. 5.7(a) - The field strength in the CHFA pattern minimum as measured on the actual site, compared with the computation with "low" and with "high" ground conductivity. Note that the measured data was taken about every three degrees, whereas the computed values are spaced one degree apart.

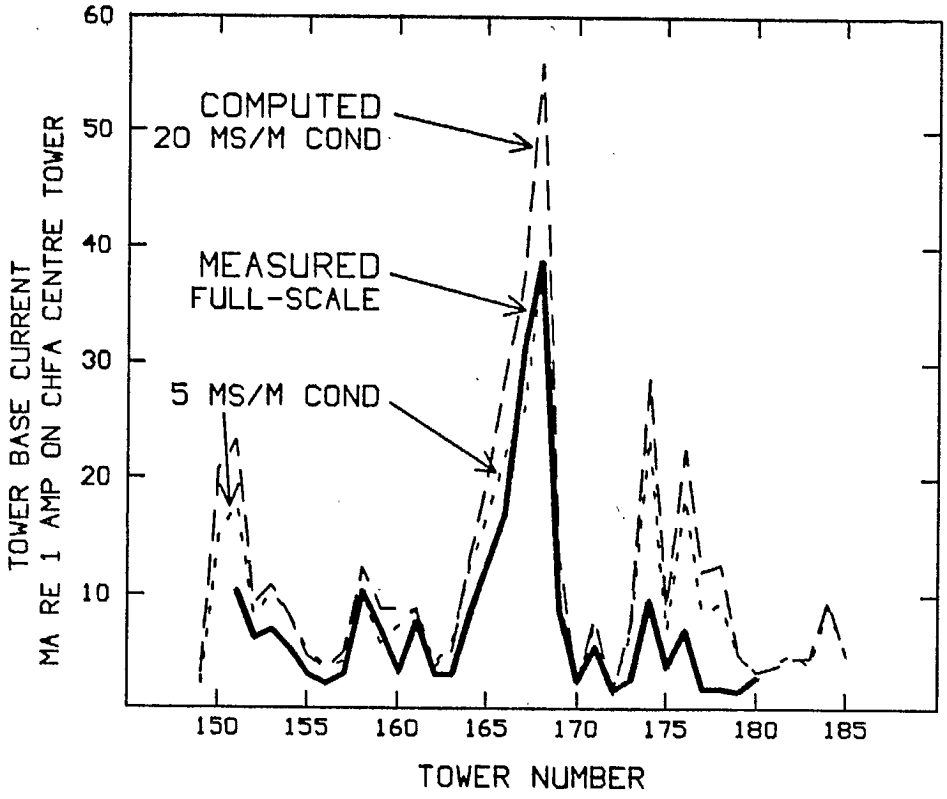

Fig. 5.7(b) - A comparison of the computed current flow at the bases of the power line towers on the "north" power line with those measured on the actual site, with all towers connected to the overhead skywire.

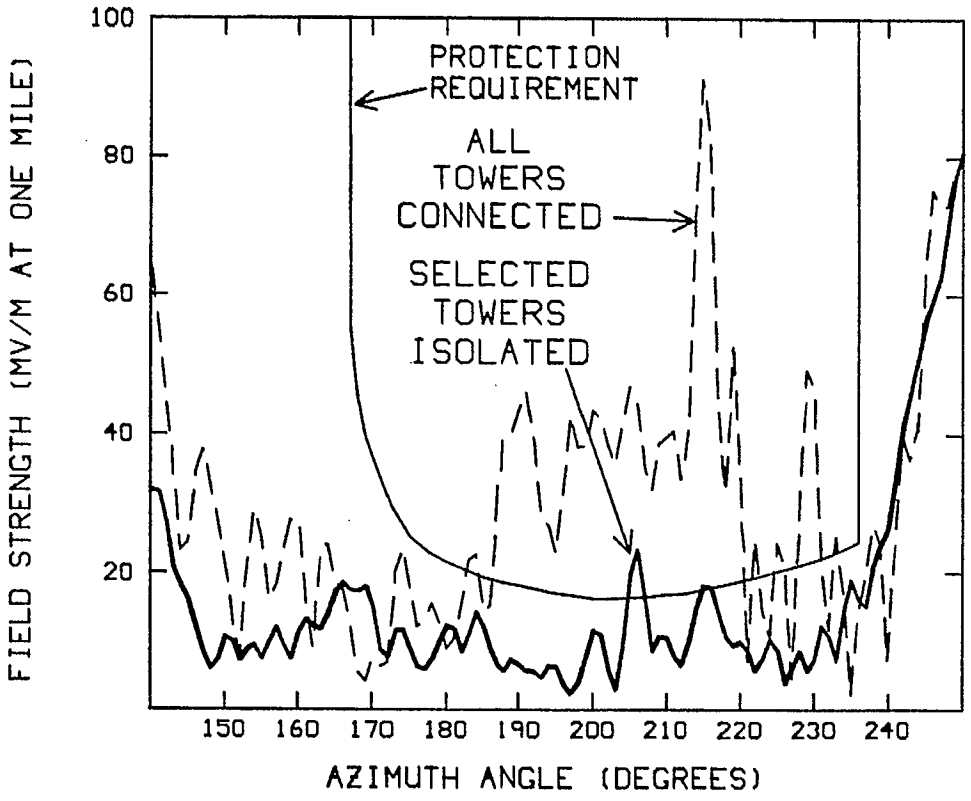

Fig. 5.8(a) - The field strength in the CHFA pattern minimum as computed with "perfect" ground conductivity, with all towers connected to the skywire, and with selected towers isolated from the skywire. A large reduction in the reradiated field has been achieved.

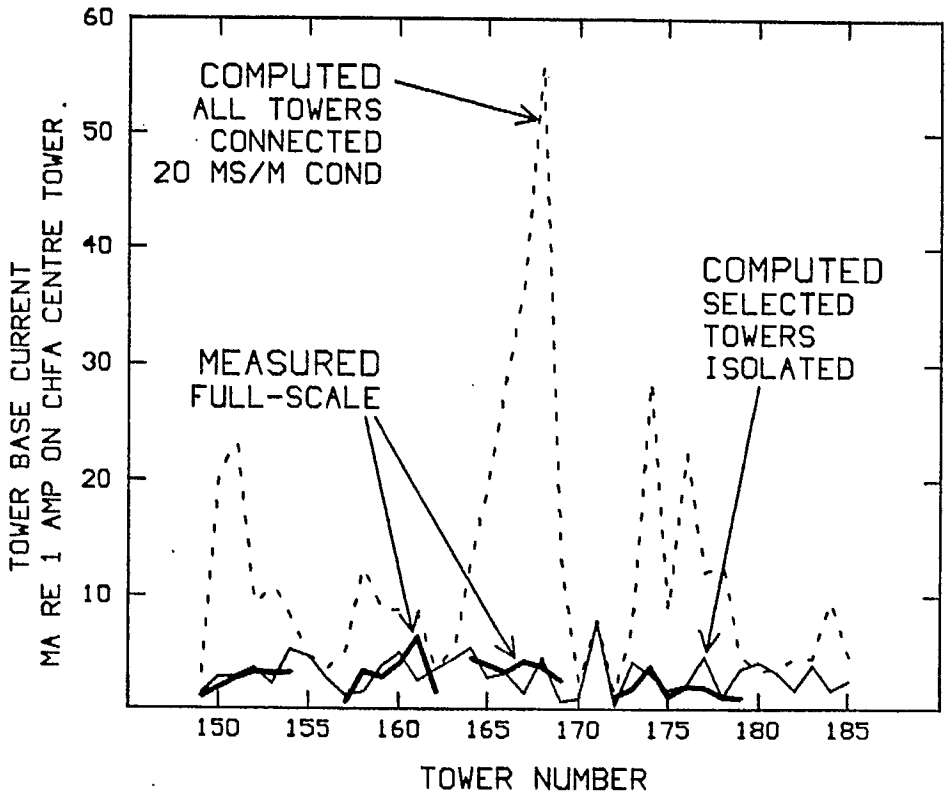

Fig. 5.8(b) - A comparison of the measured tower base currents on the towers of the "north" line with selected towers isolated from the skywire, with the tower base currents predicted by the NEC computer model.

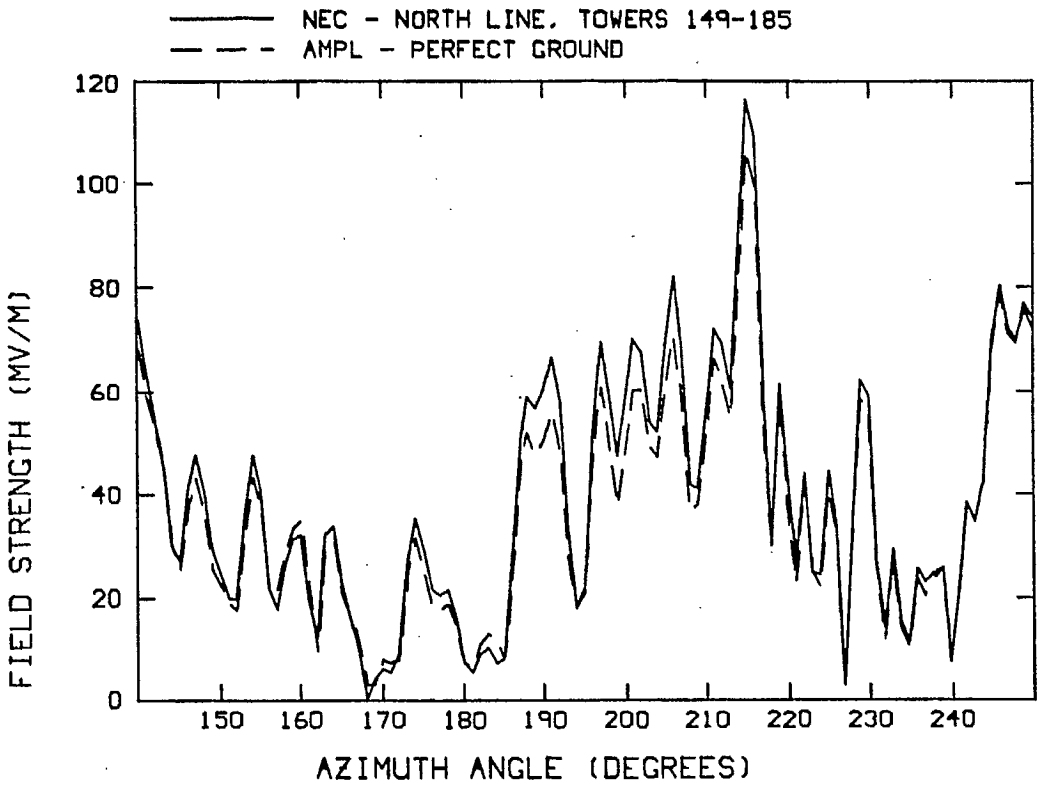

Fig. 5.9(a) - The field strength in the CHFA pattern minimum computed by AMPL, compared to that computed with the NEC program.

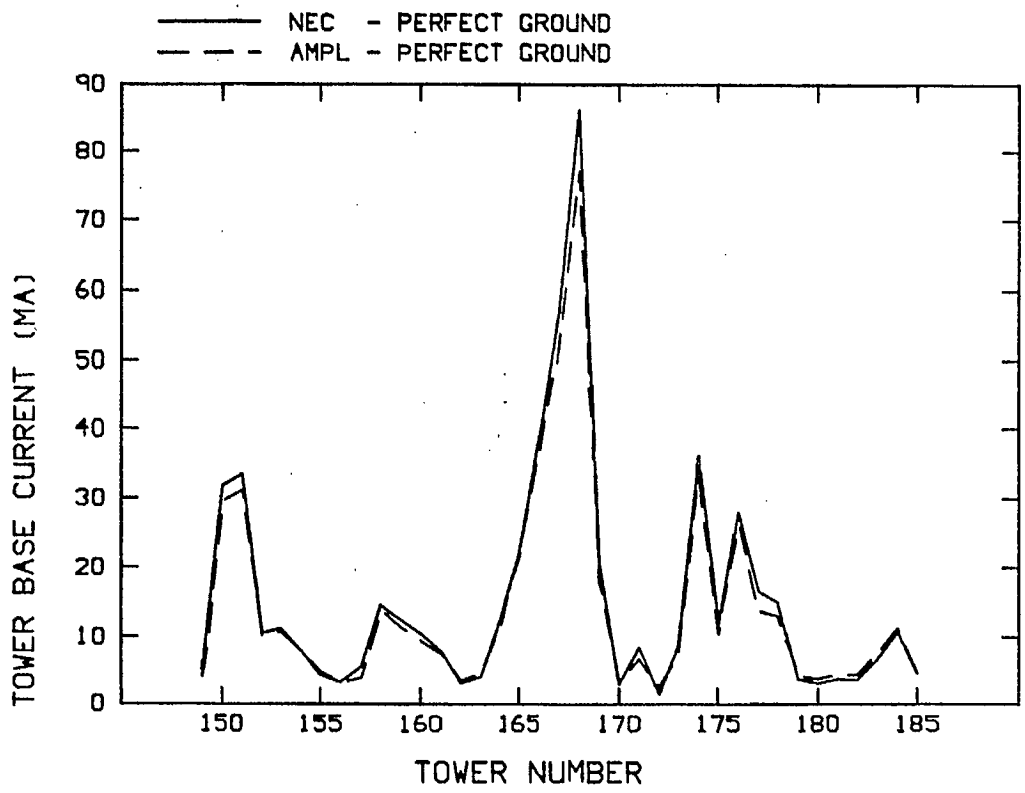

Fig. 5.9(b) - The base currents on the power line towers computed with AMPL compared to those computed with NEC, with high ground conductivity.

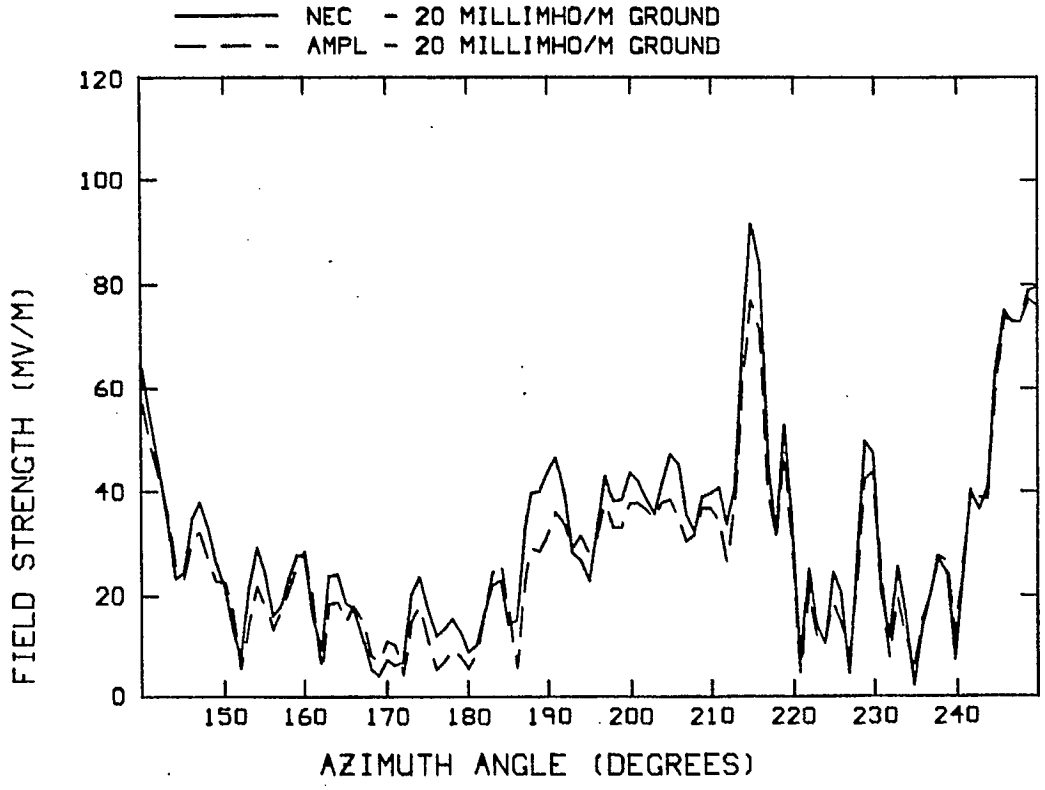

Fig. 5.10(a) - Comparison of AMPL's field strength with NEC's, with ground conductivity 20 mS/m.

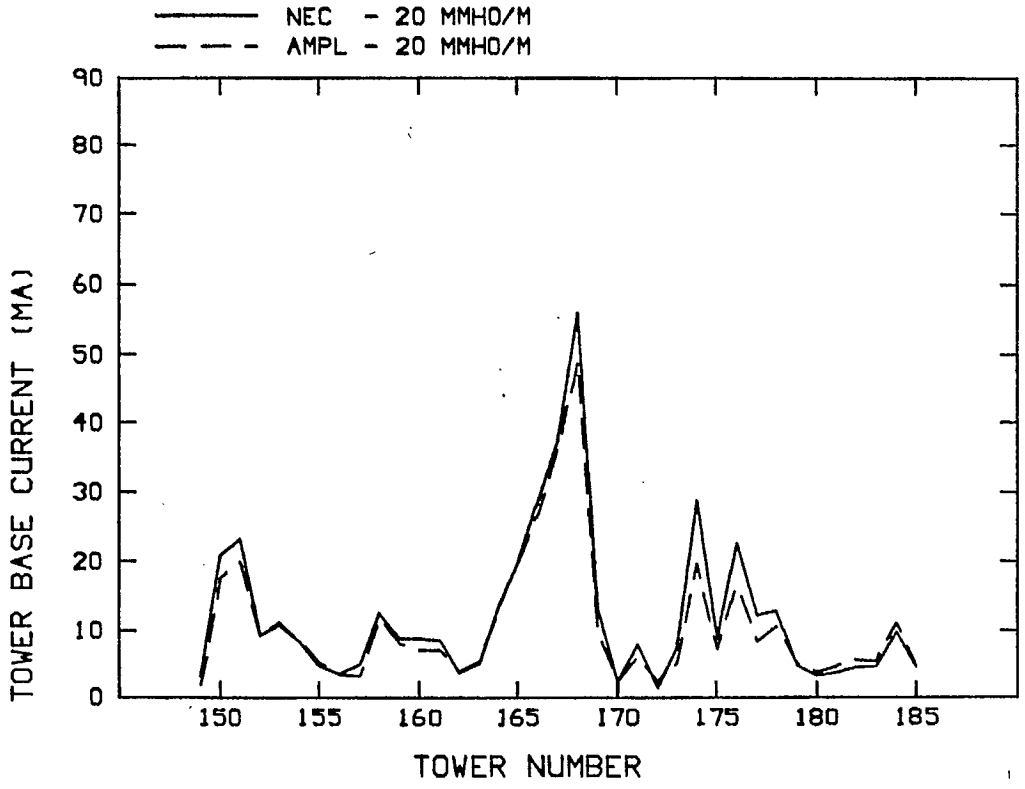

Fig. 5.10(b) - Comparison of AMPL's tower base currents with NEC's, with ground conductivity 20 mS/m.

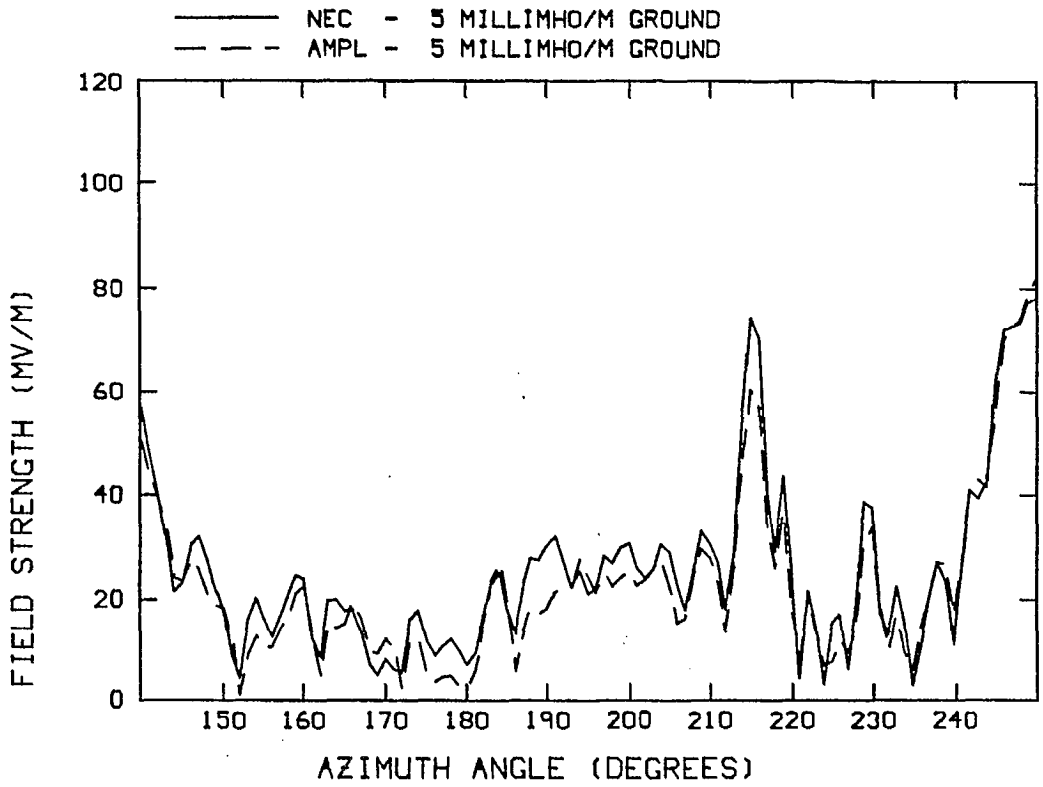

Fig. 5.11(a) - Comparison of AMPL's field strength with NEC's, with ground conductivity 5 mS/m.

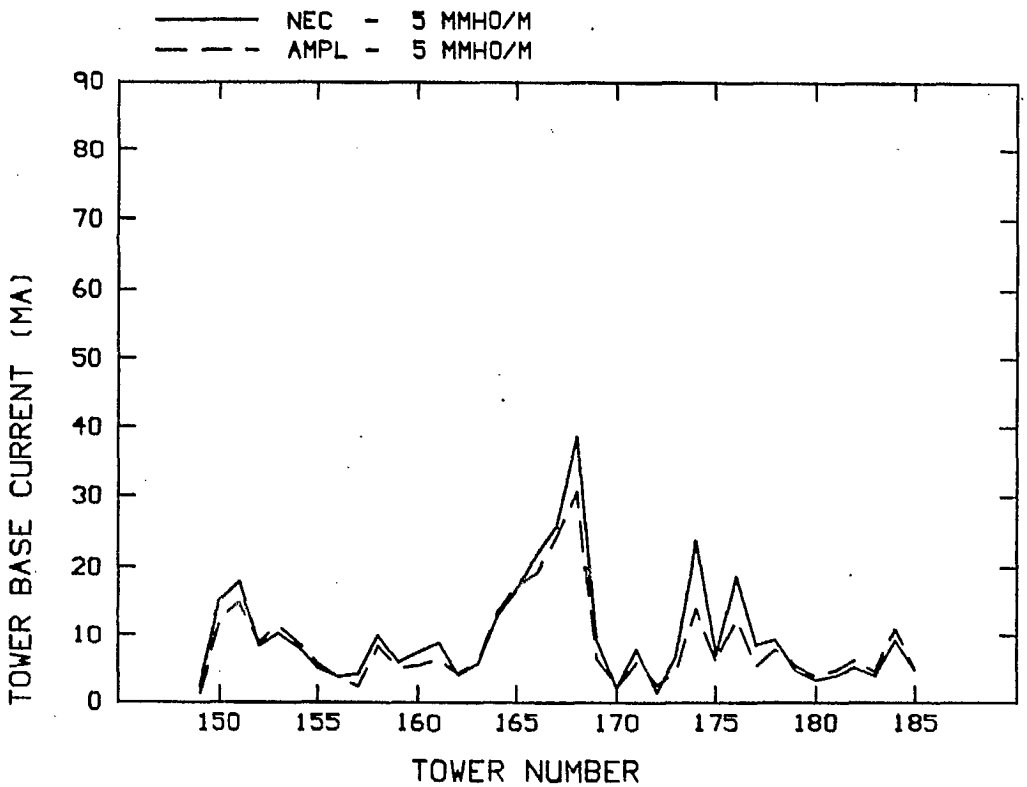

Fig. 5.11(b) - Comparison of AMPL's tower base currents with NEC's, with ground conductivity 5 mS/m.